RECYCLING AND REPROCESSING OF Nd–Fe–B PERMANENT MAGNETS VIA ELECTROCHEMICAL METHODS

Xuan Xu

Doctoral Dissertation
Jožef Stefan International Postgraduate School
Ljubljana, Slovenia

Supervisor: Prof. Dr. Kristina Žužek Rožman, International Postgraduate School and Jožef Stefan Institute

Evaluation Board:
Prof. Dr. Sašo Šturm, Chair, Jožef Stefan International Postgraduate School and Jožef Stefan Institute, Ljubljana, Slovenia
Dr. Paul J. McGuiness, Member, Jožef Stefan International Postgraduate School and Institute of Metals and Technology, Ljubljana, Slovenia
Dr. Karin Leistner, Member, Institute for Solid State and Materials Research, IFW, Dresden, Germany

MEDNARODNA PODIPLOMSKA ŠOLA JOŽEFA STEFANA
JOŽEF STEFAN INTERNATIONAL POSTGRADUATE SCHOOL

Xuan Xu

RECYCLING AND REPROCESSING OF Nd–Fe–B PERMANENT MAGNETS VIA ELECTROCHEMICAL METHODS

Doctoral Dissertation

RECIKLIRANJE IN PONOVNA PREDELAVA TRAJNIH MAGNETOV NA OSNOVI SISTEMA Nd–Fe–B Z ELEKTROKEMIJSKIMI METODAMI

Doktorska disertacija

Supervisor: Prof. Dr. Kristina Žužek Rožman

Ljubljana, Slovenia, November 2019

Intentionally left blank

To my beloved Da Miaomiao: we are going to explore and enjoy the beautiful world together, simply in Chinese, "我会陪你一起满世界，浪，浪，浪!".

–Xiao Miaomiao

Intentionally left blank

Acknowledgements

First of all, I am especially grateful to Prof. Dr. Kristina Žužek Rožman for her constant support, patience and care as my supervisor. I have benefited a lot from the freedom she avails to her students as far as exploring our own ideas and determining the immediate direction of the research. She has provided a much-needed, fresh perspective on my research and ideas. This PhD would not have been possible without her enormous encouragement, critical thinking, constructive advice and prolific discussions. I greatly respect and admire her not only as a magnificent scientist, but also as a real friend.

I am also grateful to Prof. Dr. Sašo Šturm as the Head of the Department and Prof. Dr. Spomenka Kobe for their constructive comments and discussions of this work. I thank them for their willingness to engage in conversations about all aspects of my research work and future career. Their support and enthusiasm for science had an immeasurable impact on my scientific growth.

I would like to give special thanks to my friends, Špela Trafela and Martin Topole, for their kindnesses and valuable companionship during my stay in Ljubljana. I am looking forward to our continued friendship.

I am grateful to Dr. Benjamin Podmiljšak for teaching me how to operate the VSM, glovebox, vacuum furnace, et al. in the lab; Prof. Dr. Miran Čeh and Dr. Jitka Hreščak for the thorough JEOL SEM trainings and Dr. Zoran Samardžija for the SEM analysis; Asst. Prof. Matjaž Spreitzer, Dr. Urška Gabor, Dr. Luka Kelhar and Dr. Zoran Jovanović for their expertise and time in XRD training and measurement; Dr. Marjeta Maček Kržmanc for TGA measurements; Dr. Janez Zavašnik for TEM discussion; Dr. Janja Vidmar and Katarina Marković for ICP-MS measurement and Bojan Ambrožič for FIB sessions on TEM lamellae preparation. I would like to thank Prof. Dr. Aleksander Rečnik, Prof. Dr. Slavko Bernik, Asst. Prof. Andraž Kocjan, Asst. Prof. Matej Komelj, Dr. Nina Kostevšek, Dr. Petra Jenuš, Dr. Matejka Podlogar, Dr. Marko Soderžnik, Dr. Kristina Žagar Soderžnik, Dr. Tomaž Tomše, Dr. Luka Suhadolnik, Dr. Vanja Jordan, Monika Kušter, Živa Marinko, Ipeknaz Özden, Matic Korent and Anja Korent for the fruitful and constructive discussions on the weekly meetings. I would like to express my appreciation to Sanja Fidler and Sabina Cintauer for documentation and translation support that really helped me a lot.

I am also very thankful to the European Training Network for the Design and Recycling of Rare-Earth Permanent Magnet Motors and Generators in Hybrid and Full Electric Vehicles (ETN-DEMETER) project for the financial support. I would like to thank Prof. Dr. Koen Binnemans, Dr. Peter Tom Jones, Prof. Dr. Neil Rowson, Mr. Jean-Marc Dubus, Prof. Dr. Afef Lebouc, Prof. Dr. Peter Omand Rasmussen, Dr. Irena Škulj and Ms. Rabab Naseer for their supportive efforts and biannual productive discussions on my project. I would like to acknowledge our DEMETER fellows: Anas Eldosouky, Muhammad Awais, Martina Orefice, Simona Sobekova, Basit Ali, Awais Ikram, Arnab Chakraborty, Amit Kumar Jha, Adolfo Garcia, Pranshu Upadhayay, Ziwei Li, Muhammad Farhan Mehmood, Fernando Anísio Perpétuo Coelho and Gwendolyn Bailey for their valuable friendship and fruitful collaboration throughout the project. A special thanks goes to Prof. Dr. Paul John McGuiness for all his constructive comments and efforts on my manuscripts.

Most of all, a big thank you goes to my dear Xiaojing for her constant encouragement and understanding. I am very grateful to be lucky enough to have her as my babe, who always gives me motivation and strength to cross barriers, as well as shares every happy and funny moment with me. Lastly, I cannot thank my precious family enough. I would like to thank them wholeheartedly for their unconditional love, support and understanding that in any manner made me who I am today.

Abstract

Currently, sintered neodymium-iron-boron (Nd–Fe–B) permanent magnets (PMs) have a clear domination over other rare-earth (RE) PMs, such as samarium-cobalt (Sm–Co) by means of both value and weight shares. Sintered Nd–Fe–B PM consumption has been estimated to be driven by hybrid and electric vehicles and wind turbines in the next 20 years, though the use of these magnets in other applications will support further demand growth. Generally, the sintered Nd–Fe–B PMs incorporate 20–30 wt.% of rare-earth elements (REEs) that include mainly Nd with a small addition of Dy and/or Tb, and as such represent an important secondary REEs resource. Despite that, less than 1% of REEs are being recycled from End-of-Life (EoL) products, with REE-containing PMs representing the largest share of these products. This is a very small percentage, especially if we consider that the recycling of the sintered Nd–Fe–B magnets is an important strategy for reducing the environmental dangers associated with the RE mining and overcoming the well-documented supply risks associated with the REEs.

With the aim of recycling the sintered Nd–Fe–B magnets, various approaches, such as direct re-use, alloys recovery and REEs recovery are currently at different technology-readiness levels. A direct re-use of the Nd–Fe–B magnets is considered as the most economical and ecological way. However, extra addition of REE materials, e.g., Nd hydride, is required due to the loss in the liquid phase and the non-separation of REE oxide (REO) phases. As a result, sintered Nd–Fe–B magnets produced from the repeated recycling of materials by direct re-use methods tend to have poorer magnetic properties as the number of cycles increases. Alloys recovery, such as melt-spinning and liquid-metal extraction, is able to recover both RE-transition metal (RE–TM) alloys and TM-free RE metals that are ready for new magnets making. However, the processes generally operate at 750–950 °C with long durations that are energy-intensive. REEs recovery, such as gas-slag extraction and hydrometallurgy, is applicable to both slightly and heavily oxidized magnet material with varied compositions. Especially, hydrometallurgy is seen as the most promising, as it requires relatively simple equipment to extract the REEs in a continuous operation at mild temperatures. However, this multi-step process consumes large quantities of acids and alkalis as well as large quantities of wastewater. Still, further research is needed to make the recycling processes for Nd–Fe–B magnets more economical, sustainable and environment-friendly.

Sintered Nd–Fe–B PMs consist of REE-rich grain boundaries, representing about 10–12% of the magnet, and the $Nd_2Fe_{14}B$ grains of the matrix phase, which is practically oxygen-free, accounting for 85–87% of the magnet. An electrochemical process was developed to recover the $Nd_2Fe_{14}B$ grains from the sintered Nd–Fe–B magnets. The procedure is based on the anodic etching of the sintered Nd–Fe–B magnets in a non-aqueous dimethylformamide (DMF)-0.3 mol L^{-1} $FeCl_2$ bath. Selective recovery of $Nd_2Fe_{14}B$ grains was realized within the applied current density < 5 mA cm^{-2} based on the etching priority of phases: metallic Nd > intergranular $NdFe_4B_4$ > matrix $Nd_2Fe_{14}B$. The total energy consumption of the proposed recycling route is estimated to be ~2.99 kWh kg^{-1},

which is comparable to the state-of-the-art direct re-use methods. A recycling route for the sintered Nd–Fe–B magnets is proposed based on the electrochemical etching that ends up with the $Nd_2Fe_{14}B$ grains, REE-containing electrolyte and REE-based particles, and pure Fe metal as the final products with the only consumption of $FeCl_2$ and electricity. The proposed recycling route is currently the only procedure that enables repeated recycling of sintered Nd–Fe–B magnets in a closed-loop system.

The REE-containing electrolyte with REE chlorides and $FeCl_2$ dissolved can be further treated by the conventional hydrometallurgical process for high purity of the REEs recovery. Alternatively, these chlorides can also be used as metal precursors for RE–TM alloys synthesis by electrodeposition which is promising in producing thin film magnets.

Electrodeposition of Nd–Fe from the 1-ethyl-3-methylimidazolium dicyanamide ([EMIM][DCA]) ionic liquid (IL) using metal chlorides was investigated. We observed that Nd^{3+} cannot be electro-reduced independently, although it can be co-electrodeposited inductively on a Cu substrate with the presence of Fe^{2+}. The transmission electron microscopy (TEM) analysis combined with electron-energy-loss spectroscopy (EELS) verified the formation of NdC_2 as an indirect proof that Nd^{3+} is reduced to Nd^0 during the electrodeposition process. The TEM/EELS was also able to confirm that the deposition of the Nd–Fe starts with the sole deposition of Fe, followed by the co-deposition of Nd–Fe. This is in agreement with the transition-state theory, which has the Fe initially reduced to an activated state ($\boldsymbol{Fe^*}$), where it is able to catalyse the reduction of the RE^{3+} to RE^0. This new insight into the electrodeposition process brings us a very important step closer to being able to recycle REEs efficiently and even to realize electrodeposited REE-based PM thin films at a mild temperature, thus giving us a sustainable, green-chemistry approach that provides a genuine alternative to high-temperature molten salt electrolysis.

To reduce the environmental impact of REEs recovery, a facile closed-loop process to selectively separate and recover the REEs and TMs from the sintered Nd–Fe–B magnets was demonstrated. First, using a room-temperature electrolysis step, the sintered Nd–Fe–B magnet was completely leached on the anode, while the Fe metal was selectively deposited on the cathode. By balancing the dissolution and consumption of the Fe, selective leaching of the REEs was realized, which saved 84.4% in terms of acid consumption and did not require the use of any alkali for the Fe precipitation. The REEs were selectively precipitated as REE-sodium sulfate double salts, which meant we have been able to recycle the electrolyte in a closed-loop, avoiding any wastewater discharge that has to be done using conventional hydrometallurgy. This two-step method was able to recover 92.5% of the REEs with a purity of 99.4%.

Povzetek

Po trenutnem tržnem deležu tako po vrednosti kot tudi po teži, imajo sintrani trajni magneti na osnovi sistema redka zemlja-prehodna kovina neodim-železo-bor (Nd–Fe–B) očitno prevlado nad drugimi magneti na osnovi podobne kemijske konfiguracije (npr. Sm-Co). Ocenjuje se, da bodo porabo sintranih trajnih magnetov Nd–Fe–B v naslednjih 20 letih diktirala predvsem hibridna in električna vozila ter vetrne turbine kot nadgradnja teh magnetov v že klasičnih aplikacijah. Na splošno sintrani trajni magneti Nd–Fe–B vsebujejo 20–30 ut.% elementov redkih zemelj, ki vključujejo predvsem Nd z majhnim dodatkom Dy in/ali Tb in kot takšni predstavljajo pomemben sekundarni vir. Kljub temu se manj kot 1 % elementov redkih zemelj reciklira iz odpadnih izdelkov, največji delež teh izdelkov pa predstavljajo prav trajni magneti. To je zelo majhen odstotek, še posebej, če upoštevamo, da je recikliranje sintranih magnetov Nd–Fe–B pomembna strategija za zmanjšanje okolijskih škodljivih vplivov, povezanih z rudarstvom redkih zemelj, ter za premagovanje dobro dokumentiranih tveganj oskrbe, povezanih s temi specifičnimi elementi.

Pristopi k recikliranju trajnih magnetov Nd–Fe–B so različni, npr. neposredna ponovna uporaba, pridobivanje osnovnih zlitin in pridobivanje osnovnih elementov redkih zemelj, in se trenutno izvajajo na različnih stopnjah tehnološke pripravljenosti. Neposredna ponovna uporaba magnetov Nd–Fe–B s pretaljevanjem velja za trenutno najbolj ekonomičen in ekološki način. Vendar pa zahteva dodajanje manjših količin elementov redkih zemelj (NdH_2) za kompenzacijo izgub slednjih med pretaljevanjem, saj zlitina s časom bogati na vsebnosti Nd-oksida. Kot rezultat imajo sintrani magneti Nd–Fe–B, ki so narejeni s ponavljajočim se recikliranjem s pretaljevanjem, slabše magnetne lastnosti, ki se s številom ciklov še poslabšujejo. Pridobivanje osnovne zlitine Nd–Fe–B prek pretaljevanja in hitrega ohlajanja ali prek ekstrakcije elementov redkih zemelj s tekočo kovino je sicer izvedljivo, vendar energijsko potratno, saj deluje pri povišanih temperaturah 750–950 °C in v dolgih časovnih intervalih. Pridobivanje redkih zemelj iz odsluženih magnetov je mogoče tudi s postopki plinske ekstrakcije in nadaljnje elektrolize ali s kemijskimi postopki hidrometalurgije, ki se lahko uporabljajo tako za rahlo kot močno oksidirane magnete različnih vhodnih kemijskih sestav. Predvsem se hidrometalurgija obravnava kot najbolj obetavna, saj zahteva razmeroma enostavno opremo za ekstrakcijo elementov redkih zemelj v obliki soli, v kontinuirnem delovanju pri blagih temperaturah. Vendar pa ta postopek poteka v več kemijskih korakih, ki rezultirajo v porabi velike količine kislin in alkalij ter v generaciji velike količine odpadne vode, kar še vedno predstavlja izziv. Tako smo v okviru te doktorske disertacije raziskali nove smeri, ki lahko vodile k večji ekonomičnosti ter k višji ekološki sprejemljivosti, ki bi recikliranje magnetov Nd–Fe–B dvignile na višji trajnostni nivo.

Mikrostrukturo svežih kot tudi odsluženih sintranih magnetov Nd–Fe–B sestavljajo zrna $Nd_2Fe_{14}B$ matrične faze, ki je praktično brez kisika, kar predstavlja 85–87 % magneta, ter meje med zrni, bogate z Nd, ki predstavljajo približno 10–12 % magneta, vendar preferenčno oksidirajo tekom časa uporabe. Poleg omenjenih faz Nd–Fe–B magneti vsebujejo tudi fazo $NdFe_4B_4$, ki pa po deležu predstavlja le nekaj %. Za selektivno pridobivanje zrn $Nd_2Fe_{14}B$ iz sintranih magnetov Nd–Fe–B smo razvili elektrokemijski

postopek, ki temelji na anodnem jedkanju magnetov Nd–Fe–B v organskem topilu dimetilformamidu (DMF)–0,3 mol L^{-1} z dodatkom $FeCl_2$. Selektivno rekuperacijo zrn $Nd_2Fe_{14}B$ smo uspešno izvedli znotraj okvirja uporabljene tokovne gostote < 5 mA cm^{-2} na podlagi različnih elektrokemijskih redukcijskih potencialov posameznih faz v magnetu Nd-Fe-B, po principu preferenčnega jedkanja: kovinski Nd > faza $NdFe_4B_4$ > faza $Nd_2Fe_{14}B$. Ocenjena skupna poraba energije za predlagano pot recikliranja znaša ~2,99 kWh kg^{-1}, kar je primerljivo z dosedanjimi metodami neposredne reciklaže. Predlagana pot recikliranja sintranih magnetov Nd–Fe–B na podlagi elektrokemičnega jedkanja se konča z zrni $Nd_2Fe_{14}B$ ter s čisto kovino Fe na katodi, in rezultira le v končni porabi $FeCl_2$ in elektrike. Predlagana pot recikliranja je trenutno edini postopek, ki omogoča večkratno recikliranje sintranih magnetov Nd–Fe–B v zaprtem sistemu. Zrna $Nd_2Fe_{14}B$ je moč direktno uporabiti za izdelavo novih magnetov, nastali elektrolit, ki vsebuje ione elementov redkih zemelj, njihove kloride in raztopljen $FeCl_2$, pa je mogoče nadalje obdelati s konvencionalnimi hidrometalurškimi postopki. Slednji elektrolit lahko teoretično uporabimo tudi kot osnovni elektrolit za elektro-nanašanje sistemov redka zemlja-prehodna kovina, kar je obetavno pri proizvodnji tankoslojnih magnetov.

Iz tega naslova smo raziskali elektro nanašanje oz. elektro redukcijo sistema Nd in Fe. Elektro nanašanje smo izvajali iz brezvodnega elektrolita na osnovi ionske tekočine ([EMIM][DCA]) 1-etil-3-metilimididazol diamida iz raztopin soli $NdCl_3$ in $FeCl_3$. Opazili smo, da se Nd^{3+} ne more samostojno nanašati, vendar pa ga lahko nanesemo na substrat Cu ob prisotnosti Fe. Z analizo v presevnem elektronskem mikroskopu (TEM) v kombinaciji s spektroskopijo na izgubo energije elektronov (EELS) smo dokazali prisotnost Fe in Nd v nanesenih slojih. Nd je v sloju prisoten kot NdC_2, kar nam služi kot posreden dokaz, da se je Nd^{3+} med postopkom elektronanašanja reduciral do Nd^0. Analiza TEM / EELS je tudi potrdila, da se nanašanje Nd–Fe začne z odlaganjem Fe, čemur sledi so-odlaganje Nd. Rezultat je v soglasju z razvito in predlagano teorijo t. i. prehodnega stanja. Fe, ki se najprej nanese, zreducira v aktivno stanje (***Fe****), slednji pa nadalje katalizira redukcijo Nd^{3+} v Nd^0. Ta nov vpogled v postopek elektronanašanja, predstavlja zelo pomemben korak bližje temu, da lahko učinkovito recikliramo elemente redkih zemelj in celo uresničimo idejo o elektronanašanju tankih slojev Nd-Fe, za kar učinkovitega postopka v dostopni literaturi še ni. Razviti postopek elektronanašanja predstavlja korak napram trajnostnim rešitvam pri pridobivanju in recikliranju elementov redkih zemelj, saj predstavlja zeleno in učinkovito alternativo konvencionalnim postopkom pridobivanja Nd z elektrolizo iz staljenih soli.

Da bi zmanjšali vpliv konvencionalnih postopkov (predvsem hidrometalurških) predelave elementov redkih zemelj na okolje, smo nadalje razvili tudi postopek za selektivno ločevanje in pridobivanje elementov redkih zemelj in prehodnih kovin iz sintranih magnetov Nd–Fe–B. Najprej je bil s pomočjo elektrolize pri sobni temperaturi sintran magnet Nd–Fe–B popolnoma elektrokemijsko raztopljen na anodi, Fe pa selektivno naneseno na katodi. Z uravnoteženjem raztapljanja magneta in porabe Fe na katodi smo dosegli selektivno izpiranje elementov redkih zemelj, kar je prihranilo 84,4 % v smislu porabe kisline, za precipitacijo Fe pa ni bilo treba uporabiti alkalij, kar so značilnosti hidro metalurškega postopka. Elemente redkih zemelj smo selektivno oborili kot dvojne soli (Nd, Dy)-natrijevega sulfata. S predlaganim postopkom nam je uspelo reciklirati elektrolit v zaprti zanki, pri čemer smo se izognili kakršnemu koli odvajanju odpadne vode, ki bi ga bilo treba izvesti s konvencionalno hidrometalurgijo. S tem dvostopenjskim postopkom smo uspeli pridobiti 92,5 % elementov redkih zemelj s čistostjo 99,4 %

Contents

List of Figures

Intentionally left blank

List of Tables

Intentionally left blank

Abbreviations

Alamine 308	. . . Tri-iso-octyl-amine
Alnico	. . . Al–Ni–Co alloys
BSE	. . . Backscattered electron
CV	. . . Cyclic voltammetry
Cyanex 272	. . . *bis*(2,4,4-trimethylpentyl) phosphinic acid
Cyanex 921	. . . Tri-octyl-phosphine oxide
Cyphos® IL 101	. . . Trihexyl(tetradecyl)phosphonium chloride
D2EHPA	. . . *bis*-(2-ethylhexyl)-phosphoric acid
DDPMG	. . . Direct-drive permanent magnet generator
DESs	. . . Deep eutectic solvents
DMF	. . . Dimethylformamide
EC	. . . European Commission
EDS	. . . Energy-dispersive X-ray spectroscopy
EELS	. . . Electron-energy-loss spectroscopy
EoL	. . . End-of-Life
EU	. . . European Union
EVs	. . . Electric vehicles
[EMIM][DCA]	. . . 1-ethyl-3-methylimidazolium dicyanamide
F/TE-SEM	. . . Field-/thermionic-emission scanning electron microscopy
FFT	. . . Fast Fourier transform
FIB	. . . Focused ion beam
GBP	. . . Grain boundary phase
GWEC	. . . Global Wind Energy Council
HAADF-STEM	. . . High-angle annular dark-field scanning TEM
HD	. . . Hydrogen decrepitation
HDD	. . . Hard disk drive
HDDR	. . . Hydrogenation disproportionation desorption and recombination
HDPE	. . . High density polyethylene
HEVs	. . . Hybrid electric vehicles
[Hbet][Tf_2N]	. . . *bis*(trifluoromethylsulfonyl)imide
ICP-MS	. . . Inductively coupled plasma mass spectrometry
ICP-OES	. . . Inductively coupled plasma optical emission spectrometry
ILs	. . . Ionic liquids
KS	. . . Kichizaemon Sumitomo
LSV	. . . Linear sweep voltammetry
MRI	. . . Magnetic resonance imaging
OCP	. . . Open circuit potential
ODD	. . . Optical disk drives
PC-88A	. . . 2-ethylhexyl-2-ethylhexyl-phosphonic acid
PE	. . . Polyethylene
PMs	. . . Permanent magnets
PP	. . . Polypropylene

QRE	... Quasi-reference electrode
RE	... Rare-earth
REEs	... Rare-earth elements
REOs	... Rare-earth oxides
RTILs	... Room-temperature ionic liquids
SAED	... Selected-area electron-diffraction pattern
SE	... Secondary-electron
SHE	... Standard hydrogen electrode
TEM	... Transmission electron microscopy
TGA	... Thermogravimetric analysis
TMs	... Transition metals
TODGA	... Tetraoctyl diglycol amide
UV-Vis-NIR	... Ultraviolet-visible-near infrared
XPS	... X-ray photoelectron spectroscopy
XRD	... X-ray diffraction

Symbols

a_i ... Atomic weight
B ... Flux density
BH ... Energy product
$(BH)_{max}$ ... The maximum energy product
B_r ... Remanence
c_j ... Ion concentration in the bulk solution
E ... Energy consumption
F ... Faraday constant, 96485.33 C mol^{-1}
f_i ... Mass fraction
ΔG ... Gibbs free energy
H ... Magnet field
H_c ... Coercivity
I ... Applied current
k_a ... Equilibrium constant of reaction a
k_i ... Electrochemical rate constant of reaction i
m_0 ... The observed mass loss of the Nd–Fe–B magnets
m_{Fe} ... Mass of the deposited Fe
m_t ... The theoretical mass loss of the Nd–Fe–B magnets
M_{Fe} ... Molar mass of Fe, 55.85 g mol^{-1}
n_i ... Number of electrons exchanged of element i
N_{EQ} ... The total number of equivalents from dissolving a unit mass of the alloy
R ... The universal gas constant, 8.314 J K^{-1} mol^{-1}
t ... Duration of the electrolysis/electrodeposition
t_{off} ... Resting period
t_{on} ... Deposition period
T ... Temperature
T_c ... Curie temperature
$\boldsymbol{TM}^*$ ... Transition state TM
TM_{ad} ... Adsorbed transition metal
U ... Voltage
V ... Volume
X_{RE} ... The molar fraction of REE
α_j ... Transfer coefficient
θ_j ... Adsorption coverage
η_D ... Current efficiency
$\eta_{Fe\text{-}L}$ ... Fe leaching efficiency
η_j ... Over-potential
η_L ... Leaching efficiency
φ^θ ... Standard electrode potential

Intentionally left blank

Chapter 1

Introduction

1.1 Development of PMs

Permanent magnets (PMs) are essential components in many fields of technology because they can provide magnetic flux. The magnetic properties of a PM are derived from hysteresis loop behavior (B *vs.* H in engineering or M *vs.* H in physical sciences), as shown in Figure 1.1 [1]. The relationships between the magnetic induction (B) inside a PM, the applied magnetic field (H), and the magnetization induced inside the sample by H, are defined by equation (1.1):

$$B=\mu_0(M+H) \tag{1.1}$$

where μ_0 is the permeability of the free space; M is the total magnetization of a PM.

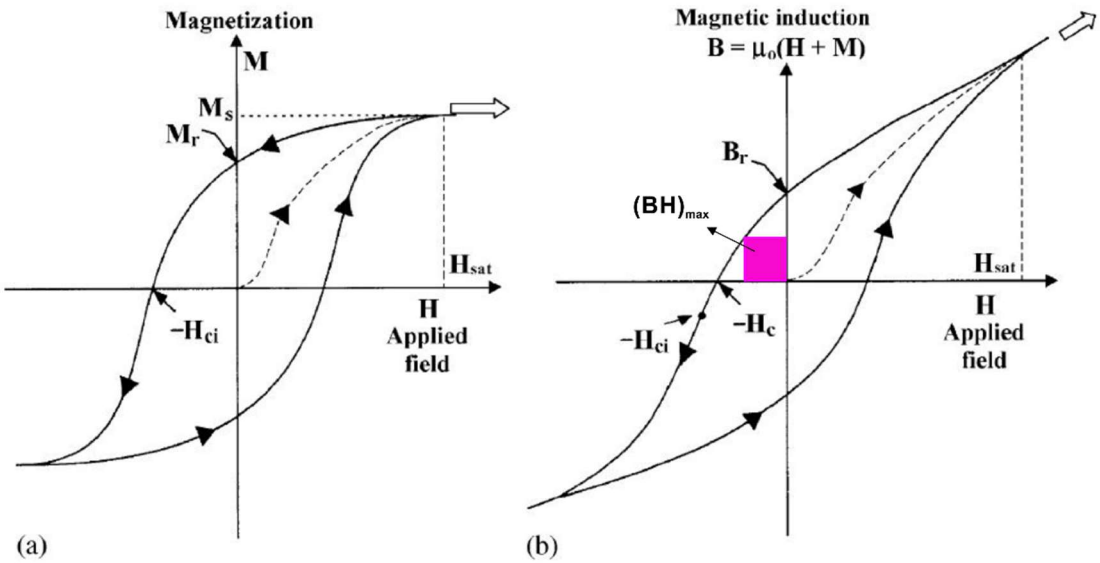

Figure 1.1: Hysteresis curves for PMs: (a) M *vs.* H and (b) B *vs.* H [1].

The M *vs.* H hysteresis loop is called the magnetization curve (Figure 1.1a). At sufficiently large values of H, the magnetization becomes constant at its saturation value, i.e., saturation magnetization (M_s). When H is decreased to zero after reaching the saturation, the magnetization is not reduced to zero but retains a certain value that is called remanent magnetization (M_r). If the applied field is then increased in the opposite direction, the magnetization will reach zero when H equals the intrinsic coercivity (H_{ci}). A

large field is needed to demagnetize a PM with large H_{ci} value. When the reversed magnetic field is further increased, saturation is reached again at $-M_s$. Reducing H to zero and then increasing it in the original direction brings the magnetization back to its saturation value, M_s. This way, the whole M *vs.* H hysteresis loop is obtained [2].

The B *vs.* H hysteresis loop is called the normal magnetization or normal induction curve that reflects the constant magnetic susceptibility after the saturation point is reached and does not saturate (Figure 1.1b). When H is decreased to zero, the induction decreases to B_r (called residual induction, or remanence) which is the same as the value of M_r. If the applied field is then reversed, the induction will decrease to zero when the negative applied field equals the coercivity, H_c. The H_c is lower than H_{ci}. The point where the product of B and H reaches its maximum value is called the maximum energy product, $(BH)_{max}$, which can be defined as an ability of a magnet to store the magnetostatic energy [1, 2]. Additionally, the Curie temperature (T_c) where a magnetic material loses its ferromagnetic properties is also an important parameter to be considered in different applications.

The magnet revolution has been brought, regarding the $(BH)_{max}$, for more than 100 years which is given by Figure 1.2a, from steels, ferrites, Alnico [aluminum-nickel-cobalt alloys, (Al–Ni–Co)] to rare-earth (RE) PMs [samarium-cobalt (Sm–Co) magnets and neodymium-iron-boron (Nd–Fe–B) magnets] [3, 4]. After the development of Kichizaemon Sumitomo (KS) steel in 1916, the progress of ferrite and Alnico is promoted, respectively. In the late 1960s, the development of hard magnetic materials has experienced a decisive jump, with the introduction of RE PMs. Driven by the growing demand for energy-efficient technologies in which PMs often play a pivotal part, the Nd–Fe–B PMs are developed to meet the need for maximized energy densities at various operating temperatures. It can be seen that the $(BH)_{max}$ of the Nd–Fe–B PMs has achieved a value almost 60 times of that of steels.

In 2016, the world market for PMs was reported with 85% ferrite, 13.5% Nd–Fe–B, 0.6% Sm–Co and 0.9% Alnico by weight, whereas with 33.9% ferrite, 61.0% Nd–Fe–B, 3.0% Sm–Co and 2.1% Alnico by value (Figure 1.2b) [5]. The common phases of ferrite are $BaFe_{12}O_{19}$ and $SrFe_{12}O_{19}$ with $(BH)_{max} < 38$ kJ m^{-3} [6]. They are cheap and relatively easy to produce, thus ferrite magnets have the largest share in terms of tonnage in the PM market. Additionally, ferrites also have very good resistance against corrosion, which makes them widely used in low-performance motor applications, sensors and other larger electronic devices. Alnico magnets have the smallest market share by both value and volume. Currently, they are being used mainly for specialized magnetic testing devices (e.g. spectrometers) which requires continuous tuning of the product. Due to their high thermal stability along with low H_c factor (inset of Figure 1.2a), they can be easily magnetized and demagnetized, making them suitable for such purposes [7]. In terms of value, two-thirds of the PMs are RE PMs. Among the RE PMs, Nd–Fe–B PMs have a clear domination over Sm–Co PMs by means of both value and weight shares. There are two different Sm–Co alloys which are being used: $SmCo_5$ and Sm_2Co_{17}. These PMs possess good H_c, high corrosion resistance and excellent thermal stability [8]. The $(BH)_{max}$ of Sm–Co magnets ranges between 120 and 260 kJ m^{-3} with the T_c of 720 °C, depending on the alloy composition [9-12]. Whereas Nd–Fe–B PMs consist of $Nd_2Fe_{14}B$ grains (matrix phase), surrounded by a Nd-rich grain boundary phase (GBP). The $(BH)_{max}$ of Nd–Fe–B PMs can reach 450 kJ m^{-3} commercially with the T_c of 312 °C [13, 14]. Beside the much lower energy density, Sm–Co PMs are much more expensive than the Nd–Fe–B PMs due to higher raw materials and manufacturing costs [15]. Furthermore, the production process for Sm–Co PMs is also more complex than that for Nd–Fe–B PMs. Additionally, Nd–Fe–B PMs can offer the smallest magnet volume under the same magnetic strength, enabling the design of the miniaturized devices, such as cameras, sensors and cell phones with high-energy

efficiencies [16]. As a result, Nd–Fe–B PMs are the inevitable option, especially for light-weight and high-performance applications.

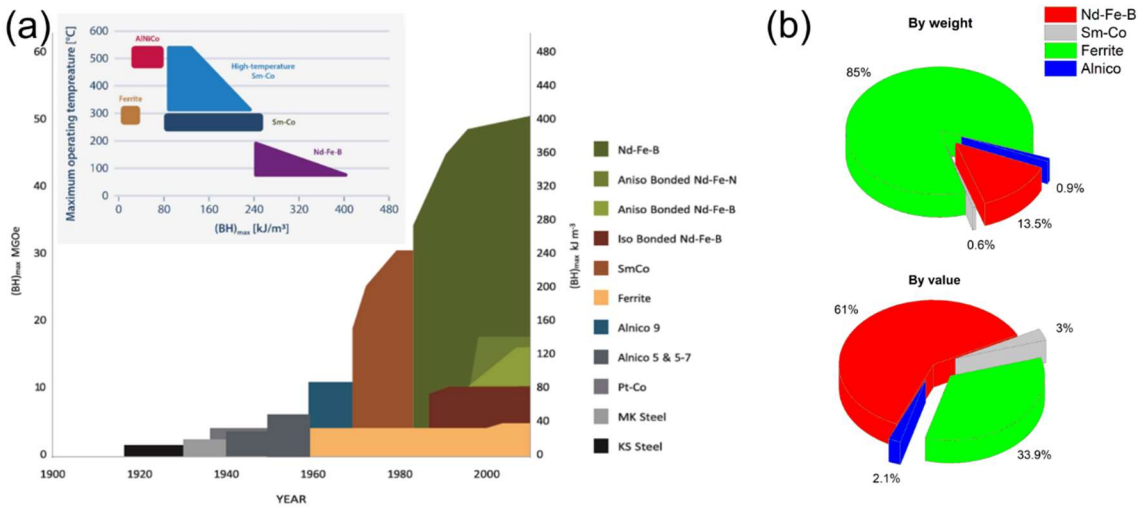

Figure 1.2: (a) Development of PMs over time with their maximum energy product, $(BH)_{max}$ [3, 4], (b) the world market share of PMs by weight (up) and by value (down) in 2016 [5].

1.2 Nd–Fe–B PMs and Their Applications

Currently, two types of the Nd–Fe–B PMs are commercially available, namely, sintered- and bonded-magnets based on the manufacturing routes. The classic powder metallurgy process for sintered-magnets and the rapid solidification process for bonded-magnets are shown in Figure 1.3 [17]. Sintered magnets are prepared by pulverizing a master alloy precursor (such as trademarked Neomax, $Nd_{15}Fe_{77}B_8$) produced by a strip casting method, followed by hydrogen decrepitation (HD) and jet milling to form microcrystalline size powders (typically 3–5 μm), continued by sintering the magnetically aligned powder into dense blocks, which are subsequently heat treated, cut to shape, surface treated, and magnetized. Bonded magnets are prepared by melt-spinning thin ribbons of the Nd–Fe–B alloy. The ribbon contains randomly oriented $Nd_2Fe_{14}B$ nano-scale grains. This ribbon is then pulverized into particles, mixed with a polymer such as polyolefin, latex or rubber, polypropylene (PP), polyethylene (PE), high density polyethylene (HDPE), polyamide, nitrile rubber or other elastomers, etc., and either compression or injection molded into bonded magnets. Although bonded magnets offer lower B_r values compared to sintered magnets due to the incorporation of non-magnetic polymers, they present several advantages such as lower weight and higher corrosion resistance with more complex geometries [18]. Nowadays, major applications for bonded Nd–Fe–B PMs are the spindle motor (used in hard disk drive, HDDs, and optical disk drives, ODD), stepper motors (used in printers, scanners, and similar equipment for very precise scanning and motion control on various medical devices and test equipment) and servo motors (used for motion control, particularly in application where precise position and speed control at high torque is required, such as machine tools, robotics, or electrical power steering systems) [19]. In 2014, the total production of the Nd–Fe–B PMs (sintered and bonded magnets) was estimated to be 79.5 kt [4], indicating a much larger market demand for sintered magnets than bonded ones (~10 kt, annually [17]). Thus, the main studies on manufacturing and recycling of the Nd–Fe–B PMs are focused on sintered ones.

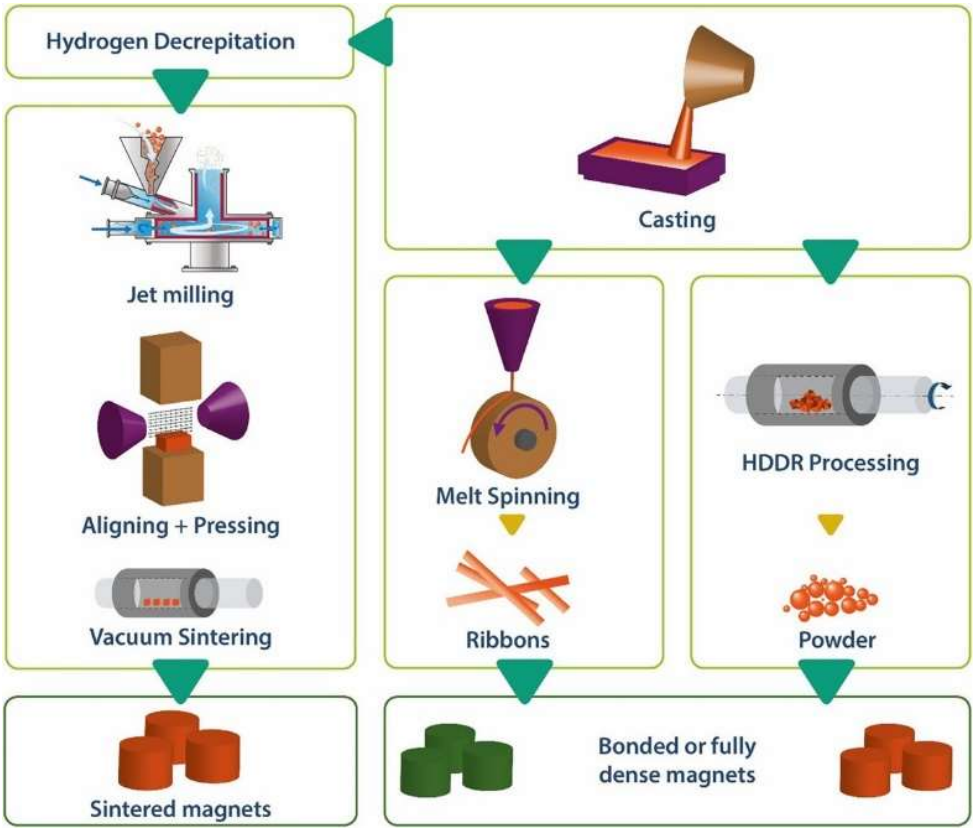

Figure 1.3: Manufacturing routes for the Nd–Fe–B PMs [17].

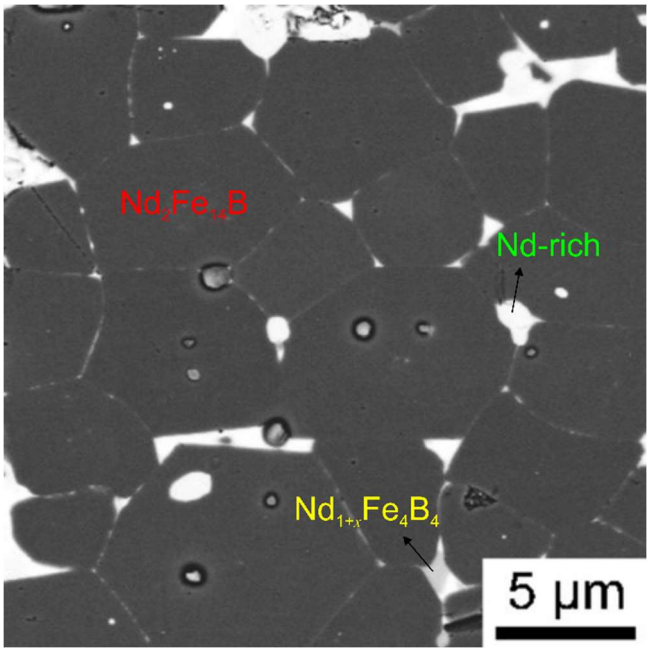

Figure 1.4: Backscattered electron image of the typical microstructure of a sintered Nd–Fe–B magnet [20].

For the sintered Nd–Fe–B PMs, typically, three equilibrium phases are formed: the hard magnetic matrix phase ($Nd_2Fe_{14}B$, 2:14:1 phase), the minor boride phase ($Nd_{1+x}Fe_4B_4$ where x is ~0.1) and the Nd-rich GBP [21] (Figure 1.4). Although sintered Nd–Fe–B PMs have a stronger magnetic strength due to the hard magnetic matrix phase, they are inferior to Sm–Co PMs regarding the resistance to oxidation and the T_c. Nd–Fe–B PMs start to lose too much of their magnetic strength if the working temperature is above 80 ℃ while they completely lose their magnetization at the working temperature above their T_c (310 ℃) for standard Nd–Fe–B alloys. Based on these facts, additives such as Dy, Tb, Gd, Nb, Co, Cu and Al are used during the magnet manufacturing process to modify some of the physical and magnetic properties to suit wide application needs. Small additions (1–8 wt.%) of Dy, Tb and Gd greatly enhance the magneto crystalline anisotropy and the H_c of the magnet by diffusing into the 2:14:1 phase, which dramatically increase the maximum operating temperature, but they also decrease the B_r and $(BH)_{max}$ due to the substitution of Nd [22-25]. Additionally, it has been observed that the amorphous Nd thin layers at the surface of the 2:14:1 grains are replaced by Dy, which plays an important role to improve the H_c in Nd–Fe–B PMs [26]. Nb is added for substitution of Fe to refine $Nd_2Fe_{14}B$ grains, resulting in a significant improvement of thermal stability and H_c [27, 28]. Co is added to increase the T_c by substitution of Co for Fe [29-31]. Cu and Al are added to improve the hot workability of the magnet alloy by forming Nd–Cu and Nd–Fe–Al eutectic alloys in the GBP which are also beneficial for corrosion resistance [32-35].

Sintered Nd–Fe–B PMs are widely used in many applications, such as industrial motors, wind turbines, sensors, magnetic resonance imaging (MRI), audios and hybrid/electric vehicles (H/EVs) (Figure 1.5) due to their high energy density [36]. Among these applications, production of HEVs and EVs is forecast to increase from 2.3 million units in 2016 to over 10.1 million units in 2026 [37], as nearly all major automotive manufacturers have developed HEV and EV models. This production growth is likely to drive a greatly increased demand for the sintered Nd–Fe–B PMs, because they are used in the powertrain in HEVs and EVs as well as in numerous other smaller applications, such as windscreen wiper motors and air conditioning systems, with up to 2.5 kg of the sintered Nd–Fe–B PMs being used in the powertrain of current models [38]. Additionally, in 2016, wind turbines were the second largest end-use applications for sintered Nd–Fe–B PMs behind consumer electronics, consuming around 8000 t of the sintered Nd–Fe–B PMs [38]. Global wind capacity is growing rapidly, with the Global Wind Energy Council (GWEC) forecasting cumulative capacity to grow by 8.8–10.6% per year through to 2022, reaching 840 GW [39]. Though figures vary by manufacturer and product, the direct-drive permanent magnet generator (DDPMG) design for wind turbines typically requires the largest volumes of the sintered Nd–Fe–B PMs at 500–700 kg/MW of installed capacity. Hybrid designs use much smaller amounts of the sintered Nd–Fe–B PMs, typically between 100 and 200 kg/MW of the installed capacity. Newer DDPMG technologies have become commercially available for large-size turbines, used mainly in offshore wind farms, which is expected to increase the volume of the sintered Nd–Fe–B PMs consumed per unit. It has been estimated that the sintered Nd–Fe–B PM consumption in the next 20 years will be driven by hybrid and electric vehicles and wind turbines, though the use of these magnets in other applications will support further demand growth [40].

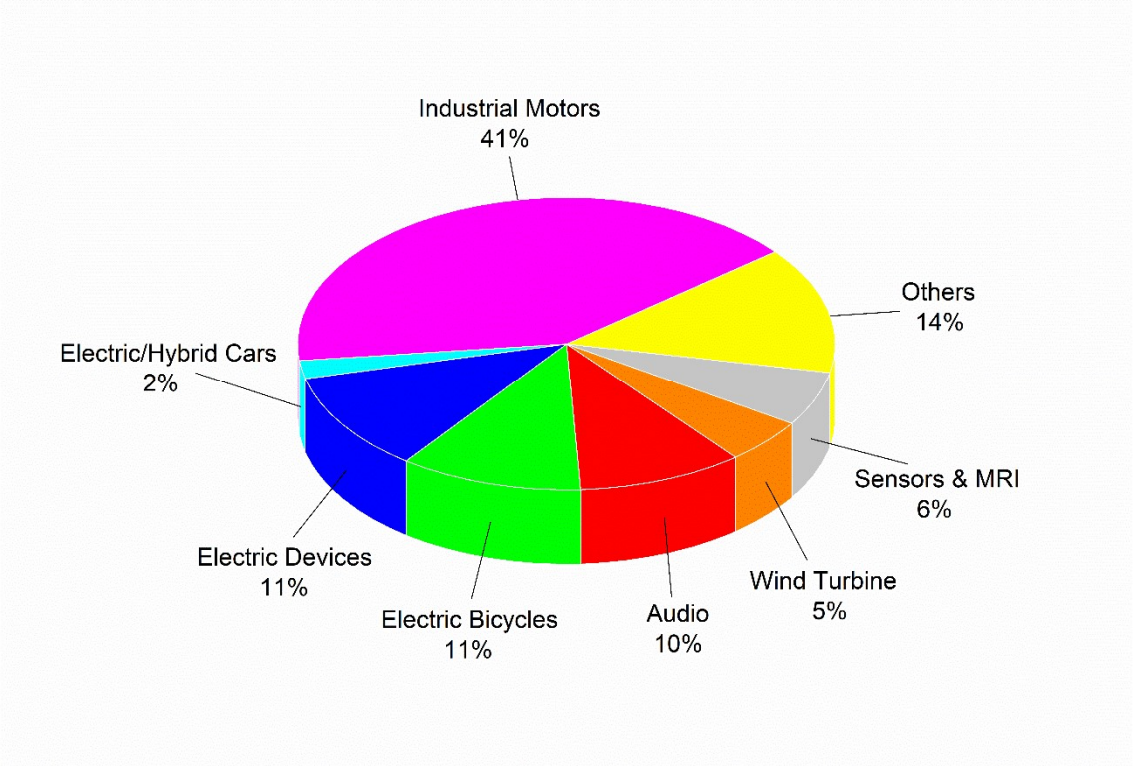

Figure 1.5: Shares of different applications in the global sintered Nd–Fe–B PM market in the year 2012 [36].

1.3 Recycling of the Sintered Nd–Fe–B PMs

Although, the chemical composition of the sintered Nd–Fe–B PMs varies from different applications. Generally, the sintered Nd–Fe–B PMs incorporate 20–30 wt.% of the rare-earth elements (REEs) that include mainly Nd with a small addition of Dy and/or Tb, they represent an important secondary REE resource [16]. Because primary mining of the REEs leads to a large environmental footprint associated with chemical usage and harmful emissions [41] and the REEs are considered the most critical based on their economic importance and supply risk [38]. Yet, despite their criticality, less than 1% of REEs are being recycled from End-of-Life (EoL) products, with the REE-containing PMs representing the largest share of these products [42]. Additionally, stricter laws, published on June 2018 by European Commission (EC), will mean that 70% of ferrous metals will have to be recycled by 2025 and, very importantly, producers will be responsible for their EoL products [43]. Therefore, the recycling of Nd–Fe–B PMs, especially sintered magnets, from the EoL products is now categorized as a "key enabling technology" [44, 45] with the prospect of positioning REEs within the circular economy.

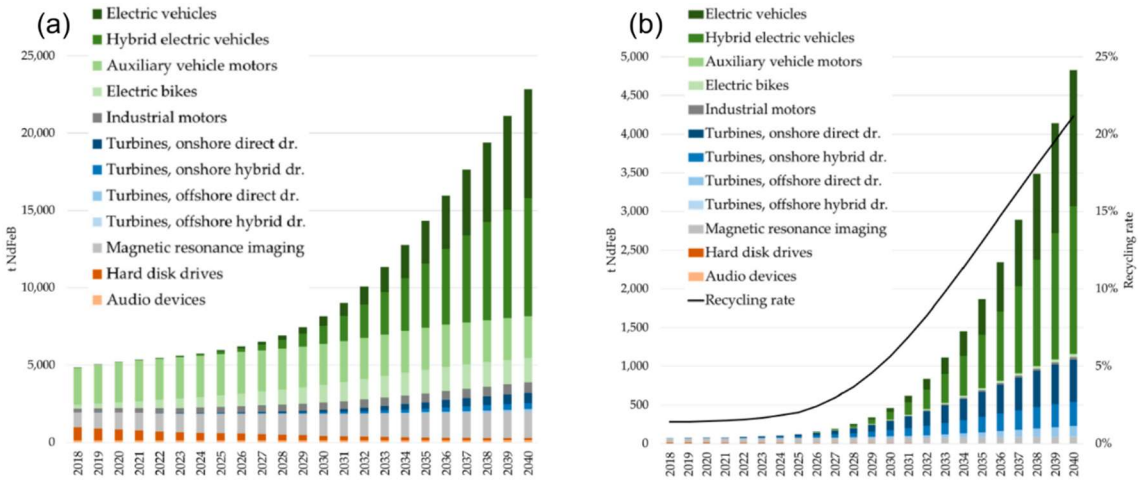

Figure 1.6: Estimation of (a) the theoretical and (b) realistic return flows by application in tons of the sintered Nd–Fe–B PMs and overall recycling rate [46].

The recycling chain of the sintered Nd–Fe–B magnets consists of the following steps: EoL products collection, magnet extraction, and recycling of the extracted magnets [47]. It should be noted that the term of "magnet scraps" is mixed in use for different magnet sources in the literature. In this thesis, the extracted Nd–Fe–B magnets from the EoL products are named as "EoL Nd–Fe–B magnet scraps". As the off-quality Nd–Fe–B magnets are inevitably generated in the manufacturing process, they are also called as "magnet scraps" in the literature [48, 49]. Here, the term "Nd–Fe–B magnet scraps" covers both the EoL Nd–Fe–B magnet scraps and the off-quality Nd–Fe–B magnets. Additionally, the wet Nd–Fe–B magnet sludge (a mixture of oil, machining chips, and other solid residue [50]) generated during the manufacturing process of cutting and polishing is termed as "Nd–Fe–B magnet swarf". Theoretically, the annual recycling potential of sintered Nd–Fe–B PMs increases slightly from 2018–2028 (Figure 1.6a) in the European Union (EU) [46]. From 2028 on, however, a sharp increase is expected due to the anticipated market penetration of H/EVs and e-bikes, with the share of wind turbines also expected to increase significantly from 2030 [46]. The total recycling potential for the EoL-sintered Nd–Fe–B PMs in the period 2018–2040 is estimated at 233 kt, corresponding to 66.6 kt of Nd and 7.9 kt Dy [46]. However, due to the fact that the extraction of magnets from the EoL products is not economic in most cases, the realistic recycling potential is predicted to be on a much lower level (Figure 1.6b) compared to the theoretical one. The annual recycling rate is predicted to increase from 1% to 21% of the theoretical potential from 2018–2040, with the overall recycling potential of about 25.7 kt of the sintered Nd–Fe–B PMs, corresponding to 7.1 kt Nd and 1.1 kt Dy. It must be noted that economic feasibility of the magnet extraction depends on the market prices for the Nd–Fe–B magnet scraps, which are strongly connected to the REE prices, and the extraction costs. Currently, in the EU, approximately 150 t of sintered Nd–Fe–B magnet scraps are collected and exported annually to China and Japan for metallurgical recycling, whereof about 40% originate from magnet production [40]. Whereas the production of the sintered Nd–Fe–B magnet scrap has been relatively constant in recent years [40]. Additionally, a large amount of the Nd–Fe–B magnet swarf that accounts for up to 30% of the total production is inevitably generated [51], which is, potentially, to be recycled. It has been estimated that a normal primary supply is unable to meet the forecast demand of Nd and Dy in their modelled demand scenarios by 2050. Although recycling is unlikely to close the wide gap between future demand and supply by 2050, in the long term, secondary supply from recycling can

meet almost 50% of the demand, i.e., by 2100 [52]. Nevertheless, high recycling potential of the sintered Nd–Fe–B magnet scraps and Nd–Fe–B magnet swarf proposes a strong demand for developing cost-effective and environmentally friendly recycling approaches in the upcoming years.

Table 1.1: Applications of the sintered Nd–Fe–B PMs and their average lifetime [46, 53, 54].

Application	Average magnet content	Estimated lifetime
Electric Vehicles	2500 g	15 years
Hybrid Electric Vehicles	1500 g	15 years
Auxiliary Vehicle Motors	175 g	15 years
Electric Bikes	270 g	15 years
Industrial Motors	--	15 years
Wind Turbines, Direct drive	650 kg/MW	>20 years
Wind Turbines, Hybrid drive	160 kg/MW	>20 years
Magnetic Resonance Imaging	2.5 t	10 years
Hard Disk Drives	5.67 g	10 years
Audio Devices	--	5–10 years

Table 1.2: Comparison of the theoretical potential and realistic returns of the sintered Nd–Fe–B PMs in tons accumulated from 2018 up to 2040 within the EU [46].

Application	Theoretical potential returns [t Nd–Fe–B]	Estimated realistic returns [t Nd–Fe–B]
Electric Vehicles	36336	7097 (28%)
Hybrid Electric Vehicles	49320	9140 (36%)
Auxiliary Vehicle Motors	60861	0 (0%)
Electric Bikes	23832	292 (1%)
Industrial Motors	10575	232 (1%)
Wind Turbines, Direct drive	5776	4678 (18%)
Wind Turbines, Hybrid drive	3066	2483 (10%)
Magnetic Resonance Imaging	31585	1579 (6%)
Hard Disk Drives	8704	174 (1%)
Audio Devices	2836	0 (0%)
Total	232891	2567 (100%)

Currently, the necessary recycling technology is not available at an industrial scale in Europe. It is simply cheaper to buy REE master alloys or newly manufactured magnets originated from primary resources than to reprocess the complex material from recycled resources [55, 56]. One of the main challenges for recycling of the sintered Nd–Fe–B PMs is the magnets extraction from the waste and EoL products, on which an emphasis should be laid in the future research and development. It should be noted that the sintered Nd–Fe–B PMs from mobility applications and wind turbines are more easily dismantled and physically concentrated due to their large contents (Table 1.1) and dominance in recycling

share in the upcoming future (Table 1.2), and even reuse of these large magnets is possible after refurbishing. For the recycling of the sintered Nd–Fe–B magnet scraps, diverse approaches are currently under development in Europe, which can be classified into: i) direct re-use, ii) alloys recovery, and iii) REEs recovery based on the form of the end-products.

1.3.1 Direct Re-Use Methods

The sintered Nd–Fe–B PMs are multi-phase materials: they have RE-rich GBP, which contain the vast majority of the oxygen (typically 300–400 ppm [47]), and represent about 10–12% of the magnet, while the $Nd_2Fe_{14}B$ matrix phase, which is practically oxygen-free, is 85–87% of the magnet [57]. Thus, a direct re-use of the magnets as a whole is currently regarded as the best route both ecologically and economically due to the minimum energy consumption in a very short loop without waste generation. This magnet-to-magnet route ends up with new magnets as the final products and is applicable only if the Nd–Fe–B magnet scraps are not highly contaminated and oxidized/corroded [58]. At present, large quantities of such magnets are not available practically, but the situation may possibly change from 2025 on according to Figure 1.6b where the recycling potential for wind turbines and H/EVs starts to increase.

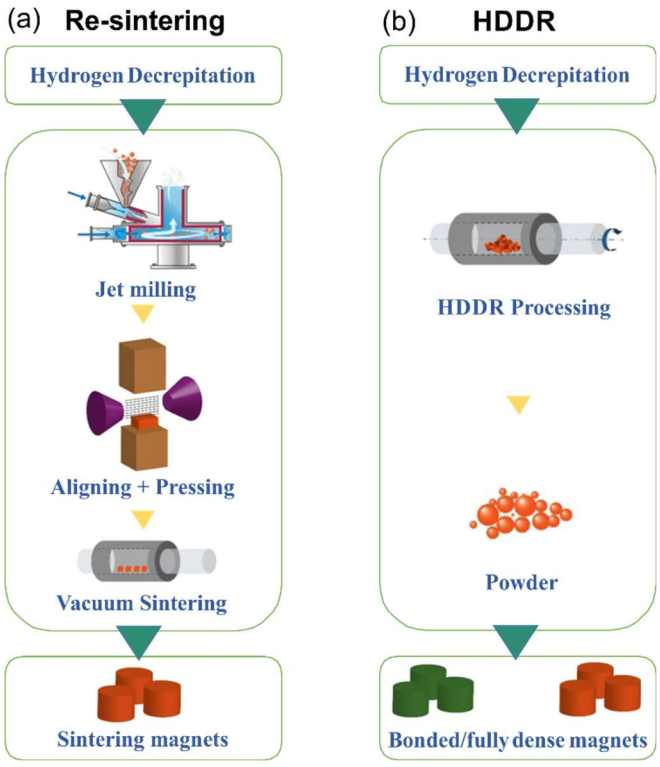

Figure 1.7: Recycling routes for the Nd–Fe–B PMs by (a) Re-sintering and (b) HDDR (the used images are rearranged based on [17]).

The direct re-use methods, including re-sintering (Figure 1.7a) and hydrogenation disproportionation desorption and recombination (HDDR, Figure 1.7b) are being developed. Generally, the Nd–Fe–B magnet scraps are pre-treated by HD process where hydrogen is absorbed into the magnet material and reacts with the intergranular GBP and $Nd_2Fe_{14}B$ matrix phase, resulting in their hydrogenation and consequent material pulverization due to the different volume expansions of the two phases [59]. The resulting

powder can be further processed via the same route for the production of a new magnet. It must be mentioned that HD process transforms the as-extracted magnets into an almost fully demagnetized powder for an easy separation of the magnetic fraction from the rest of the materials (corrosion protection layers or, depending on the device, the assembly where the magnet was fixed into) [60]. Taking into account the challenges in dismantling of the EoL products, HD provides an energy-efficient way to dismantle, demagnetize, and pulverize the magnets in one processing step.

However, the EoL Nd–Fe–B magnet scraps have a higher oxygen content (typically 2000–5000 ppm) compared to the virgin magnets (typically 300–400 ppm) [47]. This additional oxygen mainly takes place at the REE-rich, e.g., Nd-rich, GBP [61], because metallic REEs are preferentially oxidized to form rare-earth oxides (REOs) when exposed to air. Direct re-use methods recycle the EoL Nd–Fe–B magnet scraps without separation of REOs that causes problems. Due to the much higher melting temperature of these oxides compared to that of eutectic phase, e.g., metallic Nd-rich phase, they do not melt on re-sintering of the magnet scraps, resulting in reprocessed magnets lacking full density and exhibiting poor magnetic properties [62]. E. Herraiz et al. [63] recycled Nd–Fe–B magnet scraps from voice coil motors (VCM) using the HD processing and re-sintering route. The hydrogenated Nd–Fe–B powder was milled and re-sintered into new magnets at 1060 °C in the vacuum. However, the re-sintered Nd–Fe–B magnets showed a decrease in density, B_r, H_c and $(BH)_{max}$, in comparison to the starting material. The decrease in magnetic properties has been reported to be due to a loss of Nd-rich GBP as a result of oxidation. Alexandru Lixandru et al. [64] systematically investigated HDDR processing conditions for the recycling of the sintered Nd–Fe–B magnet scraps. The oxygen concentration was registered between 0.25 and 0.45 wt.% after the HDDR process, which was higher than that of the initial scrap between 0.09 and 0.26 wt.%. Furthermore, comparing the starting scrap magnets with the recycled magnets, recovery rates of ~90% in B_r and less than 80% of H_c recovery rate were achieved in the recycled HDDR magnets after the optimization of the HDDR process.

Due to the loss in the metallic REE and the increase of oxide phases in the GBP, powder blending of extra RE materials into the HD powder is a common technique to compensate for the existing REEs tied up with oxygen. Oliver Diehl et al. [65] added 2 wt.% NdH_2 to the recycled powder, inducing an increase in H_c of the recycled magnet of 9%, while remaining the same B_r as the starting scrap magnets. M. Zakotnik [66] used the GB modification technique by adding extra Dy in the range of 0.2–1.3 at.% resulting in an ~80% increase in H_c and ~6% decrease in B_r over starting material. It is clear that a higher oxygen level in the as-recycled magnet requires higher fresh REE consumption which then represents only a partial circular economy for the magnets. Furthermore, with the repeated recycling by direct re-use methods, the total volume of the non-ferromagnetic phases increases due to the addition of RE hydrides, which then reduces the saturation magnetization and therefore the B_r of the sintered Nd–Fe–B magnets. As a result, the sintered Nd–Fe–B magnets produced from the repeated recycling of materials by direct re-use methods tend to have poorer magnetic properties as the number of cycles increases.

1.3.2 RE Alloys Recovery

For recovering RE alloys from the sintered Nd–Fe–B magnet scraps, several processes are under investigation, such as re-melting-melt spinning, electro-slag refining and liquid metal extraction. These processes operate at 750–950 ℃ with the end-products of either the Nd–Fe–B master alloys that are ready for new magnets making, or transition metal (TM)-free RE alloys. They are applicable to almost all types of compositions but relative clean pieces.

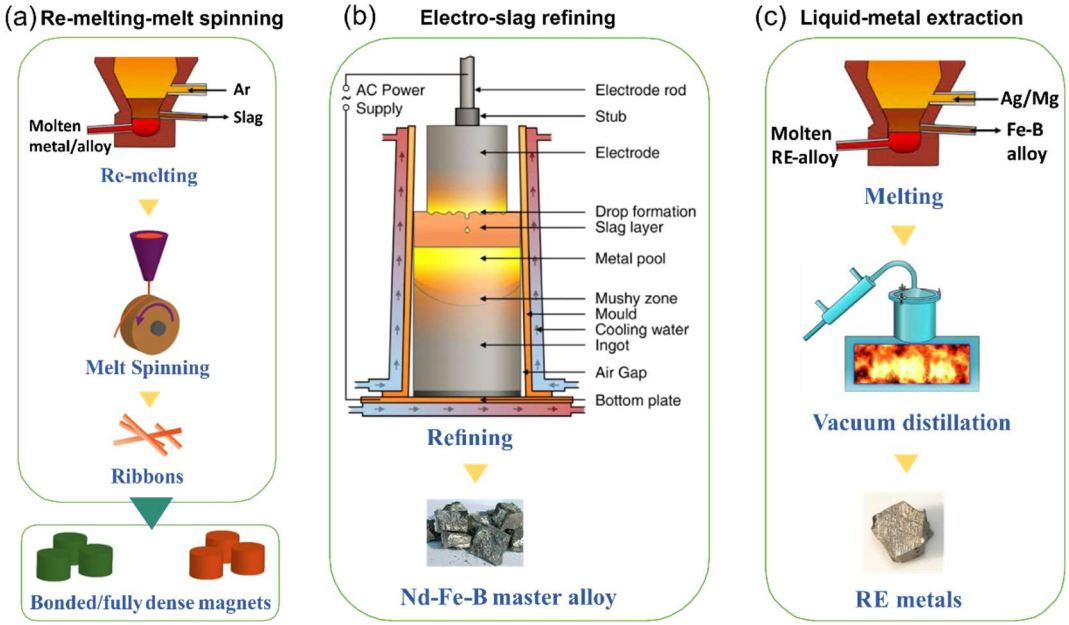

Figure 1.8: Recycling routes for the sintered Nd–Fe–B magnet scraps by (a) Re-melting-melt spinning, (b) Electro-slag refining, and (c) Liquid-metal extraction (the used images are rearranged based on [17] and Google search).

1.3.2.1 Re-Melting-Melt Spinning

Recycling sintered Nd–Fe–B magnet scraps by the re-melting-melt spinning route (Figure 1.8a) have the advantage of removing the oxides in the magnets. Generally, the magnet scraps are inductively melted and subsequently cast (melt spun) onto a water-cooled copper wheel with a high rotation speed (e.g., 30–40 m s^{-1}) [67]. The melt is rapidly solidified in the shape of flakes with cooling rates of up to 10^6 K s^{-1} during which a very fine structure (nanocrystalline or amorphous) is formed with typical grain sizes of 5–50 nm [68]. A compositional as well as microstructural optimization of the resulting flakes can be realized with the reduced oxygen content due to slag formation during melting [69, 70]. However, this energy-intensive process causes the loss of a significant amount of the REEs (around 20–30%) due to the strong affinity for oxide slags [65, 71].

1.3.2.2 Electro-Slag Refining

The electro-slag refining process (Figure 1.8b) utilises molten fluoride to extract and to separate REOs which become harmful for recycling when magnets are reproduced from EoL magnet scraps. In this process, molten fluorides like LiF-NdF_3 and LiF-DyF_3 are used as a flux and the REOs present in the Nd–Fe–B magnet scraps are extracted because the REOs dissolve in the molten fluoride flux to form REE oxyfluoride [72] which floats above the liquid alloys. Alloys that are refined by removing oxides have the oxygen content sharply reduced from 5000 ppm to less than 200 ppm by weight and are sufficiently low as the master alloy for magnets. This process is relatively simple and energy-saving to regenerate magnet alloys without oxidation, especially viable for large and clean sintered Nd–Fe–B magnet scraps, such as the broken magnets from manufacturing. However, it is not applicable to the magnet swarf with fine granules and high level of contaminations [49].

1.3.2.3 Liquid-Metal Extraction

The liquid-metal extraction (Figure 1.8c) is similar in principle to conventional low-temperature liquid-liquid solvent extraction. Liquid metals are used which can selectively dissolve the RE alloy and distribute RE metals and TMs between two immiscible liquid-metal phases. Several liquid systems including Mg–Nd and Ag–Nd were studied. In the Mg–Nd system, the high affinity of Nd for Mg causes Nd to rapidly diffuse out of the solid magnet scraps into the liquid Mg (melting point: 649 ℃) [73]. Nd is soluble in liquid Mg up to 65 at.% at 800 ℃ [74], whereas Fe is essentially insoluble (less than 0.035 at.% at 800 ℃) in molten Mg [75]. However, the theoretical extraction limit of Nd for the Mg–Nd system is 24–25 at.% [76]. The liquid Mg–Nd alloy can be separated from the Fe–B particles. Due to high vapor pressure of Mg (0.73 atm at 1300 K) and the very low vapor pressure of Nd (less than 10^{-6} atm at 1300 K) [77], Nd metal can be recovered from the alloy by vacuum distillation of Mg. The advantage of the Mg–Nd system is that Nd metal with up to 97.7% purity could be recovered directly from magnet scraps and the liquid-metal solvent can be recycled and the waste streams are kept to a minimum. However, this process is relatively slow (24–72 h) with high-energy costs during metal extraction and the Mg distillation steps. Furthermore, it cannot be applied to (partly) oxidized magnet scraps. Ag–Nd system was developed for the direct extraction of Nd from the sintered Nd–Fe–B magnet scraps, because Ag (melting point 962 ℃) dissolves Nd, but not Fe or B. Nd can be separated from the liquid alloy by oxidation of Nd to Nd_2O_3, which is insoluble in molten Ag [78]. Although Ag is more expensive than Mg, using Ag seems to be an interesting option for an industrial liquid-metal leaching process, because of the easy recyclability and re-use of the Ag metal. The extraction limit of Nd for the Ag–Nd system can reach 55 at.%. As the end product is a REO, the advantage of Ag–Nd system should be weighed, compared to the Mg–Nd system where a RE metal is finally obtained.

1.3.3 REEs Recovery

For the recovery of the REEs as raw materials, various approaches have been developed in recent years, which can be classified into glass-slag extraction, gas-phase extraction, and hydrometallurgical methods. The end-products are either RE halides (RE fluorides, REF_3 or RE chlorides, $RECl_3$) or REOs. These methods are applicable to both slightly and heavily oxidized magnet material with varied compositions.

1.3.3.1 Glass-Slag Extraction

The glass-slag extraction (Figure 1.9a) utilizes a molten flux to selectively extract REEs from the sintered Nd–Fe–B magnet scraps into a slag phase which can supercool to a glass. In this process, molten B_2O_3 (1377 ℃) is applied both as the oxidizing agent and the extraction medium in an Ar atmosphere. RE metals are selectively oxidised to REOs, leaving behind α-Fe and Fe_2B phases with the REEs (Nd, Dy and Pr) content of less than 0.01 wt.% [79]. The REEs are separated and concentrated through the formation of REOs-B_2O_3 melt, which contains 50 wt.% REOs and B_2O_3 melt (immiscibility gap). The REEs can be recovered from the glass slag by dissolving the glass slag in sulfuric acid (H_2SO_4), followed by selective precipitation of the REEs as sulfate double salts or hydroxides [80]. The REOs-B_2O_3 could also be leached with hydrochloric acid (HCl) and precipitated as REE oxalates. Although this method is suitable for the large-scale treatment of magnet scraps, it is energy-intensive and generates a lot of inorganic waste.

Bian et al. [81] improved this method by using FeO-B_2O_3 fluxes to increase the selectivity of Nd oxidation and separation of REEs from Fe. The FeO is selectively reduced to metal by the metallic Nd in molten flux due to its larger chemical potential compared

to B_2O_3 at the temperature of 1400–1550 K. The increasing temperature and prolonging holding time help the reduction of B_2O_3 contents in the oxide phase. However, the B was distributed in both oxide and metal phases that consequently formed $REBO_3$ in the oxide phase, which reduces the purity of the REOs. The extraction ratios of all REEs were more than 99.5 wt.%, and the purity of the REOs reached 98.4% when using $2FeO{\cdot}B_2O_3$ flux.

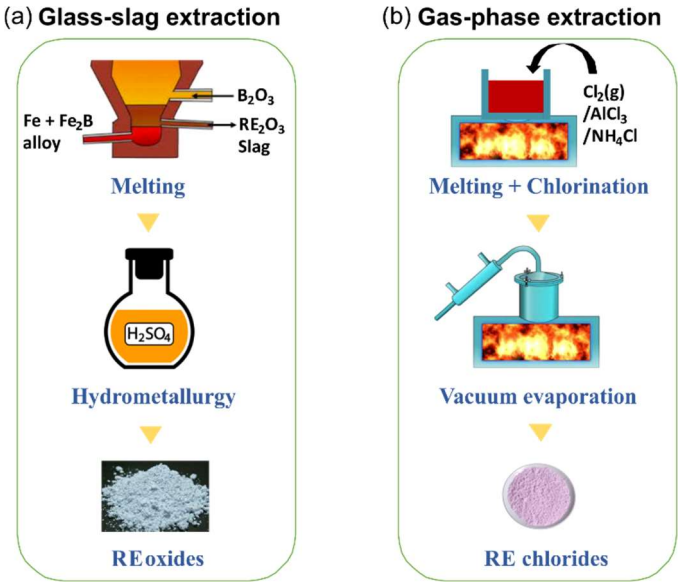

Figure 1.9: Recycling routes for the sintered Nd–Fe–B magnet scraps by (a) Re-sintering and (b) HDDR (the used images are rearranged based on Google search).

1.3.3.2 Gas-Phase Extraction

Gas-phase extraction (Figure 1.9b) is based on chemical vapor transport reactions that transform all the metals and oxides in the magnet scraps into volatile chlorides which can be separated based on differences in volatility. It is known that the $RECl_3$ form volatile chlorides with alkali metal chlorides (e.g., $KRECl_4$) and with aluminium chloride ($REAl_nCl_{3+3n}$(g) with $n = 1$–4) [82], leading to a huge increase in vapor pressure. Therefore, a stream of Cl_2 (chlorinating gas) in N_2 (carrier gas) with $AlCl_3$(g) is sent over the magnet scraps to completely chlorinate the oxides and metals to the corresponding volatile chlorides. The resulting gas-phase species are transported with the carrier gas to a tubular furnace with a temperature gradient where the metal chlorides are deposited and decomposed in the anhydrous metal chloride and $AlCl_3$ at different places in the reactor tube. The anhydrous $RECl_3$ are selectively concentrated at the temperature zone of 800–900 ℃ due to the lowest volatility. The Co and Ni chlorides are condensed at the temperature zone of 500–700 ℃ while the other TMs such as Fe, Cu, Al, etc. deposit at the last temperature zone of ≤ 350 ℃ of the furnace. Obviously, gas-phase chlorination requires relatively high temperatures and long reaction times. The $RECl_3$ have very similar volatilities, so mutual separation is not expected in the sublimation processes.

Due to the complete chlorination, more than 80% of Cl_2 gas is consumed for unwanted elements like Fe. Additionally, the $AlCl_3$ can be highly corrosive which hydrolyzes to form hydrogen chloride (HCl) gas, even with a minor amount of moisture. Therefore, selective chlorination of the magnet scraps was investigated. Selective chlorination in molten $FeCl_2$ bath combined with activated carbon addition via distillation was proposed by Uda et al. [83, 84]. Molten $FeCl_2$ acts as the reaction medium while carbon is added to convert NdOCl to $NdCl_3$. The $RECl_3$ are separated from the rest by vacuum distillation with REE yields

of ~76%. Shirayama et al. [85] utilised molten $MgCl_2$ to selectively convert REEs in the sintered Nd–Fe–B magnet scraps to $RECl_3$, leaving solid Fe–B alloy and impurity elements behind. Approximately 80% of Nd and Dy could be efficiently extracted as chloride following 12 h of reaction. Itoh et al. used NH_4Cl as the chlorination agent which easily chlorinated Nd and Nd_2O_3 to form $NdCl_3$. Although Both α-Fe and Fe_2O_3 were also chlorinated to generate $FeCl_2$, but with conversion rates of around 30 and 90%, respectively. The resultant $RECl_3$ with up to 90% yields could be consequently recovered by leaching the reacted solids with water.

1.3.3.3 Hydrometallurgical Methods

Recycling of the REE-based PMs is, traditionally, via hydrometallurgy where the whole magnet scraps are completely/partly dissolved in strong mineral acids, e.g., H_2SO_4 and HCl, and the REEs are selectively precipitated as sulfate double salts, e.g., (Nd, Na)$(SO_4)_2{\cdot}xH_2O$, oxalates or fluorides. Hydrometallurgical methods are applicable to both slightly and heavily oxidized magnet material with varied compositions. As the hydrometallurgical recycling of the sintered Nd–Fe–B magnet scraps is quite similar to the existing hydrometallurgical processing of ores for the REEs, the REE-rich leaching solutions can be injected into an existing REE separation plant after the removal of non-REEs [71]. The separated REOs or REF_3 by hydrometallurgical methods can be used in all REE-related applications apart from PMs.

Acid leaching is the most important step as it determines the extraction efficiency of valuable metals and their concentrations in the leachate as well as the selectivity against contaminants such as Fe that needs to be minimized during the REEs precipitation. Up to date, two different leaching routes are established: a complete leaching route and a selective leaching route.

Complete leaching. Complete leaching of the sintered Nd–Fe–B magnet scraps is conventionally realized in concentrated HCl, H_2SO_4 or HNO_3 solutions. The choice of acid mostly depends on the subsequent separation process: H_2SO_4 for selective precipitation and HCl for solvent extraction [86]. The usage of HNO_3 is normally avoided because it produces nitrated wastewater. H_2SO_4 solution (Figure 1.10a) is used to leach the sintered Nd–Fe–B magnet scraps due to the formation of REE sulfate followed by selectively precipitating neodymium-sodium sulfate double salt which could be converted into a variety of useful products, like REF_3 [87-89]. For treating 1 kg of the sintered Nd–Fe–B magnet scraps, 10 L of a 2 mol L^{-1} H_2SO_4 solution is required (solid-to-liquid (S:L) ratio of 10% w/v) which completely dissolves the magnet scraps and keeps the pH low enough to prevent precipitation of $Fe(OH)_3$. The pH is then raised to ~1.0 by NaOH, KOH or NH_4OH, at which a neodymium-(sodium or ammonium) sulfate double salt, $Nd_2(SO_4)_3{\cdot}M_2SO_4{\cdot}xH_2O$ or (Nd, M)$(SO_4)_2{\cdot}xH_2O$ (M = Na, K, NH_4) is formed. Fe remains in solution as long as the pH does not exceed 2.0. The RE sulfate double salt can be converted to either NdF_3 by leaching in hydrofluoric acid (HF) solution or Nd oxalate by adding an aqueous oxalic acid solution. The other REEs like Dy, Pr and Tb present in the scrap can also be recovered as the RE sulfate double salt and be converted into the REF_3 or RE oxalate. RE oxalate can then be calcined to form REOs. Both the REF_3 and REOs can be reduced to the corresponding RE metal (e.g., molten salt electrolysis [90]). After removal of the RE sulfate double salts, oxygen gas is bubbled or H_2O_2 solution is added to fully oxidize Fe^{2+} to Fe^{3+} that precipitates as yellow jarosite, $NaFe_3(SO_4)_2(OH)_6$, which is easier to filter than $Fe(OH)_3$.

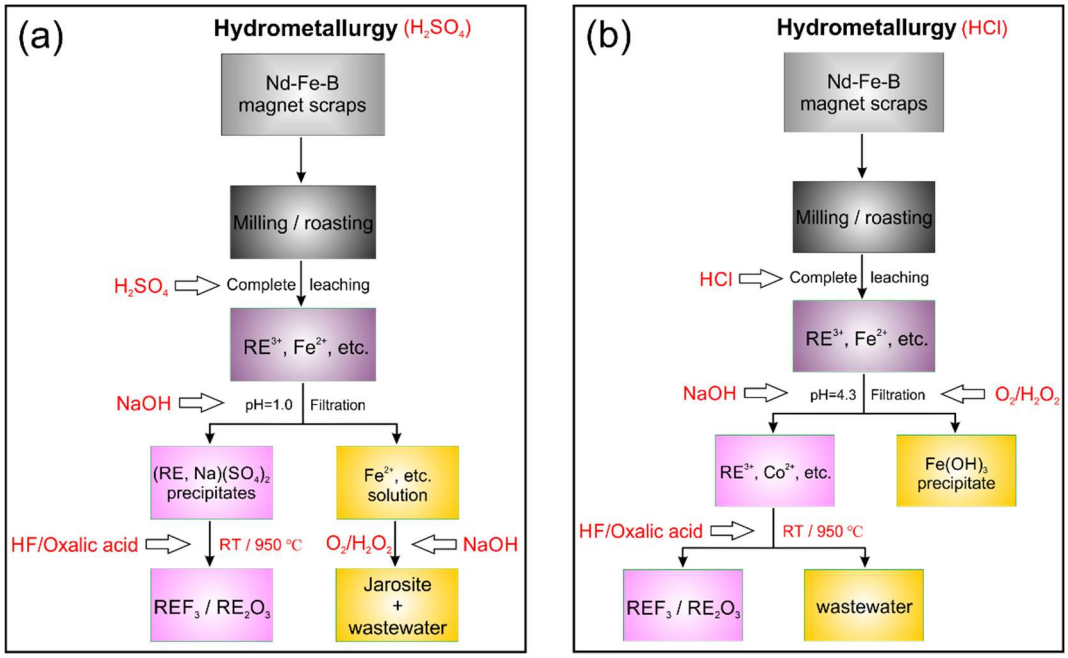

Figure 1.10: Recycling routes for the sintered Nd–Fe–B magnet scraps by hydrometallurgy using (a) H_2SO_4 and (b) HCl acid solution.

3–6 mol L^{-1} HCl solution (Figure 1.10b) with the S:L ratio of 10% w/v has been applied to completely dissolve sintered Nd–Fe–B magnet scraps [86, 91]. However, Fe leaches into the solution as Fe^{2+}, which is a stable species until a pH of 6.0 and cannot be selectively precipitated [44, 86]. Because REEs are traditionally precipitated as REE oxalates using oxalic acid, whereas iron(II) oxalates are highly insoluble [92]. On the other hand, Fe^{3+} undergoes hydrolysis and can be precipitated at a pH of 2.0 where the REEs remain as stable species in solution [93]. Therefore, the oxidation of Fe^{2+} to Fe^{3+} is required, generally by adding H_2O_2 solution as an oxidizer [91], as air oxidation of Fe^{2+} is kinetically sluggish below pH 7.0 [94]. After oxidation, the separation of Fe from other elements as precipitates (α- or/and β-FeO(OH)) can be achieved at pH 2.0–4.0 [92, 95]. The resulting solution after Fe removal is reacted with oxalic acid to form a precipitate that contains the REEs. The calcined precipitate forms REOs, which can then be returned to the initial manufacturing process for the Nd–Fe–B magnets or to any other RE-related applications.

Alternatively, the pre-treatment of the magnet scraps can be applied by an oxidative roasting at 500 to 950 ℃ to transform all Fe into Fe_2O_3, which would favor the Fe removal step after complete leaching process. It was found that the dissolution of Nd_2O_3 and Fe_2O_3 (oxidative roasting at 500 ℃) was much faster than direct leaching of the magnet using 2 mol L^{-1} H_2SO_4 solution [96]. However, it was also reported that a RE–Fe complex oxide, $NdFeO_3$, formed at high temperatures for a certain duration is more acid-resistant than the respective simple oxides (Nd_2O_3 and Fe_2O_3), suppressing the Nd extraction [97, 98]. Therefore, a prolonged leaching duration at elevated temperatures is required for the complete dissolution of this complex oxide with sufficient acid addition [99].

It has to be noted that unlike the fluoride precipitation for the REEs separation in the conventional hydrometallurgical process where NdF_3 is readily gelatinous and is, therefore, difficult to separate from solution by filtration [49]. The NdF_3 obtained from RE sulfate double salt is easy to filter which shows a significant advantage. Additionally, the solubility of RE sulfate double salts decreases with increasing temperatures which can be used for

high REEs recovery [100]. Because of this, the RE sulfate double salts are generally used for precipitation and storage of the REEs in the current industry [49].

Based on the whole recycling routes of hydrometallurgy, for the complete dissolution of 1000 kg of the sintered Nd–Fe–B magnet scraps, the required amount of H_2SO_4 is 2172 kg from which 272 kg is for Nd and 1900 kg is for Fe. Likewise, the required amount of HCl is 1622 kg, from which 202 kg is for Nd and 1420 kg is for Fe. Moreover, the consumption of base for Fe removal and effluent neutralization is correspondingly 1600 kg of NaOH or 1100 kg of CaO [101]. Additionally, due to the adverse impact of mineral acids on the environment, organic acids, e.g., acetic acid, citric acid et al., are also used and proved to be efficient for leaching Fe and Nd from ground scrap magnets [102, 103]. Organic acids are more easily degradable and less hazardous, compared to mineral acids, although longer leaching duration and higher working temperature are required.

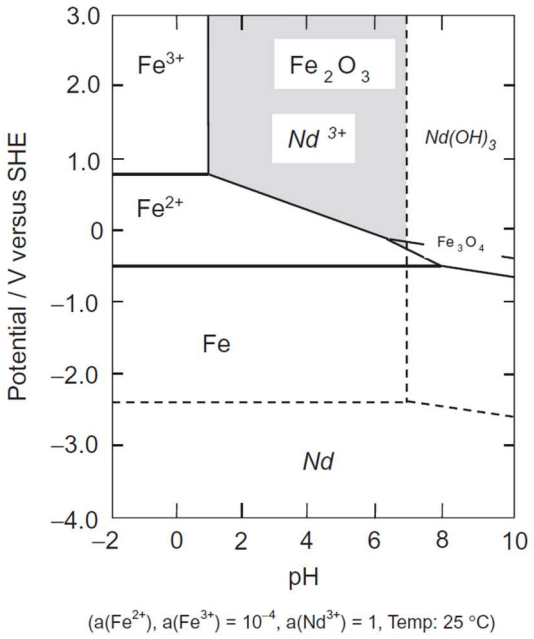

Figure 1.11: Potential-pH diagram of the Fe-H_2O and Nd-H_2O systems, where a(M^{n+}) is the activity of M^{n+} ion, (M = Fe and Nd) [101].

Selective leaching. Because the sintered Nd–Fe–B magnets consist of more than 60 wt.% of Fe which consumes the majority of the acid and alkali. A selective leaching of the REEs from the sintered Nd–Fe–B magnet scraps with reduced chemical usage is practically demanded. The basic principle of the selective leaching relies on the pH-dependent dissolution of the calcined material, which is called potential-pH diagram [101] shown in Figure 1.11. The stability region of Fe_2O_3 and Nd^{3+} at the pH 1.0–7.0 can be used, theoretically, to dissolve Nd^{3+} leaving Fe in the residue as Fe_2O_3. Koyama and Tanaka [104] reported that selective leaching was realized by using 0.02 mol L^{-1} HCl in an autoclave at 180 ℃ for 2 h after oxidatively roasting the magnet scrap at 900 ℃ for 6 h. More than 99% of REE recovery has been achieved with less than 5% of Fe extraction. On the contrary, more than 50% of Fe was leached without roasting, although more than 99% of the REEs were extracted. Selective leaching on roasted magnets at a lower temperature is also possible by increasing the initial acid concentration with prolonged etching duration (Table 1.3).

Table 1.3: Percentages of Nd, Dy, and Fe leached from the sintered Nd–Fe–B magnets after oxidative roasting [104].

HCl / mol L^{-1}	Nd / %	Dy / %	Fe / %
0.001	15.8	13.1	1.2
0.01	96.4	96.1	14.0
0.1	> 99	> 99	> 99

Leaching was done at 60 ℃ for 24 h.

Solvent extraction. After the acid leaching step, precipitation of the REEs is the easiest route to recover dissolved REEs. However, due to the similar chemical behavior of the REEs, the precipitates are separated as mixed REE compounds that have low commercial value [105, 106]. Therefore, individual separation of the REEs is desirable. Solvent extraction allows for excellent intragroup separation of the REEs, which is promising for large-scale industrial applications [107]. It is based on the formation of complexes between ligand molecules soluble in an organic phase and ions present in an aqueous phase and the transfer of these complexes to the immiscible organic phase. Individual separation is possible due to the decrease in ionic radii along with the lanthanide series, also known as lanthanide contraction. Heavier elements create stronger complexes than the lighter ones, facilitating their separation [53]. It must be noted that the separation of individual REEs requires a large number of separation stages to achieve very high purity, and thus is economically challenging. REEs recovery via solvent extraction can be done with leachates obtained after the total dissolution of magnets (Fe is present in the solution along with the REEs) and after selective leaching (no Fe is present in the aqueous phase). Typically, solvent extraction is followed by precipitation to recover the product(s) in solid form.

The most common ligands for industrial solvent extraction of the REEs are commercial organophosphorus compounds, such as the *bis*-(2-ethylhexyl)-phosphoric acid (D2EHPA). Before using D2EHPA for solvent extraction, Fe removal from the leachates is required. It has been reported that D2EHPA was used on a H_2SO_4-leachate containing Nd, Dy, Pr, Gd, Co and B with an initial pH of 5.2 [108]. Extraction equilibrium with 0.6 mol L^{-1} D2EHPA was reached within 5 min in cyclohexanone and 1-octanol. Equilibrium was achieved within 3 min using aliphatic diluents, hexane, octane, and kerosene which were most suitable for the REE separation. The REEs were completely extracted as a group using 0.9 mol L^{-1} or 1.2 mol L^{-1} D2EHPA in either octane or hexane without B or Co extraction. The separation of heavy REEs from the light REEs was achieved using 0.3 mol L^{-1} D2EHPA in hexane, without measurable B or Co extraction. The complete stripping of the REEs from the loaded organic phases was possible by using > 2 mol L^{-1} HCl solutions. Partially saponified 2-ethylhexyl-2-ethylhexyl-phosphonic acid (PC-88A) was used to separate REEs from the magnet chloride leachate after removal of Fe and Co with NaOH and NaHS, respectively [109]. Separation of the light REEs from heavy REEs was successfully realized with 1 mol L^{-1} PC-88A in kerosene, although no separation of Pr from Nd and of Dy from Tb, respectively, was carried out. Extraction of the REEs from magnet-scrap sulfate leachates with PC-88A was also reported [110]. A comparative study [111] of PC-88A and D2EHPA for the REEs recovery concluded that either extractant dissolved in kerosene is feasible to recover the REEs with high efficiencies. Mineral acids can be used to strip the metals from the loaded organic phase with the order of stripping efficiency being hydrochloric > nitric > sulfuric for D2EHPA and nitric > sulfuric > hydrochloric for PC-88A. Other extractants that have attracted a lot of interest for separation of the REEs are Tricaprylmethylammonium nitrate ([A336][NO_3]) [112, 113], *bis*(2,4,4-trimethylpentyl)

phosphinic acid (Cyanex 272) [114], Tri-octyl-phosphine oxide (Cyanex 921) [115] and Tri-iso-octyl-amine (Alamine 308) [116]. The combination of two extractants or one extractant with one ionic liquid (IL) generally gives a better synergy [117].

The magnet leachates without Fe removal were also investigated by solvent extraction. Tetraoctyl diglycol amide (TODGA) showed high selectivity for the REEs over Fe in nitrate media using the aliphatic diluents [118]. The impurity elements generally did not exceed distribution ratios of > 0.1 with very efficient stripping of the REEs (>96%) by using water. David Dupont and Koen Binnemans used the carboxyl-functionalised IL, betainium *bis*(trifluoromethylsulfonyl)imide ([Hbet][Tf_2N]) to leach the roasted magnet and simultaneously separate REEs from other elements [119]. [Hbet][Tf_2N]-H_2O system is a special thermomorphic leaching system that homogeneously leaches roasted magnet at 80 ℃ while selectively extracts Fe^{3+} in the IL phase (organic phase) at room temperature. The REEs were stripped out by adding oxalic acid with a purity above 99.9 wt.%. The [Hbet][Tf_2N] was regenerated by stripping Fe using oxalic acid. A similar study using Trihexyl(tetradecyl)phosphonium chloride (Cyphos® IL 101) to extract Fe in the organic phase while leaving REEs in the aqueous phase is also reported [120]. The separation factor for Nd/Fe was 5.0×10^6 in a 9 mol L^{-1} HCl solution by forming stable anionic chloro complexes. For separation of the REEs by ILs, the focus is on the use of hydrophobic ILs with nonfluorinated anions (chloride or nitrate). By increasing the alkyl chain lengths on the cation, the ILs can be made hydrophobic (immiscible with water) without the need of using hydrophobic fluorinated anions. The separation of the REEs is realized by re-distributing the REEs and TMs into two immiscible phases. The stripped REEs can be further separated individually using D2EHPA or PC-88A.

1.3.4 Electrochemical Recycling Processes

Electrochemistry is an integral part of recycling metals and is often used to recover metals. Electrochemical processes transport electrons from the anode (oxidation reactions) to the cathode (reduction reactions) by applying voltage between the two/three electrodes. Therefore, recycling of the sintered Nd–Fe–B magnet scraps through etching or even complete leaching could be done via oxidation reactions on the anode, while on the cathode, metals or alloys are deposited simultaneously.

1.3.4.1 Electrochemical Recovery of the RE Metals/Alloys in Molten Salts

Due to the variation of the electrochemical potential of Nd (–2.32 V *vs.* standard hydrogen electrode, SHE), Fe (–0.447 V *vs.* SHE) and B (–0.89 V *vs.* SHE) [121], the REEs can be, theoretically, leached away selectively through electrochemical anodization by controlling the potential and maintaining it in the region between dissolution of the REEs and the region in which metallic Fe, B, and other elements are stable or immune.

Y. Kamimoto et al. [122] investigated the electrochemical leaching behaviors of various elements of the sintered Nd–Fe–B magnet scraps in 59 mol% LiCl + 41 mol% KCl molten bath at 723 K (Figure 1.12a). The use of potentiostatic electrolysis enabled selective leaching of the REEs from the magnet in the potential range from –1.8 to –0.8 V (*vs.* Ag/AgCl). Control of the oxidation potential enabled control of the oxidation stage during potentiostatic electrolysis. In the first stage, the REEs were leached from the GBP of the magnets. In the second stage, the REEs were leached from the interior of the $Nd_2Fe_{14}B$ matrix phase. Although the estimated leaching ratio of the REEs was approximately 90% at –1.0 V, the leaching ratio of Fe and the cathodic deposit, as well as the energy consumption, were not specified.

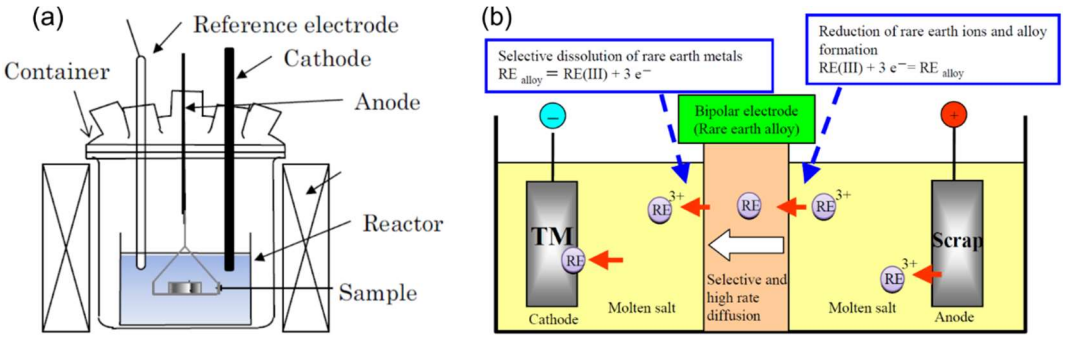

Figure 1.12: Schematic drawing of (a) selective leaching of the REEs using a sintered Nd–Fe–B magnet scrap as the anode in molten salts [122] and (b) the process for separation and recovery of the REEs using a bipolar electrode [123].

T. Oishi [123] proposed a new process based on an alloy diaphragm in a molten salt. A RE–TM alloy is used as the diaphragm, which functions as a bipolar electrode and enables selective "permeation" of the REE ions (RE^{3+}) (Figure 1.12b). The RE metals or alloys are recovered via the following steps: (i) a REE-containing material like the sintered Nd–Fe–B magnet scrap is used as the anode and the RE metals are selectively dissolved into the melt as ions, (ii) the dissolved RE^{3+} are reduced on the anode side surface of the diaphragm and the REE atoms diffuse through the diaphragm, (iii) the REE atoms are dissolved from the cathode side surface of the diaphragm as ions, and (iv) REE is finally recovered as a metal or an alloy on the cathode by reduction of the dissolved RE^{3+}. The RE^{3+} remaining in the anode room can be collected by electrolysis using another cathode in the anode room. Almost all impurities remain in the anode room as residue or anode slime. This process potentially enables the recovery of highly pure RE materials or even allows the selective recovery of the RE metals like Dy from the sintered Nd–Fe–B magnet scraps because of the high selectivity during the alloying step on the anode side surface of the diaphragm, as Konishi et al. [124] showed using a molten chloride. On the other hand, some technical problems still remain unresolved. These include low mechanical strength of the RE–TM alloys and difficulties in maintaining the alloy diaphragm at an appropriate composition. Thus, further investigations are necessary to establish whether this process is applicable to commercial use.

Additionally, the microstructure of the sintered Nd–Fe–B PMs directly influences the corresponding dissolution mechanisms. Generally, the sintered Nd–Fe–B PMs consist of $Nd_2Fe_{14}B$ grains (matrix phase), surrounded by a Nd-rich phase and a B-rich phase in the GBP [125]. It has been proposed [126, 127] that Nd-rich phases corrode preferentially because of the negative standard reduction potential of REEs, followed by the B-rich phase dissolution which can even result in pulverization of the magnet [128]. This provides a theoretical support for selective recovery of the $Nd_2Fe_{14}B$ grains from the sintered Nd–Fe–B magnet scraps.

1.3.4.2 Electrochemical Recovery of the REEs in Aqueous Solutions

Theoretically, the sintered Nd–Fe–B PMs can be anodized on the anode and dissolve into the electrolyte without using extra acid, this offers an alternative to recover the REEs from the electrolyte with the highest possible purity by conventional hydrometallurgy in a more environmentally friendly way.

A patent for processing the Nd–Fe–B magnet slag [129] claimed that a complete leaching of the magnet slag filled in a plating barrel as an anode and a simultaneous Fe

refining by cathodic deposition could be achieved in a sulfamic acid bath with an applied current density of 50 A dm^{-2}. The Nd- and Fe-containing leachate was obtained, followed by the addition of HF solution to precipitate Nd out as NdF_3. The remaining solution was sent back to the electrolysis tank for further electro-refining. However, both Fe^{3+} and Fe^{2+} can precipitate as FeF_3 [130] and FeF_2 [131] by adding HF due to their low solubility. Consequently, NdF_3 was precipitated without selectivity as a mixture of NdF_3, FeF_3 and FeF_2. Further purification of NdF_3 from the fluoride mixture was not described in the patent. Therefore, selective precipitation of Nd from the Nd- and Fe-containing leachate still needs further investigation.

Recently, Prakash Venkatesan et al. [132], developed an electrochemical recycling process to selectively extract REEs from the sintered Nd–Fe–B magnet scraps at room temperature. The sintered Nd–Fe–B magnet scrap was used as the anode to convert the elements present in the magnet scraps into the respective hydroxides. More than 97% of the REEs leached into the solution with HCl, leaving the Fe in the residue. The REEs were recovered using oxalic acid, followed by calcination to obtain REOs with high purity (99.2%). The electrochemical process precipitated > 90% of the Fe in the form of akaganeite (FeOOH) with the extra electricity consumed to convert the Fe^{2+} to Fe^{3+}. The resulting leachate in the form of wastewater could not be recycled because of the high concentration of oxalic acid remained in the solution after REE precipitation that would result in non-selective precipitation of REEs and Fe in the next batch if this oxalic acid-containing solution would be re-used. This electrolysis process is advantageous, as the leaching of the magnet scraps and the oxidation of Fe^{2+} to Fe^{3+} were done simultaneously in one step. The electrochemical conversion of Fe^{2+} to Fe^{3+} is more efficient than that of the conventional hydrometallurgical process. The whole process required an acceptable energy consumption of 3.0 kWh/kg of the sintered Nd–Fe–B magnet scraps.

1.3.4.3 RE–TM Recovery by Electrodeposition

Electrodeposition of Nd–Fe in an alloy form can be a promising alternative to RE alloy recycling route and could act as an alternative of direct PMs synthesis method. Electrodeposition is an attractive process, as it possesses many advantages such as low cost and easily maintained equipment, great flexibility, with the possibility to tailor properties to a specific application based on the composition of the solution and the operating conditions [133]. More importantly, electrodeposition enables to produce RE–TM-based magnets as thin films in micron- or even nano-size on substrates that cannot be done by the current powder-metallurgy route which typically produces magnets in millimeters or centimeters.

Currently, two categories of electrolyte are being used for electrodeposition of metals and alloys: aqueous electrolytes and non-aqueous electrolytes. Aqueous electrolytes generally contain water (as a solvent), a conductive salt, target metal salts (solutes) and some additives in dependence of the targeted application (surfactants, brighteners and so on). The advantages of these electrolytes are high solubility for metal salts, high conductivity and low viscosity. Because of the low capital investment and simplicity, metal deposition (electrodeposition or electroplating) in aqueous electrolytes has been extensively investigated [134]. The REEs commonly have a very negative reduction potential (< –2.3 V *vs.* SHE [135]), making them very difficult to deposit in a metallic form. Therefore, using aqueous solution to deposit RE-related alloys is very challenging with regards to the occurrence of the hydrogen evolution ($2H^+ + 2e^- \rightarrow H_2$, $\varphi^\theta = 0$ V *vs.* SHE) during electrolysis, a narrow electrochemical window ($2H_2O + 4e^- \rightarrow 2OH^- + H_2$, $\varphi^\theta = -0.828$ V *vs.* SHE) and low thermal stability of aqueous solutions [136]. At the potential necessary to reduce Nd, strong liberation of hydrogen and a consequent increase in pH would take

place at the interface. Nd^{3+} would hydrolyse at pH >7 [137] and in addition, Nd may interact strongly with hydroxyl ions. This phenomenon would favor the formation and incorporation of Nd oxide or hydroxide instead of Nd metal [138]. It is a fact that individual deposition of pure Nd from an aqueous solution is extremely difficult, even impossible. However, the electrodeposition of the REEs with the elements such as Fe, Ni or Co in the form of films from aqueous solutions has been reported [133, 139, 140], although the metallic state of these films has not yet been confirmed. This electrodeposition phenomenon is called "induced co-deposition" or "anomalous co-deposition" which suggests that the electrodeposition of the REEs from non-aqueous solvents together with the TMs might offer a promising alternative [141].

Non-aqueous electrolytes can be classified into three groups: molten salts, deep eutectic solvents (DESs) and ILs, based on the difference in working temperatures of electrodeposition. A classical molten salt electrolyte is obtained by melting or liquifying one or more metal salts through heating (450–1025 ℃), to counterbalance the salt(s) lattice energy. Such a solution consists of ions and their combinations and is free of any solvent molecules. Therefore, molten salts can function as solvents with good heat capacity (red heat, > 700 ℃) and high conductivity. The most common molten systems are LiCl-KCl [142], NaCl-KCl [143] and LiF-CaF_2 [144], but also other mixtures are used and investigated [136]. Molten salt electrolysis enables a continuous operation, and therefore it is suitable for mass production of many refractory metals. For making RE metals by electrolysis in molten salts, the common RE salts are REF_3 mixed with REOs, using an inert cathode like W or Mo, et al. and graphite as the sacrificial anode [90, 145]. For making RE–TM alloys, TM metals, e.g., Fe and Ni, are used as the cathode instead [146, 147]. Additionally, the regeneration of spent salts is not required in the electrolysis process [148]. Molten salt electrolysis is advantageous because it allows the simultaneous extraction and separation of metals/alloys based on their eletrochemical potentials. The existing limitation on the cell design and understanding of molten salt's behavior and optimal conditions are some of the aspects that still need to be further studied. Additionally, one big problem of molten salt electrolysis is the high-energy consumption which leads to large running costs.

A salt dissolved in a molecular solvent (generally, organic) at near ambient temperature is DES. One of the most widely used components for formation of DES is choline chloride. In combination with safe hydrogen bond donors, such as urea, carboxylic acid (e.g. oxalic, citric or amino acid) or polyols (e.g. glycerol or carbohydrates), choline chloride is capable of rapidly forming a DES [149]. Generally, DESs are liquids at a temperature lower than 150 ℃ and most of them are liquids between room temperature and 70 ℃. The electrochemical windows of DESs are around 2.5 V (varying on the substrates) with viscosities which can reach as low as 19 cP (*vs.* water, 1 cP [150]) at 20 ℃ [151, 152]. There are literature reports about the electrodeposition of the RE–TM using DESs [153-155], and organic solvents [156]. However, here the organic chemicals are generally volatile, casting doubt on the environmental credentials of the process.

ILs are generally defined as those salts composed solely of ions (cations and anions) with melting points below 100 ℃ [157]. A typical IL contains a large organic cation as well as an inorganic or an organic anion. This highly asymmetric structure makes it difficult for the cations and anions to stack closely with each other, thus effectively prohibiting IL's crystallization and lowering its melting point [158]. Salts having a low melting point are liquids at room temperature, or even lower, and form a new class of liquids usually called room-temperature ionic liquids (RTILs). One of the most important properties of ILs is the extremely high electrochemical stability, of which cathodic limit can be as negative as –3.3 V *vs.* Fc/Fc^+ (Fc: ferrocene, $Fe(C_5H_5)_2$), while the anodic limit can be as positive as +5.4 V *vs.* Li/Li^+ [159]. Therefore, almost all the metal elements in the periodic table are theoretically possible to be reduced or oxidized electrochemically within this window. In

fact, the electrodeposition of Nd using imidazolium and phosphonium-based ILs was reported [160-163]. However, the oxygen contents up to 50 at.% in the deposits make these materials of little practical value. To confirm the valence state of the deposited REEs, such as Nd, X-ray photoelectron spectroscopy (XPS) was used in these earlier studies. However, the binding energies of metallic Nd (Nd^0) and Nd oxide (Nd_2O_3) are very close, i.e., 980.5–981.5 eV and 981.7–982.3 eV, respectively, making it almost impossible to differentiate between the two states [164]. Sophisticated methods to characterize the RE-containing deposit on chemical composition, crystallography and valence state are strongly needed. Furthermore, the availability of literature describing electrochemical co-deposition of the RE–TM using ILs is quite limited. Therefore, finding a stable electrolyte system with high ionic conductivity and wide electrochemical window and avoiding the oxidation of the deposit will be critically required to recycle the sintered Nd–Fe–B PMs in alloy forms.

Additionally, a deep understanding of the mechanism for the co-deposition of the RE–TM, so far, has not been reported. It is well known that some elements with negative electrochemical standard potentials cannot be electrodeposited in metallic form from aqueous solutions, but they can be co-deposited with TMs, forming alloys [165]. For example, metallic tungsten cannot be deposited alone from an aqueous solution, but it does deposit in the presence of $Fe^{2+/3+}$ in solution, forming metallic alloys [166-168]. For Fe–W co-deposition, catalytic mechanisms induced by adsorbed species such as hydrogen (H_{ad}) or the adsorbed TM (TM_{ad}) are proposed [169, 170]. A "catalytic reduction" theory was proposed by Holt and Vaaler [171] to explain the reduction of aqueous tungstate solutions in the presence of zero-valence TM elements (i.e., Ni, Co and Fe). Another mechanism, proposed by Clark and Lietzke [172], emphasizes the role of hydrogen, where there is an initial deposition of a partially reduced tungstate film on the cathode, followed by the catalytic reduction of this film by hydrogen in the presence of freshly deposited Fe, Co, or Ni. The third mechanism is based on the formation of TM tungstate complexes that are precursors to tungsten alloys, as introduced by Younes-Metzler et al. [173] In this concept mixed-metal soluble complexes were used by adding a complexing regent of citrate [166] or gluconate [174] as a prerequisite for the TM–W co-deposition. The latter two mechanisms rely on active hydrogen produced by the electrolysis of water and the formation of TM–tungstate coordination compounds with certain complexing reagents that help realize the co-deposition process. The "catalytic reduction" theory opens a way to further investigate the co-deposition of the RE–TM in both aqueous and non-aqueous solutions.

1.4 Summary of the Literature Review

To summarize the literature survey of the sintered Nd–Fe–B PMs recycling, diverse approaches are being developed and used for different purposes with regards to final product application. To make new PMs as the final products using recycled materials, the direct re-use methods are generally considered as the most ecological and economical route. However, the direct re-use methods cannot separate the REOs and thus result in an unsustainable recycling problem. Alternatively, RE alloys recovery can be considered as a promising route. Currently, the re-melting-melt spinning method and electro-slag refining method are able to remove REOs, realizing the RE alloys recycling. However, these methods operate at high temperatures leading to 10–30 wt.% of REEs loss. Separating the RE alloys and the REOs under a mild temperature will reduce the energy consumption and REEs loss that makes it more cost-effective. Although the liquid-metal extraction method requires a long processing duration and a large energy input, the recovered RE metals are valuable and can be used for other applications, apart from PMs.

REEs recycling in ionic forms (REOs or $RECl_3$) as the end products by glass-slag methods and gas-phase extraction generally requires medium to high temperatures for prolonged durations along with the use of non-recyclable and/or unstable chemicals, which has huge environmental impacts. Hydrometallurgical methods based on strong mineral acid leaching are indispensable as they can deal with all types of magnets with a different composition and oxidation state. Especially the magnet swarf generated from cutting, polishing processes are mixing with water as sludge. REE-containing oxides produced from glass-slag recycling process and re-melt spinning recycling process need to be treated further. The magnet swarf and REE-containing oxides can be processed mainly by hydrometallurgical methods to recover REEs in the form of REF_3 or REOs as raw materials. However, hydrometallurgical methods have such a high environmental footprint due to the consumption of large amounts of chemicals and the generation of considerable wastewater that the recovery of the REEs through selective leaching is strongly demanded. As Fe consists > 60 wt.% of the magnet scraps that consumes the majority of chemicals, selective leaching of the REEs, leaving Fe behind, would greatly reduce the chemical consumption and wastewater generation. Since the pre-treatment of the magnet waste by oxidation roasting allows the selective leaching with a diluted mineral acid, efforts can be focused on the combination of oxidative roasting and diluted mineral acid leaching or even organic acid leaching that will give a good selectivity on REEs leaching over Fe/Fe_2O_3 with a high REEs recovery.

It must be noted that the experimental work on recycling in this thesis was performed on the sintered Nd–Fe–B PMs.

Intentionally left blank

Chapter 2

Aims and Hypothesis

2.1 Problem Description

The total recycling potential for the EoL sintered Nd–Fe–B PMs in the period 2018–2040 is estimated at 233 kt [46], which triggers the development of the corresponding recycling methods. In terms of making new sintered PMs from the sintered Nd–Fe–B magnet scraps, the direct re-use methods are generally considered as the most ecological and economical routes. However, they are not able to separate REOs from the the sintered Nd–Fe–B magnet scraps. An addition of extra RE alloys is required to reach fully dense magnets due to the high molten point of the REOs in the GBP [62], which consequently represents only a partial circular economy for the sintered Nd–Fe–B PMs. Furthermore, with the repeated recycling by direct re-use methods, the total volume of the non-ferromagnetic phases increases due to the addition of REE hydrides, which then reduces the saturation magnetization and therefore the remanence of the sintered Nd–Fe–B PMs. As a result, the sintered Nd–Fe–B PMs produced from the repeated recycling of materials by direct re-use methods tend to have poorer magnetic properties as the number of cycles increases.

Electrodeposition of Nd–Fe in an alloy form can be a promising alternative to RE alloy recycling route, as well as an alternative of direct PMs synthesis method. However, electrodeposition of Nd–Fe in an alloy form is challenging due to the very negative reduction potential of Nd^{3+}. Finding a stable electrolyte system with high ionic conductivity and wide electrochemical window and avoiding the oxidation of the deposit is critically required to recycle the sintered Nd–Fe–B PMs in alloy forms. Additionally, a deep understanding of the mechanism for the co-deposition of the RE–TM is still unclear.

To recover the REEs from the sintered Nd–Fe–B magnet scraps, hydrometallurgy is currently the only realistic route to recover REEs from the sintered Nd–Fe–B magnet scraps as it can be incorporated into the existing REE separation plants. But such methods require 2172 kg of H_2SO_4 and 1600 kg of NaOH to treat 1000 kg sintered Nd–Fe–B magnets, together with the generation of around 10000 liters of wastewater [101]. The acid and alkali cannot be recycled in a closed-loop and the wastewater and solid waste, e.g., jarosite [71], have to be further treated, all of which adds to the costs. The state-of-the-art methods, including the electrochemical and thermal pre-treatment of the magnets that facilitate the separation of REEs from Fe, still cannot avoid the generation of wastewater.

2.2 Aims

1.) To electrochemically recover the RE alloys ($Nd_2Fe_{14}B$ matrix phase) from the sintered Nd–Fe–B magnet scraps at room temperature as an alternative to molten

salt electrolysis. As the sintered Nd–Fe–B magnets contain 87~92% hard magnetic alloy $Nd_2Fe_{14}B$ matrix phase which is barely oxidized during their lifetime due to the protection of the GB (typically Nd–rich phase) [57]. Therefore, a direct electrochemical recovery of the $Nd_2Fe_{14}B$ grains for fresh Nd–Fe–B PMs making would directly reduce the chemical usage and energy consumption.

2.) To electrochemically deposit Nd–Fe alloy from non-aqueous solutions. The electrodeposition of Nd–Fe in the metallic/alloy forms at mild temperatures can be regarded as another way of RE alloy recycling of the sintered Nd–Fe–B magnet scraps. More importantly, it will directly influence the area of producing the nanostructured magnets for the micro-electro-mechanical system devices, especially using the recycled sources, and would dramatically reduce the manufacturing cost and alleviate the environmental footprint.

3.) To electrochemically recycle REEs and Fe from the sintered Nd–Fe–B magnet scraps, via the selective leaching of the REEs using room-temperature electrolysis. As REEs only account for up to 30 wt.% of the PMs, selective leaching of the REEs, leaving metallic Fe behind will largely reduce the chemical consumption.

Main Goals of the Dissertation:

1.) Recovering the $Nd_2Fe_{14}B$ grains from the sintered Nd–Fe–B magnets by selectively electrochemical etching the Nd-rich GBPs in an organic electrolyte. For that purpose, we used the magnet as the anode, the Nd-rich GBPs of which were preferentially etched (anodized) during electrolysis, leaving the $Nd_2Fe_{14}B$ grains behind. Investigation of the etching mechanism would facilitate the high recovery of $Nd_2Fe_{14}B$ grains which makes the recycling process economically feasible.

2.) Electrodeposition of Nd–Fe in metallic form from non-aqueous solutions and investigation of the mechanism for the RE–TM co-deposition.

3.) Selective leaching of the REEs from the sintered Nd–Fe–B magnets by electrolysis, Fe metal electrodeposition and selective precipitation of REEs with recyclable electrolyte.

2.3 Hypothesis

2.3.1 Hypothesis 1

Generally, the sintered Nd–Fe–B magnet scraps consist of $Nd_2Fe_{14}B$ grains (matrix phase, accounting for 87~92% [57]), surrounded by a Nd-rich (including metallic Nd, NdO and Nd_2O_3 [175, 176]) phase and a B-rich phase ($Nd_{1+x}Fe_4B_4$ where x is ~0.1 [21]) in the GBP. It has been proposed [126, 127] that Nd-rich phases corrode preferentially because of the negative standard reduction potential of REEs, followed by the B-rich phase dissolution which can even result in pulverization of the magnet [128]. This provides a theoretical support for selective recovery of the $Nd_2Fe_{14}B$ grains from the Nd–Fe–B magnet scraps. Due to the difference in electrochemical potential of Nd (–2.32 V *vs.* SHE), Fe (–0.447 V *vs.* SHE) and B (–0.89 V *vs.* SHE) [121], metallic Nd can be preferentially etched electrochemically, compared to Fe and B.

We hypothesize that the electrochemical etching priority of all the metallic phases in the sintered Nd–Fe–B magnet scraps depends on their Nd content. Therefore, the metallic Nd and B-rich phase in the GBP can be preferentially etched electrochemically by tuning the applied potential or current density, leaving behind the magnetic $Nd_2Fe_{14}B$ grains for recovery. As the sintered Nd–Fe–B magnet scraps are quite sensitive to oxygen and water, a non-oxygen and non-water system is required to prevent the oxidation of the recovered

$Nd_2Fe_{14}B$ grains that can readily be oxidized. As the NdO and Nd_2O_3 are electrochemically inert and thus they will remain solid state as particles even after electrochemical etching. A magnetic separation of the $Nd_2Fe_{14}B$ grains from these oxide particles can be realized using an external magnet. The recovered $Nd_2Fe_{14}B$ grains without oxidation are potentially aimed for direct re-use for new magnet synthesis. Therefore, RE alloy recycling could be realized at room temperature by selective etching of the GBP using an electrochemical anodization method.

2.3.2 Hypothesis 2

RE metals and alloys are quite sensitive to water and oxygen due to the nature of their very negative electrode potential. The evolution of hydrogen is inevitable during the RE metals/alloys electrodeposition in aqueous electrolytes. This hydrogen evolution then increases the pH of the solution, thereby favoring the formation of the REE hydroxides and oxides [138]. Therefore, electrodeposition of the Nd–Fe from non-aqueous solution is required to avoid hydrogen evolution and thus would help the Nd–Fe alloys making, which realizes the RE alloy recycling. Indeed, there are literature reports about the electrodeposition of RE alloys using DESs and organic solvents [153-155, 177]. But here the organic chemicals are generally volatile, casting doubt on the environmental credentials of the process. ILs with their high ionic conductivity, wide electrochemical window, lack of volatility and a very low vapor pressure also look promising [178]. In fact, the electrodeposition of Nd using imidazolium and phosphonium-based ILs was reported [160-163], but oxygen contents up to 50 at.% in the deposits make these materials of little practical value. It is a fact that individual deposition of pure Nd metal is extremely difficult due to its very negative reduction potential. However, Nd^{3+}, as well as many other REEs, can be deposited together with one or more metals from the TM group [179-181]. This electrodeposition phenomenon is called "induced co-deposition". Although electrodeposition studies of Nd–Fe from ILs as well as the co-deposition mechanism are up to now scarce in the literature, being able to electrodeposit REE metals and RE–TM alloys at a mild temperature from ILs would be promising in terms of the environmental footprint of the REE industry. It has been reported that metallic tungsten cannot be deposited alone from an aqueous solution, but it does deposit in the presence of $Fe^{2+/3+}$ ions in the solution, forming metallic alloys [166-168].

We hypothesize that the mechanism for RE–TM co-deposition might be similar to that of TM–W co-deposition. A "catalytic reduction" theory was proposed by Holt and Vaaler [171] to explain the reduction of aqueous tungstate solutions in the presence of zero-valence TM elements (i.e., Ni, Co and Fe). In this process, the reduction of TM^{2+} to TM^0 occurs first; it then catalyzes the tungsten deposition until the surface is covered with it, preventing any further tungsten deposition. This process continues until a new layer of the TM element forms. The observation of laminated structures was the basis for this concept by Younes and Gileadi [182], although how the zero-valence state of a TM element catalyzes tungsten deposition was not elaborated. We hypothesize that the mechanism for RE–TM co-deposition might be similar to that of TM–W co-deposition. Inspired by the "catalytic reduction" theory of W–Fe, here we introduce an induced co-deposition mechanism for RE–TM based on the transition-state theory, which assumes that the transition-state TM ($\boldsymbol{TM^*}$) is the catalyzer for the RE^{3+} reduction to RE^0.

2.3.3 Hypothesis 3

Although, hydrometallurgy is currently the only realistic route to recover REEs from the sintered Nd–Fe–B magnet scraps. A large amount of the mineral acids and alkalis is required to completely leach the sintered Nd–Fe–B magnet scraps and to neutralize the

leachate. Fe consists of more than 60 wt.% of the sintered Nd–Fe–B magnet scraps which consumes the majority of the mineral acids during the acid-leaching process and alkalis during Fe removal process which generates large amounts of Fe-based solid waste, e.g., jarosite [101]. Additionally, after Fe removal and REE precipitation processes, large amounts of wastewater containing oxalic acid are inevitably generated that need further treatment. Selective leaching of REEs from the EoL Nd–Fe–B, leaving Fe unleached, is practically demanded as it would largely reduce the chemical consumption. Electrochemistry can be used as an integral part of recycling of REE-based PMs as it is often used to recover metals at room temperature. Actually, the anodic dissolution of Nd–Fe–B magnet scraps, generating Nd^{3+} (as one example of REEs), Fe^{2+} et al. into the electrolyte, has been reported [132]. While on the cathode selective deposition of Fe it could be achieved due to the large difference of Nd^{3+}/Nd^{0} (–2.3 V *vs.* SHE) and Fe^{2+}/Fe^{0} (–0.47 *vs.* SHE) in electrode potential, leaving Nd^{3+} in the electrolyte.

Therefore, we hypothesize that the selective leaching of the REEs could be achieved by leaching the sintered Nd–Fe–B magnet scraps on the anode that dissolves Nd^{3+}, Fe^{2+} et al. into the electrolyte (Fe^{2+} production), while simultaneously depositing Fe metal in the cathode (Fe^{2+} consumption), where the net production/consumption of Fe^{2+} in the whole process is maintained around zero (balanced Fe^{2+} concentration in the electrolyte). To maintain the balanced Fe^{2+} concentration in the electrolyte, the leaching efficiency of Fe^{2+} from the Nd–Fe–B magnet anode should be tuned as close as the current efficiency of Fe deposition on the cathode. Furthermore, as the electrolyte contains both Nd^{3+} and Fe^{2+}, selective precipitation of Nd^{3+} is required. Na_2SO_4 will be used as the precipitant to precipitate Nd^{3+} in the form of $(Nd, Na)_2(SO_4)_2{\cdot}xH_2O$ which is a typical Nd raw material ready for industrial application [49]. After recovering Nd, the electrolyte can be re-used for the next electrochemical processing.

Chapter 3

Materials and Methods

3.1 Materials

Selective recovery of the $Nd_2Fe_{14}B$ grains from the sintered Nd–Fe–B magnets: As sintered Nd–Fe–B magnets are quite sensitive to oxygen and water, in order to prevent the oxidation of the recovered $Nd_2Fe_{14}B$ grains that can readily be oxidized, a protective Ar atmosphere for material handling and non-aqueous solvents for the electrochemical experiments need to be used. To select the most suitable solvent, important points need to be considered: i) the solvent should not be based on water, because of the oxidation issues, ii) it should have high solubility for $FeCl_2$ to have a high conductivity of the electrolyte; ii) it should have high vapor pressure, so it can be recovered by distillation and re-used. After considering these facts, the economic feasibility together with environmental and safety issues have to be considered. For this study dimethylformamide (DMF, >99%, Sigma-Aldrich, Germany) was selected for all the electrochemical etching experiments as it fulfils the first three criteria. Here we have to emphasize that precautions have to be met when working with this solvent according to safety regulations [183]. Iron(II) chloride tetrahydrate ($FeCl_2 \cdot 4H_2O$, > 99.99%), and molecular sieves (4A) were used and purchased from Sigma-Aldrich. Prior to use, molecular sieves that were dried under vacuum at 160 ℃ for more than 24 hours were added to the DMF to remove any water. $FeCl_2 \cdot 4H_2O$ was dehydrated under vacuum at 140 ℃ for 24 hours. All the dried chemicals were stored inside a closed bottle in an argon-filled glove box with water and oxygen contents below 1 ppm. The water concentration in the electrolyte was less than 50 ppm, as determined with a Karl Fischer titration (C20S, Mettler-Toledo, Switzerland). The sintered Nd–Fe–B magnets were supplied by Magneti Ljubljana d.d., Slovenia, and were used as model materials of the EoL PMs. These magnets were demagnetized and mechanically polished to remove the protective coating on the surface (Al/Al_2O_3). The chemical compositions of the magnet scrap were measured with inductively coupled plasma optical emission spectrometry (ICP-OES, Perkin Elmer Optima 5300 DV), with the results listed in Table 3.1. Despite Nd, the addition of Dy (1–8 wt.%) [25, 184] in the sintered Nd–Fe–B magnets is typical for high temperature application such as hybrid electric vehicles and electric motors.

Table 3.1: Elemental composition of the sintered Nd–Fe–B magnets.

Element	Content (wt.%)	Element	Content (wt.%)
Nd	26.01	Ga	0.22
Dy	7.20	Al	0.12
Fe	61.83	Cu	0.11
Pr	0.58	Co	2.93
B	0.90	Total	99.90

Electrochemical deposition of the Nd–Fe from an ionic liquid: 1-ethyl-3-methylimidazolium dicyanamide ([EMIM][DCA], > 98%), iron(II) chloride tetrahydrate ($FeCl_2 \cdot 4H_2O$, > 99.99%), hydrochloric acid (HCl, 37%), and neodymium(III) chloride hexahydrate ($NdCl_3 \cdot 6H_2O$, > 99%), and molecular sieves (4A) were used and purchased from Sigma-Aldrich. Prior to use, molecular sieves that were dried under vacuum at 160 ℃ for more than 24 hours were added to the [EMIM][DCA] to remove any water. $FeCl_2 \cdot 4H_2O$ and $NdCl_3 \cdot 6H_2O$ were dehydrated under vacuum at 140 ℃ for 24 hours. All the dried chemicals were stored inside a closed bottle in an argon-filled glove box with water and oxygen contents below 1 ppm. The water concentration in the electrolyte was less than 50 ppm, as determined with a Karl Fischer titration (C20S, Mettler-Toledo, Switzerland).

Selective recovery of the REEs and Fe metal from the sintered Nd–Fe–B magnets: iron(II) sulfate heptahydrate ($FeSO_4{\cdot}7H_2O$, > 99%), ammonium sulfate ($(NH_4)_2SO_4$, > 99%), sodium citrate dihydrate ($Na_3cit{\cdot}2H_2O$, > 99%), sodium sulfate (Na_2SO_4, > 99%), boric acid (H_3BO_3, > 99%) and sulfuric acid (H_2SO_4, 98%) were used and purchased from Sigma-Aldrich. The sintered Nd–Fe–B magnets were supplied by Magneti Ljubljana d.d., Slovenia, and were used as model materials of EoL PMs. These magnets were demagnetized and mechanically polished to remove the protective coating on the surface (Al/Al_2O_3). The chemical compositions of the magnet scrap were measured with ICP-OES (Perkin Elmer Optima 5300 DV), with the results listed in Table 3.2.

Table 3.2: Elemental composition of the sintered Nd–Fe–B magnets.

Element	Content (wt.%)	Element	Content (wt.%)
Nd	23.71	Ga	0.25
Dy	6.55	Al	0.06
Fe	64.23	Cu	0.12
Pr	0.78	Co	2.13
B	1.12	Total	98.95

3.2 Selective Recovery of the $Nd_2Fe_{14}B$ Grains from the Sintered Nd–Fe–B Magnets

A three-electrode cell (Figure 3.1) with a potentiostat (Gamry, Reference 600, USA) was used during the experiment:

- A Pt wire (> 99.99%, diameter $\phi = 0.5$ mm) was used as the quasi-reference electrode (QRE), because the potential obtained using a Pt QRE is stable and reproducible in DMF at a mid-range temperature.

- A sintered Nd–Fe–B magnet with varied effective surface areas or a Pt wire (> 99.99%, diameter $\phi = 0.5$ mm, with an effective area of 0.047 cm^2) was used as the working electrode.
- An inert Pt plate (30 mm × 10 mm, with an effective area of 2.0 cm^2) or a Cu foil (40 mm × 30 mm, with an effective area of 10 cm^2) was used as the counter electrode.

The initial electrolyte bath consisted of 15 mL of DMF with 0.3 mol L^{-1} $FeCl_2$.

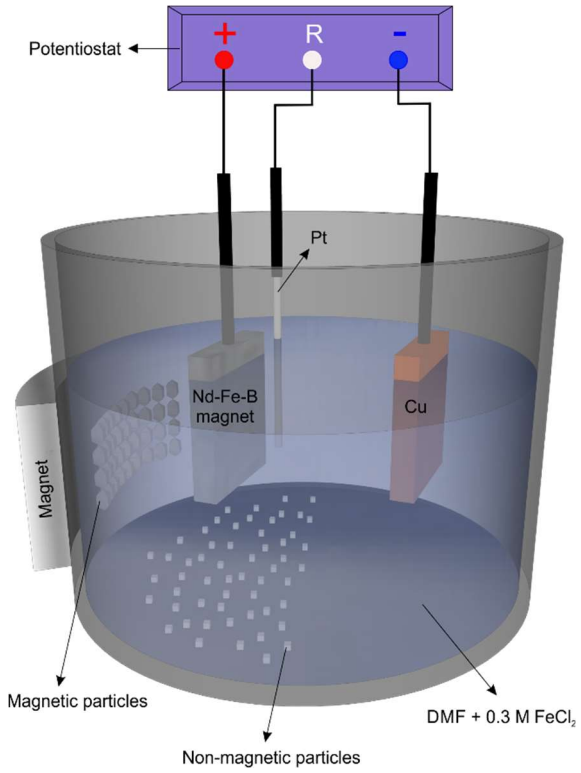

Figure 3.1: Schematic illustration of the electrochemical cell for recovering the $Nd_2Fe_{14}B$ grains from the sintered Nd–Fe–B magnets; (1) A sintered Nd–Fe–B magnet (anode), (2) A Cu foil (cathode), (3) Pt wire (QRE), (4) Electrical conductors for the connection to the power supply, (5) Electrolyte, (6) Magnetic particles, (7) Non-magnetic particles and (8) An external commercial Nd–Fe–B magnet.

3.2.1 Linear Sweep Voltammetry

The electrochemical behaviors of the sintered Nd–Fe–B magnets in 15 mL of DMF containing 0.3 mol L^{-1} $FeCl_2$ at room temperature were evaluated using linear sweep voltammetry (LSV). In order to observe the microstructure evolution of the sintered magnet during electrochemical etching, a polished sintered Nd–Fe–B magnet (2 mm × 2 mm × 30 mm) was used as the working electrode with effective areas of 0.05 cm^2. A Pt wire (> 99.99%, diameter $\phi = 0.5$ mm, with an effective area of 0.047 cm^2) was also used as the working electrode to make a comparison with the sintered Nd–Fe–B magnet. Another Pt wire (> 99.99%, diameter $\phi = 0.5$ mm) was used as the QRE. All the potentials reported herein were referred to the Pt QRE. A Pt plate (30 mm × 10 mm) was selected as the counter electrode, with an effective area of 2 cm^2. The LSV experiments were carried

out in a potential range from open circuit potential (OCP) to 1.0 V (*vs.* Pt) with a scanning rate of 40 mV s^{-1}.

3.2.2 Electrochemical Etching of the Sintered Nd–Fe–B Magnets

A Cu foil substrate (40 mm × 30 mm) was employed as the cathode with an effective area of 10 cm^2 and a polished sintered Nd–Fe–B magnet (2 mm × 5 mm × 30 mm) was used as the anode with the effective area of 0.25 cm^2. A Pt wire (> 99.99%, diameter $\phi = 0.5$ mm) was used as the QRE. The applied current density was within the range 2–48 mA cm^{-2} for various times. In order to obtain a higher yield of particles, a Cu foil substrate (40 mm × 30 mm) was employed as the cathode with an effective area of 10 cm^2 and a polished sintered Nd–Fe–B magnet (2 mm × 15 mm × 30 mm) was used as the anode with an effective area of 5 cm^2. A Pt wire (> 99.99%, diameter $\phi = 0.5$ mm) was used as the QRE. A current of 10 mA (the corresponding anode current density was 2 mA cm^{-2} and the cathode current density was 1 mA cm^{-2}) was applied for 360 min. A few studies have reported that REEs and TMs could be co-deposited in organic solvents [154, 156]. In order to obtain REE-free metal on the cathode, the cathode current density in the current study was controlled at 1 mA cm^{-2}, because the literature [185] suggests that a Nd–Fe film would be obtained at a cathode current density > 1 mA cm^{-2}. All the experimental procedures were carried out in an Ar atmosphere at room temperature.

3.2.3 $Nd_2Fe_{14}B$ Grains Collection after the Electrochemical Etching

Since the magnetic particles of the $Nd_2Fe_{14}B$ grains formed after the electrochemical etching tended to be attracted by the anode, after every 60 min the etched anode was put close to an external magnet to separate these particles from the anode. After the electrochemical etching, the $Nd_2Fe_{14}B$ grains are collected magnetically and washed three times ultrasonically using DMF. The non-magnetic REE-based particles were collected by filtering the electrolyte after etching.

3.3 Electrochemical Deposition of the Nd–Fe from an Ionic Liquid

3.3.1 Cyclic Voltammetry

A three-electrode cell with a potentiostat was used for all the electrochemical measurements. The electrochemical behaviors of the Fe^{2+} and Nd^{3+} in 10 mL of [EMIM][DCA] containing 0.03 mol L^{-1} $FeCl_2$ and 0.1 mol L^{-1} $NdCl_3$ at 110 °C were evaluated using cyclic voltammetry (CV). Pt wires (> 99.99%, diameter $\phi = 0.5$ mm) were used as the working electrode and the QRE. A Pt plate (> 99.99%, 30 mm × 10 mm) was selected as the counter electrode. The areas of the working electrode and the counter electrode immersed in the electrolyte were 4.71 mm^2 and 80 mm^2, respectively. The CV experiments were carried out in a potential range from –2.0 V to 0 V (*vs.* Pt) for at least 50 cycles with a scanning rate of 10–100 mV s^{-1}.

3.3.2 Electrodeposition of Nd–Fe

For the electrodeposition experiments, a Cu substrate (5 mm × 5 mm) was employed as the cathode and an Fe plate (25 mm × 15 mm) was used as the anode in 10 mL of [EMIM][DCA] containing 0.015/0.03 mol L^{-1} $FeCl_2$ and 0.1 mol L^{-1} $NdCl_3$ at 110 °C. The

Cu substrate was used instead of Pt because the cathodic parts of the CVs on the Pt and Cu electrode are similar. Before use, they were degreased with acetone, followed by an acid treatment (1 mol L^{-1} HCl) to remove the surface oxides and finally dried. All the experimental procedures were carried out in an Ar-filled atmosphere at 110 °C. The deposition process was realized by using a constant potential of –1.4 V and a pulsed current of i_{on} = –4 to –24 mA cm^{-2} for different times. The as-deposited samples were washed with dried DMF to remove any electrolyte adhered to the surface.

3.4 Selective Recovery of the REEs and Fe Metal from the Sintered Nd–Fe–B Magnets

A three-electrode cell (Figure 3.2) with a potentiostat was used during the experiment:

- A Ag/AgCl (3 mol L^{-1} KCl) electrode was used as the reference electrode,
- A polished sintered Nd–Fe–B magnet with varied effective surface areas or a Pt wire (> 99.99%, diameter ϕ = 0.5 mm, with an effective area of 0.047 cm^2) was used as the working electrode. An external magnet was put inside a glass tube to hold the anode to the side wall of the glass tube. It was observed that pulverization of the magnet led to loose magnetic particles that were no longer in electrical contact. However, the external magnet kept the loose magnetic particles attached to the anode for continuous leaching, and
- A Pt plate (30 mm × 10 mm)/Cu foil (40 mm × 60 mm) was used as the counter electrode, with an effective area of 2.0 cm^2/8–16 cm^2.

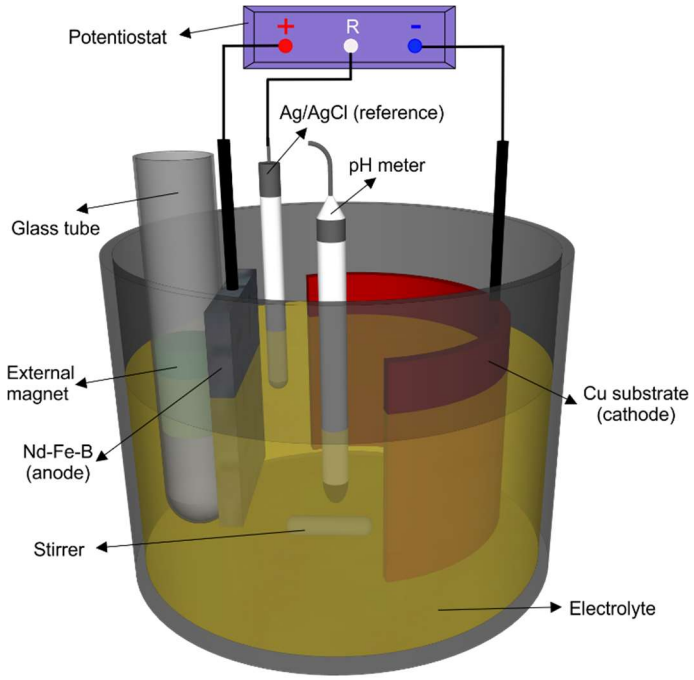

Figure 3.2: Schematic of the electrochemical cell for leaching the sintered Nd–Fe–B magnets and the deposition of Fe at room temperature.

3.4.1 Linear Sweep Voltammetry

The electrochemical behaviors of the Nd–Fe–B magnets in 70 mL of an aqueous bath containing 0.6 mol L^{-1} $FeSO_4$, 0.4 mol L^{-1} $(NH_4)_2SO_4$, 0.175 mol L^{-1} Na_3cit and 0.4 mol L^{-1} H_3BO_3 with the pH of 4.0 (Mettler-Toledo, S210) were evaluated using LSV at room temperature. In order to observe the microstructure evolution of the sintered magnet during electrochemical etching, a polished sintered Nd–Fe–B magnet (2 mm × 2 mm × 30 mm) was used as the working electrode with effective areas of 0.05 cm^2. A Pt wire (> 99.99%, diameter $\phi = 0.5$ mm, with an effective area of 0.047 cm^2) was also used as the working electrode to make a comparison with the sintered Nd–Fe–B magnet. The sintered Nd–Fe–B magnet and the Pt wire working electrode had an effective area of 0.05 and 0.047 cm^2, respectively. A Pt plate (30 mm × 10 mm) was selected as the counter electrode, with an effective area of 2 cm^2. An Ag/AgCl (3 mol L^{-1} KCl) electrode was used as the reference electrode. The LSV experiments were carried out in a potential range from OCP to 1.0 V (*vs.* Pt) with a scanning rate of 100 mV s^{-1}.

3.4.2 Influence of Anodic Current Density on the Leaching of the Sintered Nd–Fe–B Magnets

The electrolyte bath contained 0.6 mol L^{-1} $FeSO_4$, 0.4 mol L^{-1} $(NH_4)_2SO_4$, 0.175 mol L^{-1} Na_3cit and 0.4 mol L^{-1} H_3BO_3. A polished Nd–Fe–B magnet (30 mm × 15 mm × 5 mm) connected with a Pt wire as the conductor was used as the anode with the effective area of 2.0 cm^2. A copper foil (40 mm × 60 mm) with an effective area of 8–16 cm^2 was dipped into the electrolyte as the cathode and the back of the foil was masked with insulating tape. An Ag/AgCl (3 mol L^{-1} KCl) electrode was used as the reference electrode. Currents of 100, 150 and 200 mA were applied (initial current density of 50, 75 and 100 mA cm^{-2} on the anode, respectively, and 12.5 mA cm^{-2} on the cathode) to investigate the leaching efficiency of the sintered Nd–Fe–B magnet and the corresponding energy consumption. The electrolyte was agitated magnetically via a magnetic PTFE-coated stirring bar at a constant rotating speed of 500 rpm. Some 4 mol L^{-1} H_2SO_4 was added to the electrolyte dropwise every 10 min to keep the pH between 3.5 and 4.5, measured with a pH meter (Mettler-Toledo, S210) immersed in the electrolyte throughout the experiment.

3.4.3 Influence of Sodium Citrate Concentration on Fe Deposition

The electrolyte bath contained 0.6 mol L^{-1} $FeSO_4$, 0.4 mol L^{-1} $(NH_4)_2SO_4$ and 0.4 mol L^{-1} H_3BO_3 with the Na_3cit concentration varying from 0.05 to 0.175 mol L^{-1}. Four pieces of polished sintered Nd–Fe–B magnets (30 mm × 15 mm × 5 mm) connected with a Pt wire as the conductor were used as the anode with the effective area of 8.0 cm^2. A copper foil (40 mm × 60 mm) with an effective area of 16 cm^2 was dipped into the electrolyte as the cathode and the back of the foil was masked with insulating tape. An Ag/AgCl (3 mol L^{-1} KCl) electrode was used as the reference electrode. A current of 200 mA was applied with the initial current density of 25 mA cm^{-2} on the anode and 12.5 mA cm^{-2} on the cathode. The electrolyte was agitated magnetically via a magnetic PTFE-coated stirring bar at a constant rotating speed of 500 rpm. Some 4 mol L^{-1} H_2SO_4 was added to the electrolyte dropwise every 10 min to keep the pH between 3.5 and 4.5, measured with a pH meter immersed in the electrolyte throughout the experiment. Every 1 hour, 0.2 mL solution was sampled for a concentration measurement of total dissolved Fe and the weight of deposited Fe was measured for current efficiency calculation.

3.4.4 One Batch of Electrolysis

The electrolysis experiment (electrochemical leaching and electrodeposition of Fe happening simultaneously) was performed for 8 hours as a single batch. The electrolyte bath contained 0.6 mol L^{-1} $FeSO_4$, 0.4 mol L^{-1} $(NH_4)_2SO_4$, 0.175 mol L^{-1} Na_3cit and 0.4 mol L^{-1} H_3BO_3. Four pieces of polished sintered Nd–Fe–B magnets (30 mm × 15 mm × 5 mm) connected with a Pt wire as the conductor were used as the anode with the effective area of 8.0 cm^2. A copper foil (40 mm × 60 mm) with an effective area of 16 cm^2 was dipped into the electrolyte as the cathode and the back of the foil was masked with insulating tape. An Ag/AgCl (3 mol L^{-1} KCl) electrode was used as the reference electrode. A current of 200 mA was applied with the initial current density of 25 mA cm^{-2} on the anode and 12.5 mA cm^{-2} on the cathode. The electrolyte was agitated magnetically via a magnetic PTFE-coated stirring bar at a constant rotating speed of 500 rpm. Some 4 mol L^{-1} H_2SO_4 was added to the electrolyte dropwise every 10 min to keep the pH between 3.5 to 4.5, measured with a pH meter immersed in the electrolyte throughout the experiment. Every 1 hour, 0.2 mL solution was sampled for a concentration measurement of total dissolved Fe and the weight of deposited Fe was measured for current efficiency calculation.

3.4.5 Selective Precipitation of the REEs

After the electrolysis step, 0.57 grams of Na_2SO_4 was added to the electrolyte solution, followed by heating at 70 ℃ for 2 hours to selectively precipitate REEs based on a description in the literature [186]. While the solution was warm, the precipitates were obtained by filtration and were washed thoroughly with water, followed by drying at 105 °C for 12 hours. The filtrate was recycled back to the electrolysis cell for the next electrolysis batch.

3.4.6 Calculations

The leaching efficiency (η_L) for the dissolution of the sintered Nd–Fe–B magnets was calculated as follows:

$$\eta_L = \frac{m_0}{m_t} \times 100(\%) \tag{3.1}$$

where m_0 and m_t are the observed and theoretical mass loss of the magnets, respectively. The observed mass loss was calculated as the mass change of the magnet before and after the electrolysis. The theoretical mass loss for the magnet was calculated as [132]

$$m_t = \frac{I * t}{F * N_{EQ}} \tag{3.2}$$

where I is the applied current, A; F is the Faraday constant, 96485.33 C mol^{-1}; t is the time of the electrolysis, s; and N_{EQ} is the total number of equivalents obtained from dissolving a unit mass of the alloy [187]:

$$N_{EQ} = \sum \frac{f_i * n_i}{a_i} \tag{3.3}$$

where f_i, n_i, and a_i are the mass fraction, the number of electrons exchanged, and the atomic weight, respectively, of the ith alloying element.

The Fe leaching efficiency ($\eta_{Fe\text{-}L}$) from the magnets is estimated based on the leaching efficiency of the magnets under a constant current. We assumed that the $Nd_2Fe_{14}B$ phase accounts for 90% by weight, while the GBP accounts for 10% [57]. There are two extreme cases: the GBP contains only i) metallic Nd or ii) Nd_2O_3 (without considering other phases, e.g., $NdFe_4B_4$, due to their negligible content). In the case of i), the formula for the magnets can be written as $Nd_{2.83}Fe_{14}B$, under a constant leaching without selectivity (reaction (3.4)), the Fe leaching efficiency is calculated as

$$Nd_{2.83}Fe_{14}B - 39.49e^- \rightarrow 2.83Nd^{3+} + 14Fe^{2+} + B^{3+} \tag{3.4}$$

$$\eta_{Fe\text{-}L} = \eta_L * \frac{14*2}{2.83*3+14*2+1*3} \times 100\ (\%) = 70.9\% * \eta_L \tag{3.5}$$

In the case of ii), the formula of the magnets can be written as $Nd_2Fe_{14}B$, because the Nd_2O_3 is electrochemically inert and thus does not consume charge (current). Under a constant leaching without selectivity (reaction (3.6)), the Fe leaching efficiency is calculated as

$$Nd_2Fe_{14}B - 37e^- \rightarrow 2Nd^{3+} + 14Fe^{2+} + B^{3+} \tag{3.6}$$

$$\eta_{Fe\text{-}L} = \eta_L * \frac{14*2}{2*3+14*2+1*3} \times 100\ (\%) = 75.7\% * \eta_L \tag{3.7}$$

Generally, both metallic Nd and Nd_2O_3 are present in the GB; therefore, the Fe leaching efficiency ($\eta_{Fe\text{-}L}$) under a constant current should be in the range of (70.9–75.7%)*η_L. Specifically, when the magnet is leached with a η_L of 100%, $\eta_{Fe\text{-}L}$ is in the range 70.9–75.7%.

The current efficiency (η_D) of the Fe deposition on the cathode is calculated as

$$\eta_D = \frac{m_{Fe}/M_{Fe}}{I * t/2F} \times 100(\%) \tag{3.8}$$

where m_{Fe} is the mass of the deposited Fe on the cathode, g; M_{Fe} is the molar mass of Fe, 55.85 g mol^{-1}; I is the applied current, A; t is the duration of the electrolysis, s; and F is the Faraday constant, 96485.33 C mol^{-1}.

The recovery (%) of REEs from the Nd–Fe–B magnets is calculated as

$$\%R = \frac{\text{REEs in REE sulphate double salts (\%)} \times \text{Recovered REE sulphate double salts (g)}}{\text{REEs in magnet (\%)} \times \text{Amount of leached magnet (g)}} \tag{3.9}$$

The energy consumption, E (kWh kg^{-1}) is calculated as

$$E = \frac{U * I * t}{3600 * m_0} \tag{3.10}$$

where U is the voltage measured between the magnet anode and the copper cathode, V; I is the applied current, A; t is the duration of the electrolysis, s; and m_0 is the amount of magnet dissolved, kg. Thus the reported values are kilowatt-hours per kilogram of the magnet.

3.5 Material Characterization

3.5.1 Scanning Electron Microscopy

The morphology and chemical composition of the sintered Nd–Fe–B magnets, Nd–Fe deposits, $Nd_2Fe_{14}B$ grains, non-magnetic REE-based particles and REE-based precipitates were determined using a field-/thermionic-emission and scanning electron microscope (F/TE-SEM, JSM-7600F and 5800, JEOL, Japan) equipped with an energy-dispersive X-ray spectrometer (EDS) system INCA (Oxford Instruments, United Kingdom). An accelerating voltage of 18 kV was used with a working distance of 15 mm for the imaging and the EDS analysis in JSM-7600F. In order to achieve good accuracy for the quantitative elemental analysis, the efficiency of the EDS detector was calibrated at 18 kV using a pure Co-standard. For the JSM-5800, an accelerating voltage of 20 kV was used with a working distance of 10 mm for the imaging and the EDS analysis.

3.5.2 Transmission Electron Microscopy

Two Nd–Fe deposits annealed at 350 and 750 °C for 30 min, respectively, were analyzed by a transmission electron microscope (TEM, JEM-ARM200F, JEOL). A focused ion beam (FIB, FEI HeliosNanolab 650) was used to prepare the electron-transparent lamellae from these two samples (the conditions: accelerating voltage ~30 kV down to 1 kV, probe current 9.3 nA down to 73 pA with the incidence angles from 2° to 7° were carefully monitored throughout the whole etching process in order not to alter the samples structure and composition). The lamellae were investigated with TEM equipped with a cold field-emission gun, a scanning unit (STEM), and high-angle annular dark-field (STEM-HAADF) and annular bright-field (STEM-ABF) detectors. Low beam currents of 16 nA and low accelerating voltage of 80 kV were used to reduce the knock-on-damage to the sample.

3.5.3 X-ray Diffraction Analysis

The crystal structure of the sintered Nd–Fe–B magnets, Nd–Fe deposits, $Nd_2Fe_{14}B$ grains, non-magnetic REE-based particles and REE-based precipitates were determined with an X-ray diffractometer (XRD, PANalytical, Netherlands) using Cu-$K_{\alpha 1}$ radiation ($\lambda = 1.5406$ Å).

3.5.4 Thermogravimetric Analysis and Thermal Annealing

Thermogravimetric analysis (TGA) of the [EMIM][DCA] IL was conducted using a STA1500 (Rheometric Scientific) in a nitrogen atmosphere between 30 and 800 ℃ with a temperature ramp of 10 ℃ min^{-1}. Using the TGA, an annealing experiment was performed under Ar (99.999%) at 350 and 750 ℃ for 30 min (Carbolite, MTF 12, England). The ratio of Nd/(Nd + Fe) in the deposit is expected to remain the same after annealing at 350 ℃ and 750 ℃, as the phase changes of the deposits with 12 at.% of Nd, which would correspond to Nd_2Fe_{17} composition, would not happen until the temperature ~1100 ℃, where the Nd_2Fe_{17} phase would transform to Fe (bcc) and liquid phase via peritectic reaction, according to the phase diagram of Fe–Nd [188].

3.5.5 Inductively Coupled Plasma Mass Spectrometry

The concentration of the REEs, i.e., Nd, Dy and Pr as a whole, was analyzed by mass spectrometry with inductively coupled plasma (ICP-MS, Agilent 7700, Agilent Technologies, Tokyo, Japan). The quality of the analytical measurements was checked by

the analysis of the standard reference material SPS-SW1 (Reference material for measurements of elements in surface waters) obtained from Spectrapure Standards (Oslo, Norway).

3.5.6 Ultraviolet-Visible-Near Infrared Spectrophotometry

The concentration of total dissolved Fe in aqueous solution was determined using the 1,10-phenanthroline method [189] using an ultraviolet-visible-near infrared (UV-Vis-NIR) spectrophotometer (LAMBDA 950, PerkinElmer, USA) at $\lambda = 510\,\text{nm}$ for the Fe-phen complexes.

Chapter 4

Results and Discussion

4.1 Selective Recovery of the $Nd_2Fe_{14}B$ Grains from the Sintered Nd–Fe–B Magnets

The recycling of the sintered Nd–Fe–B magnet scraps can be classified into: i) direct re-use methods, ii) pyrometallurgical processing and iii) hydrometallurgical separation and recovery [47, 71, 190]. In terms of new magnets production using the recycled Nd–Fe–B magnet scraps, pyrometallurgical processing working at high temperature is energy-intensive, while hydrometallurgical routes require multi-processing steps with a large amount of chemical consumption and wastewater generation. In contrast, the direct re-use methods such as the re-sintering [63, 66], and HDDR [59, 64, 191] of the sintered Nd–Fe–B magnet scraps are generally regarded as the most economical and ecological ways because they provide short processing steps with zero-waste generation. However, the high oxygen content (typically 2000–5000 ppm) in the REE-rich GBP of the sintered Nd–Fe–B magnet scraps severely limits their recycling potential [47, 61]. These REOs (mainly Nd_2O_3) cannot be extracted, resulting in reprocessed sintered magnets, lacking full density and exhibiting poor magnetic properties. Therefore, extra RE hydrides are generally added to compensate for the existing REOs [66, 192]. This then represents only a partial circular economy for the magnets [193]. Additionally, the REE-rich phases, i.e., REOs, are non-ferromagnetic [194]. With the repeated recycling by direct re-use methods, the total volume of the non-ferromagnetic phases increases due to the addition of the RE hydrides, which then reduces the saturation magnetisation and therefore the remanence of the sintered Nd–Fe–B magnets. Consequently, the sintered Nd–Fe–B magnets produced from the repeated recycling of materials by direct re-use methods tend to have poorer magnetic properties as the number of cycles increases.

The sintered Nd–Fe–B magnets consist of the REE-rich GBs, representing about 10–12% of the magnet, and the $Nd_2Fe_{14}B$ grains, which are practically oxygen-free, accounting for 85–87% of the magnet [57]. Thus, a direct recovery of the $Nd_2Fe_{14}B$ grains, leaving REOs behind as a starting point would provide a sustainable recycling route for the fresh Nd–Fe–B PMs production with high magnetic properties.

Herein, we describe an electrochemical process to recover the $Nd_2Fe_{14}B$ matrix grains from the sintered Nd–Fe–B magnets based on the etching priority of different phases in the magnets. As a result, the $Nd_2Fe_{14}B$ matrix grains and the REOs were disconnected from each other after electrochemical etching that allowed a magnetic separation of the matrix $Nd_2Fe_{14}B$ grains. DMF, a non-aqueous solvent, was used to prevent the oxidation of the recovered $Nd_2Fe_{14}B$ grains as they are quite sensitive to oxygen and water.

4.1.1 Microstructural Investigation of the Sintered Nd–Fe–B Magnets

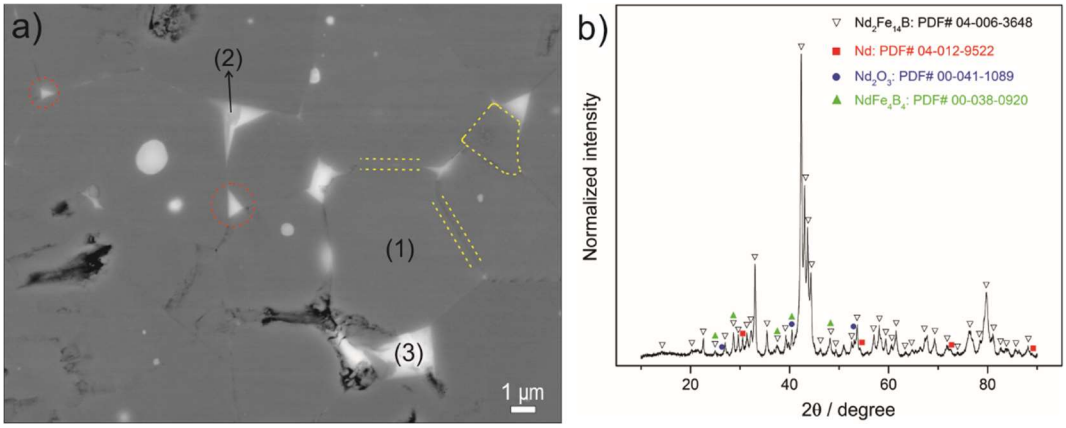

Figure 4.1: (a) BSE-SEM image and (b) XRD pattern of a sintered Nd–Fe–B magnet.

Figure 4.1a shows a back-scattered electron (BSE)-SEM image of a polished sintered Nd–Fe–B magnet. The dark-grey phase is the matrix phase, labelled (1), which consists of 83.51 at.% Fe, 9.02 at.% Nd, 3.99 at.% Dy and 3.48 at.% Co based on EDS. The light-grey phase, labelled (2), consists of 63.58 at.% Fe, 30.02 at.% Nd, 2.38 at.% Dy and 4.02 at% Ga, while the white phase, labelled (3), contains 30.23 at.% Nd, 3.89 at.% Dy and 65.88 at.% O. The bright intergranular region surrounding the grey phase (1) are the GBPs (labelled with yellow dashed lines in Figure 4.1a). The observed phases are in accordance with literature reports, with the thickness of the GBs being less than 10 nm [176, 195-197]. The analysis of the GB and the triple point (labelled with red dashed circles) is, however, not reliable in our case, because of its small volume. Figure 4.1b shows the XRD pattern of the polished sintered Nd–Fe–B magnet, from which the $Nd_2Fe_{14}B$ (PDF# 04-006-3648), metallic Nd (PDF# 04-012-9522) and Nd_2O_3 (PDF# 00-041-1089) phases are observed. Combining the XRD result with the microstructure, the grey phase (1) is the $(Nd_{1-x}Dy_x)_2Fe_{14}B$ matrix phase, i.e., labelled as "$Nd_2Fe_{14}B$". Based on the stoichiometry from the EDS, the light-grey phase (2) is the $NdFe_4B_4$ [198], the peaks of which are overlapping with the peaks of $Nd_2Fe_{14}B$ phase in the XRD pattern, because it represents just a few percent of the total (Figure 4.1b). The white phase (3) is a mixture of Nd_2O_3 and Dy_2O_3 phases, where the characteristic peaks of the Dy_2O_3 phase are not visible due to there being only a small amount. According to the literature [196, 199], the GBP is Nd-rich material, which mostly consists of metallic Nd and a mixture of different Nd-based oxides.

4.1.2 LSV Study on the Sintered Nd–Fe–B Magnets

Figure 4.2 shows the LSV of a Pt electrode (black curve) and an initial sintered Nd–Fe–B magnet (red curve) in DMF containing 0.3 mol L^{-1} $FeCl_2$ with a scan rate of 40 mV s^{-1}. For all the electrolysis experiments, the following reactions are possible at the anode:

$$Fe^{2+} - e^- \rightarrow Fe^{3+} \tag{4.1}$$

$$Nd^0 - 3e^- \rightarrow Nd^{3+} \tag{4.2}$$

$$NdFe_4B_4 - 23e^- \rightarrow Nd^{3+} + 4Fe^{2+} + 4B^{3+} \tag{4.3}$$

$$Nd_2Fe_{14}B – 37e^- \rightarrow 2Nd^{3+} + 14Fe^{2+} + B^{3+} \quad (4.4)$$

The cathodic reaction is the reduction of Fe^{2+} to produce metallic Fe:

$$Fe^{2+} + 2e^- \rightarrow Fe \quad (4.5)$$

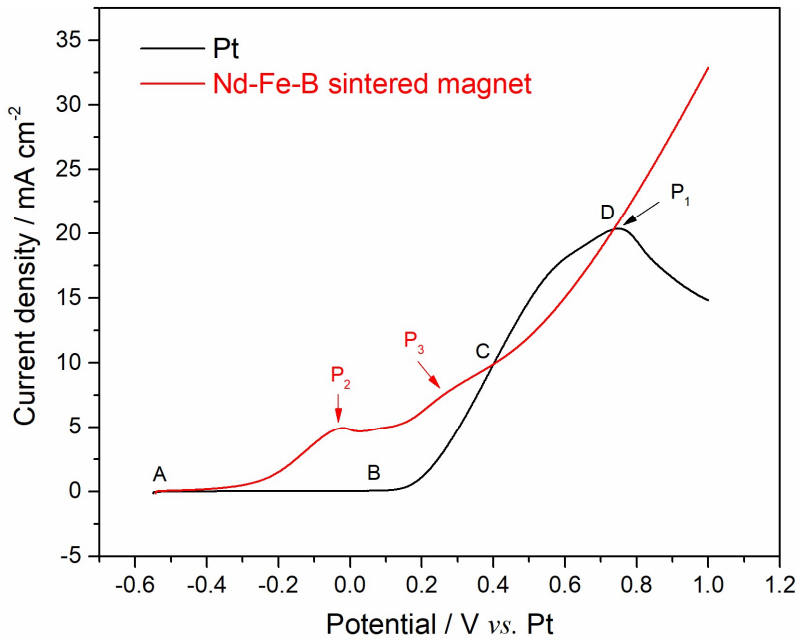

Figure 4.2: LSV of a Pt-wire working electrode (black curve) and an initial sintered Nd–Fe–B magnet (red curve) in DMF containing 0.3 mol L^{-1} $FeCl_2$, 40 mV s^{-1}, room temperature.

When using Pt as the working electrode (black curve), the current density started to increase at ~0.15 V along the BC line due to the onset of the oxidation of Fe^{2+} (reaction (4.1)) that includes also the oxidation of $[FeCl_3(DMF)]^-$ [200, 201] complex that might explain the mild current peak at ~0.55 V and the peak current (P_1) attributed to $[FeCl_4]^{2-}$ [200, 201] oxidation at the potential of 0.75 V. When the Nd–Fe–B magnet was used as the working electrode, the current density started to increase at the potential of –0.40 V, shown by the red curve. The peak (P_2) of 5 mA cm^{-2} recorded at –0.02 V was responsible for the oxidation of metallic Nd in the grain boundaries (reaction (4.2)) due to its very negative electrode potential (–2.32 V *vs* standard hydrogen electrode, SHE) [135]. The peak (P_3) at 0.30 V is likely a combined oxidation of the $NdFe_4B_4$ phase (reaction (4.3)) with an oxidation of Fe^{2+} (reaction (4.1)). From point C on, the current density regularly increases along CD on the red curve which is the response of the oxidation of all the Nd-containing phases together with the Fe^{2+} oxidation (reactions (4.1)–(4.4)). Accordingly, the etching priority of the phases inside the magnet is as follows: metallic Nd (in the grain boundary) > $NdFe_4B_4$ > $Nd_2Fe_{14}B$ (magnetic phase). This is in good agreement with the previous reports [202-205].

4.1.3 Electrochemical Etching of the Sintered Nd–Fe–B Magnets

Based on the etching priority from the LSV, selective etching of the metallic Nd-rich phase from the GB could be realized by applying a potential of < –0.02 V (corresponding to < 5 mA cm^{-2}) on the anode, while applying potentials of higher than 0.40 V (corresponding to > 9.9 mA cm^{-2}) would lead to the non-selective etching of all the phases present, e.g., the metallic Nd-rich phase, the $NdFe_4B_4$ and $Nd_2Fe_{14}B$.

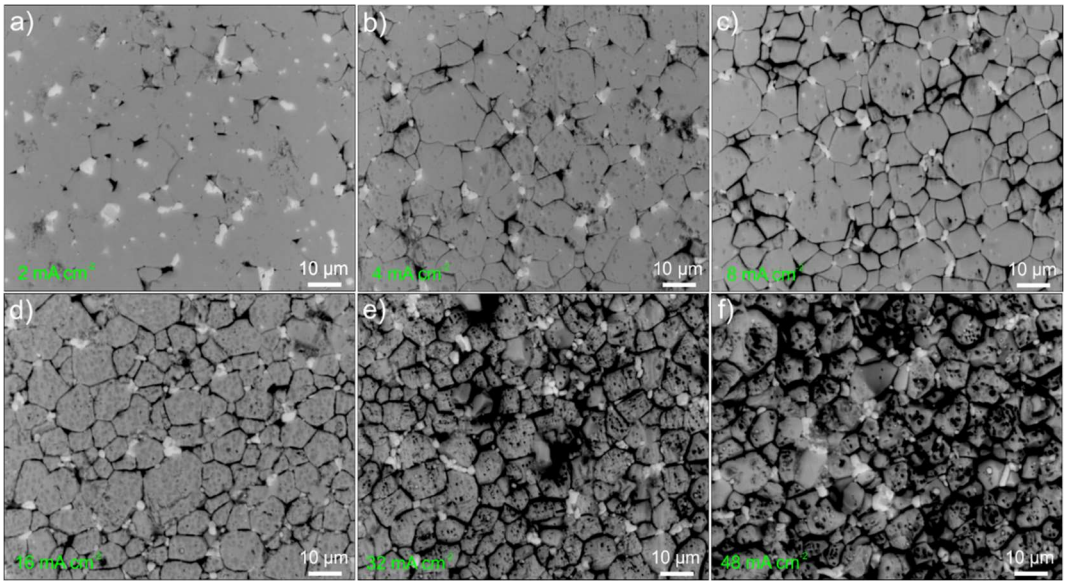

Figure 4.3: BSE-SEM images of the sintered Nd–Fe–B magnets after electrochemical etching with a current density of (a) 2 mA cm^{-2} (b) 4 mA cm^{-2}, (c) 8 mA cm^{-2}, (d) 16 mA cm^{-2}, (e) 32 mA cm^{-2}, and (f) 48 mA cm^{-2} for 2 min at room temperature.

The BSE-SEM images of the polished sintered Nd–Fe–B magnets after electrochemical etching with a current density of 2–48 mA cm^{-2} for 2 min at room temperature are shown in Figure 4.3. The Nd-rich triple points are preferentially etched at 2 mA cm^{-2} due to the more negative electrochemical potential caused by the higher Nd content (Figure 4.3a). The Nd-rich GBs connected with the triple points were also slightly etched. A longer etching time is needed to completely etch away the GBs surrounding the $Nd_2Fe_{14}B$ grains. Whereas the GBs were further etched with the increasing applied current density of 4 mA cm^{-2} (Figure 4.3b) and were completely etched at 8 mA cm^{-2} (Figure 4.3c) within 2 min, exposing the single $Nd_2Fe_{14}B$ grains on the polished magnet surface. Clearly, the average thickness of the gaps between the $Nd_2Fe_{14}B$ grains was, roughly, ~100 nm and ~300 nm with the etching current density of 4 and 8 mA cm^{-2}, respectively. As the thickness of the GB of the sintered Nd–Fe–B magnet is generally < 10 nm [176, 195-197], the much larger thickness of the gaps between the $Nd_2Fe_{14}B$ grains after etching at 4 and 8 mA cm^{-2} for 2 min indicates that the etching of the edges of the $Nd_2Fe_{14}B$ grains happened together with the etching of the GBs. When the applied current density was further increased from 16 to 48 mA cm^{-2}, aggressive etching on the $Nd_2Fe_{14}B$ grains is clearly observed (Figure 4.3d–f). Dense craters on the surface of the $Nd_2Fe_{14}B$ grains were formed by etching at 16 mA cm^{-2} (Figure 4.3d). When the current density of 32 mA cm^{-2} was applied, the morphology (Figure 4.3e) consists of electrochemically inert Nd/Dy oxides (white phase) and porous $Nd_2Fe_{14}B$ grains in which an average diameter of the pores is roughly 500 nm. A more porous structure of the $Nd_2Fe_{14}B$ grains with an average diameter of the pores around 1

μm was observed under the applied current density of 48 mA cm^{-2} (Figure 4.3f). Therefore, it can be concluded that for a constant etching time, a higher applied current density results in more aggressive etching of the $Nd_2Fe_{14}B$ grains. A low current density, e.g., 2 mA cm^{-2} could be applied with a long etching time to completely etch the GBs and consequently to obtain the $Nd_2Fe_{14}B$ grains.

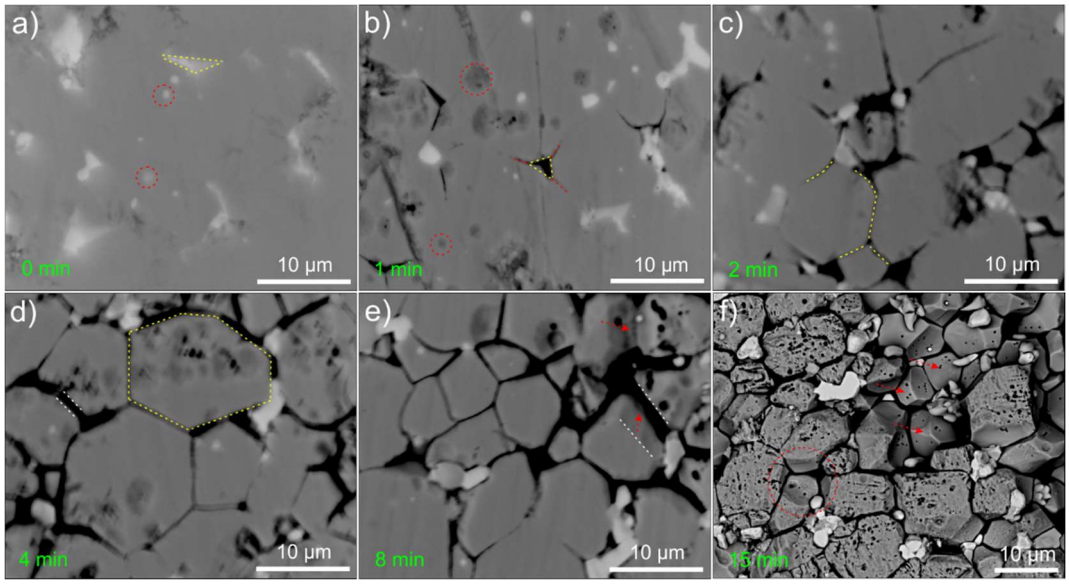

Figure 4.4: BSE-SEM images of the sintered Nd–Fe–B magnets after electrochemical etching with a current density of 2 mA cm^{-2} for (a) 0 min, (b) 1 min, (c) 2 min, (d) 4 min, (e) 8 min and (f) 15 min at room temperature.

Figure 4.4 shows the progression of the etching effect on the microstructure of a polished sintered Nd–Fe–B magnet surface when applying a current density of 2 mA cm^{-2} for 0–15 min at room temperature. The roundish (labelled by the red dashed circle, Figure 4.4a) and triangular (labelled by the yellow dashed triangle, also called a "triple point", Figure 4.4a) white phases present on the polished surface of the sintered Nd–Fe–B magnets (Figure 4.4a) with the GBs are Nd-rich phases, which are etched away first. Consequently, craters (labelled by the red dashed circle, Figure 4.4b) and an empty triple point (labelled by the yellow dashed triangle, Figure 4.4b) connecting with the partially etched GBs (labelled by red dashes, Figure 4.4b) were observed after etching for 1 min. The GBs surrounding the $Nd_2Fe_{14}B$ grains were further etched away when the etching time was extended to 2 min (labelled by the yellow dashes, Figure 4.4c). When the polished sintered Nd–Fe–B magnet was etched for 4 min under an applied current density of 2 mA cm^{-2}, the GBs were completely etched away, exposing the $Nd_2Fe_{14}B$ grains and leaving behind the Nd-based oxide phases (the white phase in the triple points of Figure 4.4d), which are not prone to electrochemical oxidation. The size of the $Nd_2Fe_{14}B$ grains varies from 5 μm to 10 μm. The gaps (labelled by the white dashes, Figure 4.4d) between the $Nd_2Fe_{14}B$ grains (the thickness of the gaps varies from ~500 nm to ~1 μm) were formed after preferential etching of the metallic phases in the GBs. The thicker gaps after etching than the thickness of the initial GBs (< 10 nm) [176, 195-197] indicate that some etching of the $Nd_2Fe_{14}B$ grain edges also occurred. The edges of the $Nd_2Fe_{14}B$ grains were further etched perpendicular to the polished surface with a prolonged etching time of 8 min (red dashed arrows, Figure 4.4e). When the sintered Nd–Fe–B magnet was etched for 15 min, the polished surface was progressively etched, resulting in a porous structure for the $Nd_2Fe_{14}B$ grains (Figure 4.4f). Some vacancies (e.g., the position labelled by a red dashed circle, Figure 4.4f) observed on

the magnet surface indicate that the $Nd_2Fe_{14}B$ grains detached from the rest of the magnet after the complete etching of the surrounding GBs. The second layer of the $Nd_2Fe_{14}B$ grains (labelled with red dashed arrows, Figure 4.4f) was much less damaged with the GB completely etched. This indicates that etching of the GBs of the sintered Nd–Fe–B magnet reached more than 2 layers of the $Nd_2Fe_{14}B$ grains to a depth of 10–20 µm within 15 min when applying a current density of 2 mA cm^{-2}.

4.1.4 The Etching Mechanism of the Sintered Nd–Fe–B Magnets

In order to understand the etching process in a three-dimensional space, a mechanism for the electrochemical etching of the sintered Nd–Fe–B magnet with metallic Nd at both the GBs and triple points in a water- and oxygen-free organic electrolyte is illustrated in Figure 4.5.

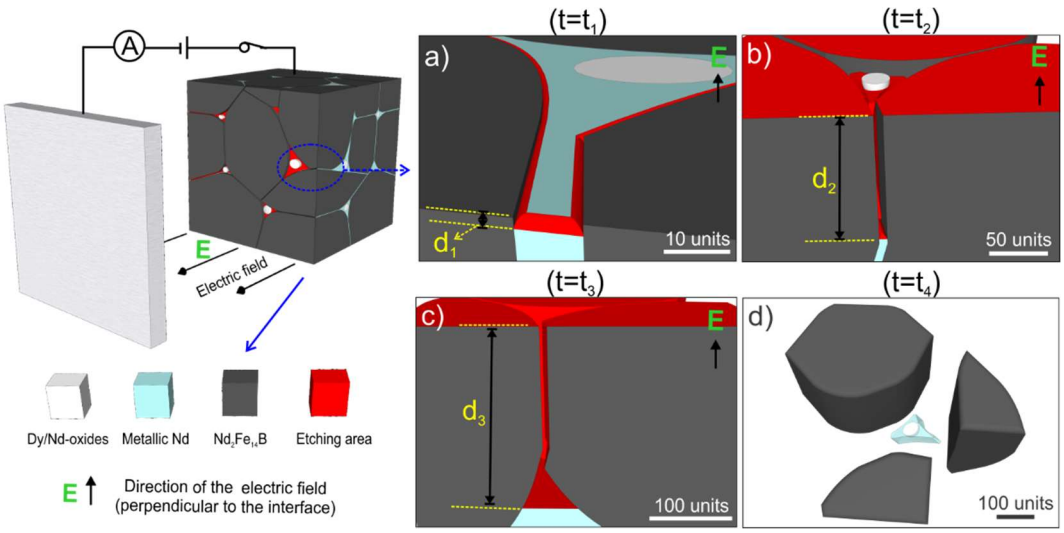

Figure 4.5: Schematic illustration of the microstructural evolution of a sintered Nd–Fe–B magnet with metallic Nd in the GBP during electrochemical etching/anodization in a water- and oxygen-free organic electrolyte.

For simplicity, only the planar surface of the magnet directly facing the cathode is considered to be subject to the electrochemical etching and the low current density (< 2 mA cm^{-2}) is considered to selectively etch the sintered magnets. At the very beginning $t = t_1$, the anodization begins with the etching of metallic Nd, most probably at the interfaces of the Nd-rich phase and the $Nd_2Fe_{14}B$ grains, as the electrochemical potential is always higher at the electrode edges [206]. As shown in Figure 4.5a at $t = t_1$ (red colored regions), an etching depth of d_1 is reached. Etching of the magnet proceeds until $t = t_2$, when a certain thickness (d_2) of the metallic Nd has been etched away, now exposing the $Nd_2Fe_{14}B$ grains (Figure 4.5b). At $t = t_2$, the metallic Nd in the triple points might not be etched completely, depending on its volume at the triple point, as shown in Figure 4.5b. The etching depth d for $t \rightarrow t_2$ increases. Consequently, the exposed area of the anode/magnet becomes larger with $t \rightarrow t_2$, which decreases the current density and the over-potential for etching the metallic Nd. As a result, the etching rate of the metallic Nd in the GB reduces with $t \rightarrow t_2$. When a constant current is applied and in order to keep the charge balanced, the etching of the $Nd_2Fe_{14}B$ grains needs to occur at d_2 at $t = t_2$ (Figure 4.5b, red-colored region). At $t = t_3$, the etching reaches a depth of d_3, at which point the etching of the $Nd_2Fe_{14}B$ grains proceeds both on the front interface and the side interfaces (Figure 4.5c, red-colored region) in parallel with the deeper etching of the Nd-rich phase. When the

latter is completely etched ($t = t_4$), the partially etched $Nd_2Fe_{14}B$ grains and the Dy/Nd-oxides detach from the magnet surface (Figure 4.5d).

4.1.5 Recovery of the $Nd_2Fe_{14}B$ Grains from the Sintered Nd–Fe–B Magnets

To monitor the overall etching process and to avoid etching the $Nd_2Fe_{14}B$ grains for high rates of recovery, electrochemical etching of a sintered Nd–Fe–B magnet with an applied current of 10 mA (the corresponding current density of 2 mA cm^{-2}) was conducted for 360 min. The magnetically collected particles are shown in Figure 4.6a. These are individual particles confirming that $Nd_2Fe_{14}B$ grains can be extracted through selective etching of the Nd–Fe–B magnet. The EDS result shows that the compositions of the grey phase (83.24 at.% Fe, 9.98 at.% Nd, 2.63 at.% Dy and 4.15 at.% Co) are similar to those of the initial polished magnet shown in Figure 4.1a.

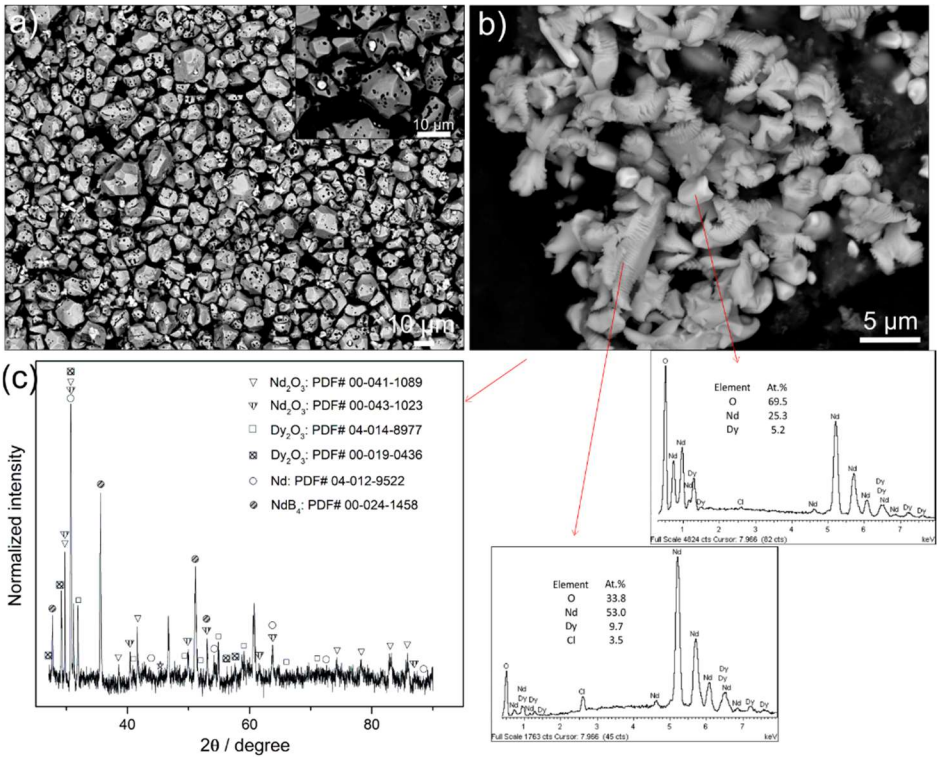

Figure 4.6: BSE-SEM images of (a) collected magnetic powder after electrochemical etching (360 min), (b) collected non-magnetic particles by filtration after the electrochemical etching (360 min) with EDS spectra and (c) the corresponding XRD pattern. Etching conditions: 10 mA (2 mA cm^{-2}), room temperature, no stirring.

For the 1.61 grams of the sintered Nd–Fe–B magnet treated at 10 mA (2 mA cm^{-2}) for 40 h, 1.08 grams of the $Nd_2Fe_{14}B$ grains were obtained. Accordingly, 67.2% of the Nd–Fe–B magnet was recovered in the form of the $Nd_2Fe_{14}B$ grains and the energy consumption per kilogram of the obtained $Nd_2Fe_{14}B$ grains was calculated to be 0.58 kWh. Around 20% of the $Nd_2Fe_{14}B$ grains was etched and dissolved into the electrolyte (assuming that the initial sintered Nd–Fe–B magnet contained 87% of $Nd_2Fe_{14}B$ grains [57]). This is caused by i) the decreasing over-potential for etching the metallic Nd during the etching process that forces the etching of the $Nd_2Fe_{14}B$ grains according to the etching mechanism (Figure 4.5) and ii) untimely removal of the $Nd_2Fe_{14}B$ grains from the magnet anode after the complete

etching of the surrounding GBP. However, the recovery of the $Nd_2Fe_{14}B$ grains can be further improved by using an ultrasonic bath during the electrochemical etching process to remove the $Nd_2Fe_{14}B$ grains from the magnet anode in time.

The non-magnetic particles collected by filtrating the electrolyte after electrolytic etching are presented in Figure 4.6b. The particles in two different geometries, round shape and elongated ribbed shape, are observed. The round particles and the elongated ribbed particles mainly consist of Nd, Dy and O, in which the oxygen content (O/(Nd + Dy + O)) is ~69 at.% and ~35 at.% (Figure 4.6b). The spectra also show the Cl (< 3.5 at.%) coming from the incomplete washing of the particles with DMF. It must be noted that boron (B) is not shown in the EDS spectra due to it being a light element, which cannot be detected by EDS. Figure 4.6c shows the XRD pattern of the non-magnetic particles obtained by filtration after anodic etching of the sintered Nd–Fe–B magnet. The confirmed phases are Nd_2O_3 (PDF# 00-041-1089 and PDF# 00-043-1023), Dy_2O_3 (PDF# 04-014-8977 and PDF# 00-019-0436), Nd (PDF# 04-012-9522) and NdB_4 (PDF# 00-024-1458). Combined with the EDS results, the round particles contain Nd_2O_3 and Dy_2O_3 phases, while the elongated ribbed particles consist of Nd_2O_3, Dy_2O_3, Nd and NdB_4 phases.

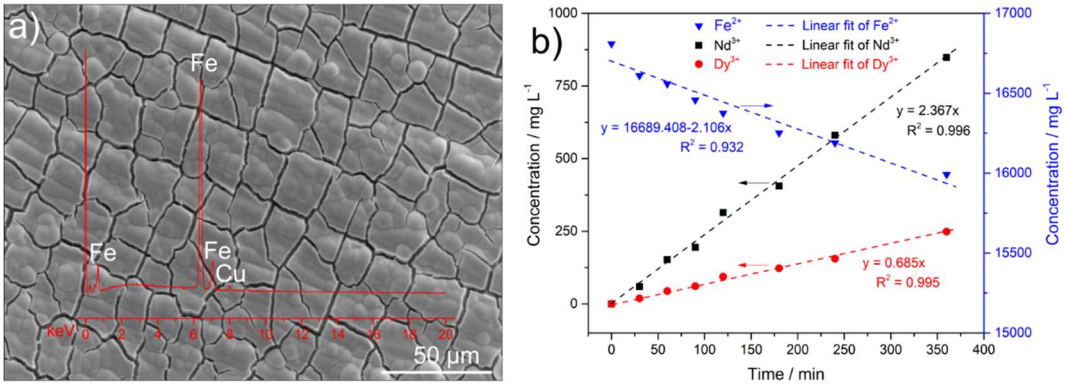

Figure 4.7: (a) The SE-SEM image of the deposit on the cathode with EDS spectrum (inset). (b) The influence of etching time on the concentrations of Fe^{2+} (blue curve), Nd^{3+} (black curve) and Dy^{3+} (red curve) and in the electrolyte. Conditions: Applied current 10 mA, the corresponding anode current density: 2 mA cm^{-2} and cathode current density: 1 mA cm^{-2}, room temperature, no stirring.

On the cathode, a deposit was obtained after a deposition of 60 min on a Cu substrate/cathode (in the period 301 to 360 min) which is shown in Figure 4.7a. Some cracks are observed from the secondary electron (SE)-SEM image of the deposited film. The EDS spectrum (inset of Figure 4.7a) indicates that only Fe was deposited on the Cu substrate. This is because the concentration of Fe^{2+} in the electrolyte was much higher than that of Nd^{3+} and Dy^{3+}, and the standard electrode potential of Fe^{2+}/Fe (–0.447 V) is much lower than those of RE^{3+}/RE (< –2.2 V), both of which result in the preferential deposition of Fe. Additionally, the current efficiency of the Fe deposition was 99.6%, because of the use of DMF, which is electrochemically stable, avoiding the hydrogen evolution that generally happens in aqueous solutions [138]. The concentrations of dissolved Nd^{3+}, Dy^{3+} and Fe^{2+} are monitored along with the etching time of 360 min (Figure 4.7b) at the applied current of 10 mA (the corresponding anode current density is 2 mA cm^{-2}). It can be seen from Figure 4.7b that the concentrations of Nd^{3+} and Dy^{3+} in the electrolyte increase with the increasing etching time and exhibit a linear relationship (correlation coefficient, R^2 = 0.996 and 0.995, respectively), from which the etching rate of the Nd^{3+} and Dy^{3+} are calculated as 2.367 and 0.685 mg L^{-1} min^{-1}, respectively. The concentration

of Fe^{2+}, in contrast, decreases with the increasing etching time, which indicates that the consumption of Fe^{2+} in the electrolyte due to electrodeposition on the cathode was larger than the amount of Fe^{2+} dissolved into the electrolyte by etching from the anode. The net consumption rate of Fe^{2+} is calculated as 2.106 mg L^{-1} min^{-1}. Therefore, the only chemical consumption for recovering the $Nd_2Fe_{14}B$ grains is $FeCl_2$.

4.1.6 Recycling Route for the Sintered Nd–Fe–B Magnets Based on the Electrochemical Recovery of the $Nd_2Fe_{14}B$ Grains

A recycling route for the sintered Nd–Fe–B magnet scraps is proposed based on the electrochemical etching (Figure 4.8). The obtained $Nd_2Fe_{14}B$ grains are used as raw materials for new magnet making. The REE-containing electrolyte and REE-based particles can be further treated by the conventional hydrometallurgical process for high purity of > 99% REEs recovery [47, 71] followed by molten salt electrolysis [101] for making RE metals/alloys which can be used together with the obtained $Nd_2Fe_{14}B$ grains for new sintered Nd–Fe–B magnet making. DMF can be recovered by distillation and re-used in a closed-loop with minimized safety risk and environmental impact. Upon that the overall REEs mass balance from the initial magnet is 100% preserved which forms a circular economy.

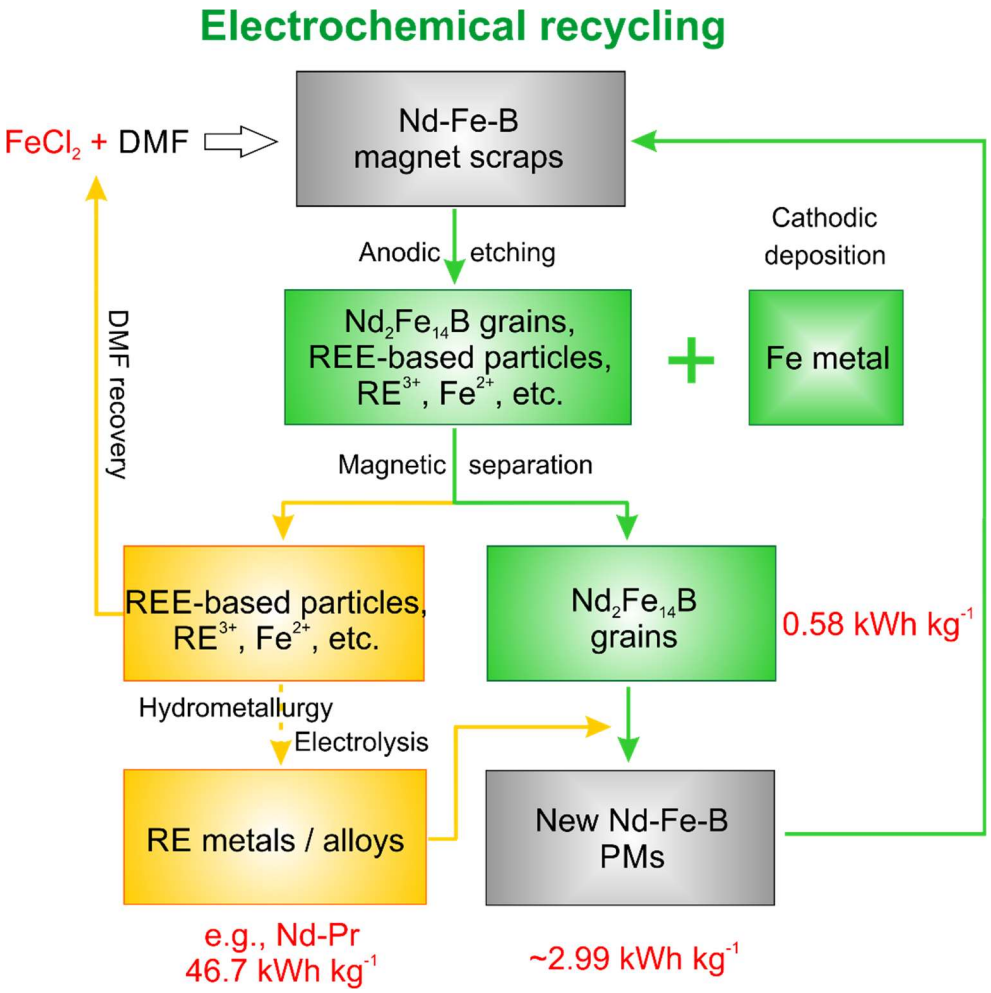

Figure 4.8: Flowsheet of electrochemical recycling of the sintered Nd–Fe–B magnets.

Table 4.1: Energy consumption of making sintered Nd–Fe–B magnets via different recycling routes.[a]

Route	Energy consumption (kWh kg^{-1})	References
Hydrometallurgy	30.0~33.4	[207]
Direct re-use	~3.0	[207]
Electrochemical recycling	~2.99	This study

[a] The detailed calculation of energy consumption is based on the available literature.

To make new sintered Nd–Fe–B magnets using the recovered $Nd_2Fe_{14}B$ grains as the starting material, the addition of RE metals or alloys, e.g., Nd hydride [65] and Nd–Pr hydride [207] are expected to reach fully dense magnets with the formation of GBs. 1.9 wt.% of Nd–Pr hydride/cycle is generally added in direct re-use methods to compensate for the loss of the Nd with the continuous recycling cycles due to Nd_2O_3 formation in the GBs [65, 207]. Upon that the energy consumption for producing 1.0 kg of the sintered Nd–Fe–B magnets via direct re-use methods is ~3.0 kWh when using the direct re-use methods, with 1.9 wt.% of Nd–Pr hydride additive [207]. The total energy consumption for making new sintered Nd–Fe–B magnets via the proposed electrochemical recycling route, therefore, includes: i) the energy consumed for recovering the $Nd_2Fe_{14}B$ grains, ii) the energy consumed for additive RE metals or alloys making [207], here we are considering the double addition of the Nd–Pr hydride (~4 wt.% Nd–Pr hydride) as we have to compensate for the whole Nd-rich GBP, and, iii) the energy consumed for the new sintered Nd–Fe–B magnet processing steps. The energy consumption per kilogram for making Nd–Pr hydride associated with mining the ores is 46.7 kWh [207], and the energy consumption per kilogram of the obtained $Nd_2Fe_{14}B$ grains was calculated to be 0.58 kWh. Considering also the magnet processing steps, such as sintering (0.46 kWh kg^{-1}) and annealing (0.08 kWh kg^{-1}) [207], the total energy consumption of the magnet-manufacturing process with blending 4 wt.% of Nd–Pr hydride (1.87 kWh) using the proposed electrochemical recycling route is estimated to be ~2.99 kWh kg^{-1}. It has to be emphasized that the proposed electrochemical recycling route requires a constant amount of the additive per cycle irrespective of the number recycling cycles as the Nd-rich phase does not pick up oxygen while recycling, unlike in the direct re-use methods. Consequently, higher total energy consumption is expected for direct re-use methods with the repeating recycling cycles. For comparison, the energy consumption of the hydrometallurgical route is regarded the same as that of the traditional magnet-manufacturing route associated with mining the ores, due to their similar production process [40]. The total energy consumption for producing 1.0 kg of the sintered Nd–Fe–B magnets is 30.0–33.4 kWh using the traditional magnet-manufacturing route [207] (Table 4.1) if we consider the conventional additive of the Nd–Pr hydride. However, the additive can be replaced by other alloys, such as Nd–Cu [176] and Ce [208] that would lead to a much lower energy footprint. As a whole, the proposed electrochemical recycling route proves itself to be comparable in energy demand to the direct re-use methods, but it proves to be more sustainable in the long term.

In this section, we propose a facile and cost-effective electrochemical recycling process that selectively recovers the $Nd_2Fe_{14}B$ grains from the sintered Nd–Fe–B magnets at room temperature. The anodic etching mechanism is based on fine-tuning of the applied current density < 5 mA cm^{-2} to exploit the etching priority series of the phases present in the pristine sintered Nd–Fe–B magnet: metallic Nd > intergranular $NdFe_4B_4$ > matrix $Nd_2Fe_{14}B$, which allows the preferential etching of their surrounding REE-rich GBs, leaving the individual $Nd_2Fe_{14}B$ grains behind for magnetic separation. The total energy

consumption of the proposed electrochemical recycling route is estimated to be ~2.99 kWh kg^{-1} which is, in the long term, expected to be economically more feasible while offering considerably more flexibility.

4.2 Electrochemical Deposition of the Nd–Fe from an Ionic Liquid

In Section 4.1, selective etching of the sintered Nd–Fe–B magnets on the anode ends up with $Nd_2Fe_{14}B$ grains, REE-based particles and REE-containing electrolyte. According to the proposed recycling route for the sintered Nd–Fe–B magnet scraps (Figure 4.8), the REE-containing electrolyte can be further treated by distillation to recover DMF for re-use and REE-based chlorides that are ready for the conventional hydrometallurgical process for high purity of > 99% REEs recovery [47, 71] followed by molten salt electrolysis [101] for making RE metals/alloys. Alternatively, electrodeposition of RE–TM, e.g., Nd–Fe, alloys at mild temperatures using the REE-based chlorides as metal sources would, theoretically, be a promising RE alloy recycling route and could act as an alternative of the direct PMs synthesis method. Compared to the hydrometallurgical process, it would avoid the multi-step REE separation and reduction processes that consume large amounts of chemicals and thermal energy.

However, it is very difficult to deposit REEs in a metallic form because they generally have a negative reduction potential of < –2.3 V *vs.* SHE [135]. There are literature reports about the electrodeposition of RE alloys using DESs and organic solvents [153-155, 177]. But here the organic chemicals are generally volatile, casting doubt on the environmental credentials of the process. ILs with their high ionic conductivity, wide electrochemical window, lack of volatility and a very low vapor pressure, also look promising [178].

In this section, the IL, [EMIM][DCA], was used as the electrolyte for the electrodeposition of the Nd and Fe. [EMIM][DCA] is an oxygen-free IL that exhibits a low viscosity (21 cP at 20 ℃), which ensures a high mass-transfer efficiency and a high conductivity, both of which are beneficial for electrodeposition [209]. DCA-based ILs with a good coordination ability were already applied to RE metal electrodeposition [210], as metal chlorides are found to dissolve well in the DCA-based ILs by forming complexed anions [211]. The electrochemical behaviors of the Nd^{3+} and Fe^{2+} were investigated, from which a co-deposition mechanism for RE–TM was proposed with a kinetic model. A detailed study using TEM combined with electron-energy-loss spectroscopy (EELS) was performed in order to locally investigate the chemical composition of the deposit and the valence state of the deposited Nd.

4.2.1 Electrochemical Behaviors of Fe^{2+} and Nd^{3+} in [EMIM][DCA] IL

The CV was used to investigate the electrochemical behaviours of the Fe^{2+} and Nd^{3+} in [EMIM][DCA] as shown in Figure 4.9.

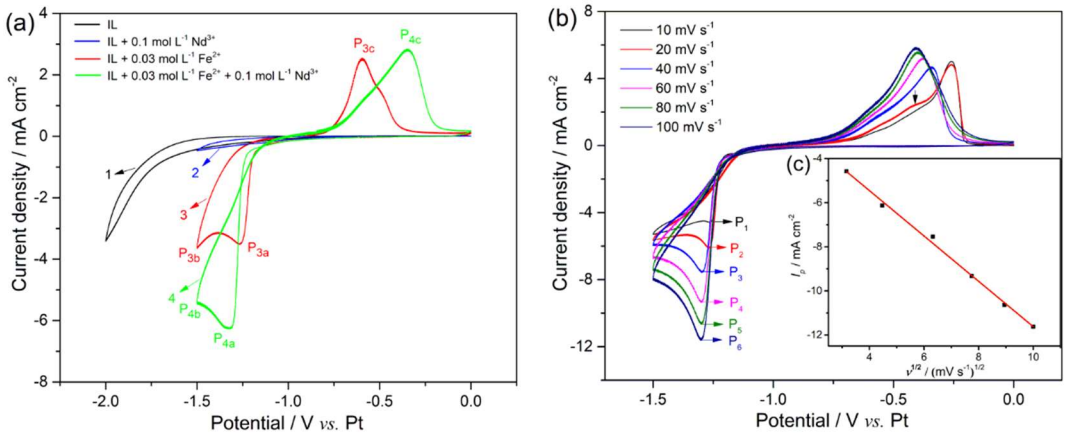

Figure 4.9: (a) CV of a Pt electrode in (1) [EMIM][DCA], (2) $FeCl_2$ (0.03 mol L^{-1})-[EMIM][DCA], (3) $NdCl_3$ (0.1 mol L^{-1})-[EMIM][DCA] and (4) $FeCl_2$ (0.03 mol L^{-1})-$NdCl_3$ (0.1 mol L^{-1})-[EMIM][DCA], 110 ℃, 40 mV s^{-1}, (b) CV of a Pt electrode in $FeCl_2$ (0.03 mol L^{-1})-$NdCl_3$ (0.1 mol L^{-1})-[EMIM][DCA] with a scan rate from 10–100 mV s^{-1} and (c) Plot of I_p–$v^{1/2}$, 110 ℃.

The black curve (curve 1) in Figure 4.9a shows the CV of the [EMIM][DCA] solution at a scan rate of 40 mV s^{-1}. The current starts to increase from –1.5 V *vs.* Pt and this can be attributed to the decomposition of the $[EMIM]^+$ cation [212], which indicates the cathodic limit potential of the [EMIM][DCA]. For this reason, the potential scan was stopped at –1.50 V in all the subsequent CVs. In the blue curve (curve 2) that represents the Nd^{3+} solution, there is no significant current increase observed up to –1.50 V, which indicates that the Nd^{3+} reduction is not induced on its own in this IL system, most probably due to the very negative reduction potential of Nd^{3+} [135]. It should be noted that the current increases from –1.25 V to –1.5 V in both curve 1 and curve 2 that is typically observed in the CV curves of the ionic liquids, called potential-dependent double layer charging current [213]. With the increasing potential, the charging current response of the double layer increases accordingly. The red curve (curve 3) and the green curve (curve 4) are the CVs of the $FeCl_2$-[EMIM][DCA] and $FeCl_2$-$NdCl_3$-[EMIM][DCA], respectively. The starting point for the Fe^{2+} reduction in curve 3 is –1.19 V, while the reduction peak (P_{3a}) appears at –1.25 V and the corresponding oxidation peak (P_{3c}) is present at –0.60 V. A small current shoulder appeared after P_{3c} at around –0.5 V is observed. Similar reports could be found from other studies [214, 215] which attributed the shoulder to a strong interaction, such as the desorption [213] of the Fe^{2+} complex on the electrode surface. In curve 4, the current increase that can be ascribed to the starting point for the Fe^{2+} and Nd^{3+} co-reduction is observed at –1.25 V, while the reduction peak (P_{4a}) appears at –1.30 V, with a much higher peak current, both of which are shifted negatively compared to curve 3. The reason for the more negative starting point for the Fe^{2+} and Nd^{3+} co-reduction (at –1.20 V) is probably due to the reduced coverage of Fe^{2+} on the cathode as a result of the addition of Nd^{3+}, according to the Nernst equation [206], and the more negative reduction potential is due to the more negative reduction potential needed for the Nd^{3+}. The peak current for Nd^{3+} and Fe^{2+} (6.5 mA cm^{-2} at –1.30 V) that is higher than in the case of Fe^{2+} reduction (3.5 mA cm^{-2} at –1.25 V) indicates that the reduction of Nd^{3+} contributed to the current increase. Because Nd^{3+} could not be reduced by itself as described in curve 2, the peak current increase of curve 4 can be only ascribed to the co-deposition of Nd and Fe, compared to that of curve 3. It should be noted that the peaks of P_{3b} in curve c and P_{4b} in curve d are ascribed to the electrochemical decomposition of

the IL. Because it has been shown from the black curve which is for pure IL that the decomposition of the IL should start from –1.5 V. The decomposition potential for the IL shifted positively from –1.5 V to ~–1.4 V after the Fe^{2+} deposition peak. It has been already reported that zero-valence Fe is able to catalyze the decomposition of imidazolium cations [216, 217] and upon that P_{3b} and P_{4b} coming after the peak of Fe^{2+} deposition and Fe^{2+} + Nd^{3+} co-deposition, respectively, could be ascribed to the catalytic decomposition of the IL by Fe. The oxidation peak (P_{4c}) at –0.33 V in curve d is more positive and wider, with a higher peak current than those in curve 3, which can be attributed to the co-reduction of Nd and Fe.

Figure 4.9b shows the CV of $FeCl_2$-$NdCl_3$-[EMIM][DCA] at different scan rates, ranging from 10 mV s^{-1} to 100 mV s^{-1}. The reduction peaks shift from –1.20 V to –1.30 V with an increasing scan rate, where the peak current increases from 5.0 mA cm^{-2} to 12.0 mA cm^{-2}. The oxidation peaks of the Nd and Fe deposits in the reversed scan are observed in the potential range –0.81 V to –0.22 V and show an increase in intensity and a shift towards a more negative potential at higher scan rates. This indicates that the oxidation of Nd and Fe is faster at a higher scan rate due to the faster electron-transfer rate. A broad shoulder and a secondary oxidation peak (where the arrow points in Figure 4.9b) in the oxidation zone are also developed at higher scan rates, as a result of the Nd and Fe compounds beginning to form, which can oxidize as separate phases at high scan rates [218]. The potential difference between the cathodic (P_{4a}) and the anodic (P_{4c}) peak of Nd–Fe is larger than 800 mV (Figure 4.9a, curve 4). A plot of I_p–$v^{1/2}$ is shown in Figure 4.9c, and can be described by the Randles-Sevcik equation [206, 219], which categorises the Nd and Fe co-reduction process as irreversible and controlled by diffusion.

4.2.2 Theoretical Mathematical Model of the RE–TM Co-Deposition Based on the "Transition-State Theory"

The results obtained from the CV study presented in Figure 4.9 show the co-reduction of Nd (RE) together with the deposition of Fe (TM); however, the theoretical background to support the processes of how the RE^{3+} is reduced inductively with TM^{2+} remains unclear. It is a fact that individual deposition of pure Nd metal is extremely difficult due to its very negative reduction potential. However, Nd^{3+}, as well as many other REEs, can be deposited together with one or more metals from the TM group [179-181]. This electrodeposition phenomenon is called the "induced co-deposition". It was found that in DESs, Nd^{3+} cannot be reduced alone to Nd^0, but it can be inductively co-deposited with Fe^{2+} [154, 155]. These studies indicated that co-deposition is possible, using a potential that is much more positive than that for the individual deposition of the REEs. However, an explanation for why RE^{3+} could be reduced in the presence of Fe^{2+} at a more positive potential was not presented in detail.

It is well known that some elements with negative electrochemical standard potentials cannot be electrodeposited in metallic form from aqueous solutions, but they can be co-deposited with TMs, forming alloys [165]. For example, metallic tungsten cannot be deposited alone from an aqueous solution, but it does deposit in the presence of $Fe^{2+/3+}$ ions in the solution, forming metallic alloys [166-168]. For Fe–W co-deposition, three possible co-deposition mechanisms have been proposed. A "catalytic reduction" theory was proposed by Holt and Vaaler [171] to explain the reduction of aqueous tungstate solutions in the presence of zero-valence TM elements (i.e., Ni, Co and Fe). In this process, the reduction of TM^{2+} to TM^0 occurs first; it then catalyzes the tungsten deposition until the surface is covered with it, preventing any further tungsten deposition. This process continues until a new layer of the TM element forms. The observation of laminated structures was the basis for this concept by Younes and Gileadi [182], although how the

zero-valence state of a TM element catalyzes tungsten deposition was not elaborated. Another mechanism, proposed by Clark and Lietzke [172], emphasizes the role of hydrogen, where there is an initial deposition of a partially reduced tungstate film on the cathode, followed by the catalytic reduction of this film by hydrogen in the presence of freshly deposited Fe, Co, or Ni. Without the inducing element, the tungstate ion is only partially reduced ($WO_4^{2-} \rightarrow WO_2$) [220], and due to its low over-potential with respect to hydrogen evolution, it cannot be further reduced. The third mechanism is based on the formation of TM tungstate complexes that are precursors to tungsten alloys, as introduced by Younes-Metzler et al. [173]. In this concept mixed-metal soluble complexes were used by adding a complexing regent of citrate [166] or gluconate [174] as a prerequisite for the TM–W co-deposition. The latter two mechanisms rely on active hydrogen produced by the electrolysis of water and the formation of TM–tungstate coordination compounds with certain complexing regents that help to realize the co-deposition process. The "catalytic reduction" theory opens a way to further investigate the co-deposition of the RE–TM in both aqueous and non-aqueous solutions.

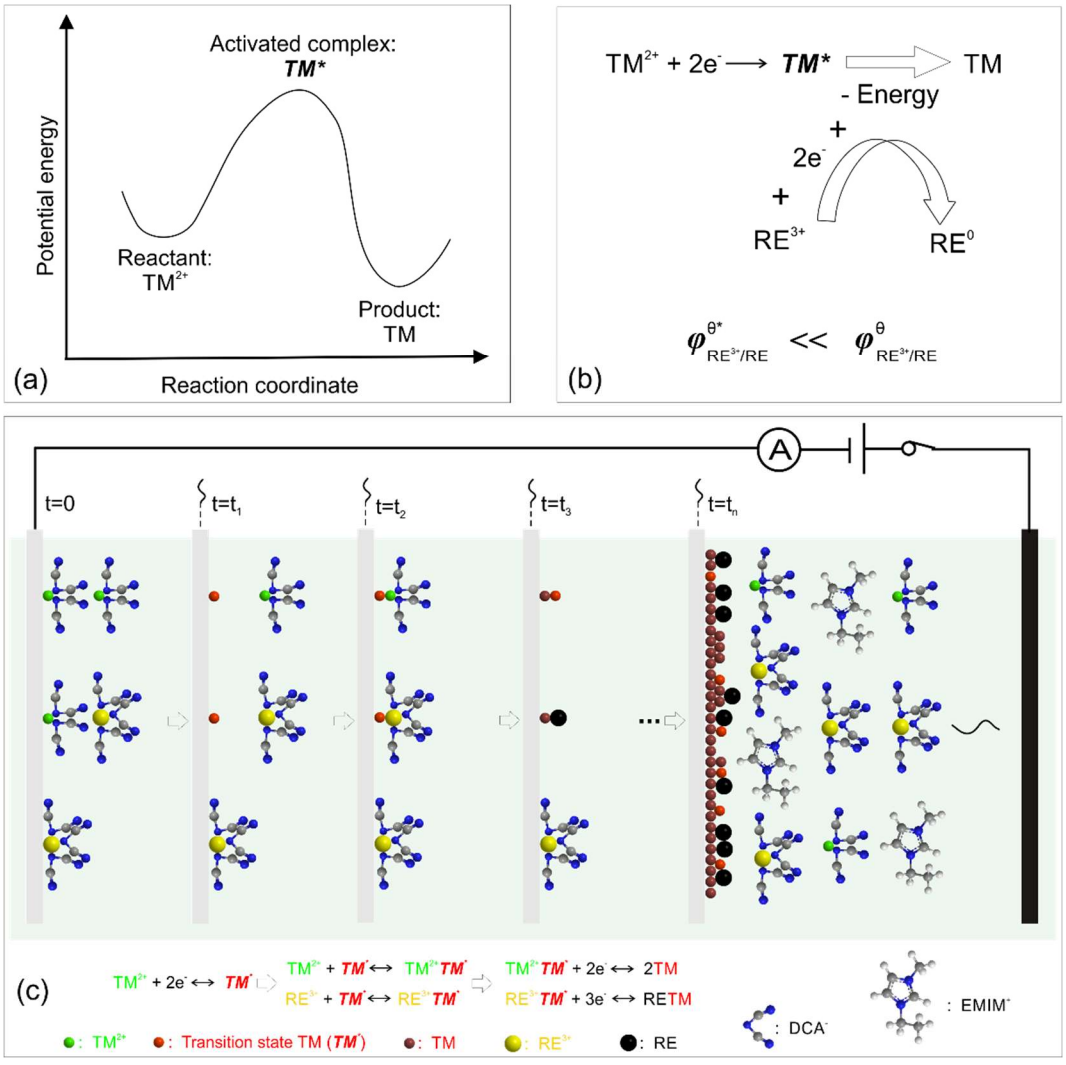

Figure 4.10: (a) Free energy changes during a reaction, (b) reaction paths of RE–TM co-deposition process, and (c) schematic of the induced co-deposition process in a locally enlarged view.

We assume that the mechanism for RE–TM co-deposition might be similar to that of TM–W co-deposition. Inspired by the "catalytic reduction" theory of W–Fe, here we introduce an induced co-deposition mechanism for RE–TM based on the transition-state theory, which assumes that the transition-state TM ($\boldsymbol{TM}^*$) is the catalyzer for the RE^{3+} reduction to RE^0. With this assumption, the influence of the substrate on the deposition of the RE–TM is neglected. According to Henry Eyring [221], reactions proceed through a well-defined transition state or activated complex, as shown in Figure 4.10a. The standard free-energy change in the transition from the reactant [e.g., TM^{2+}] to the activated complex (e.g., $\boldsymbol{TM}^*$) is ΔG_R, whereas the complex is elevated above the product (e.g., TM) by ΔG_P. Therefore, the transition-state complex is ready to release some energy (G_P) to reach a thermodynamically stable state (i.e., the ground state). It should be noted the quantitative energy transferred from one atom to another is still not clear yet, as the modern investigations of the validity of the transition-state-theory are still going on [222-224]. The most common postulate is called the strong-collision assumption that large enough amounts of energy are transferred in molecular (atomic in this case) collisions [225]. Based on this theory, an assumption is made that the TM^{2+} is reduced first to the zero valence state with a high energy ($\boldsymbol{TM}^*$, activated state or transition state, shown in Figure 4.10b), from which some of the energy can be transferred to the RE^{3+} to reduce its energy barrier, which makes it ready to be reduced at a much more positive potential ($\varphi^{\theta*}_{RE^{3+}/RE}$) than its standard electrode potential ($\varphi^{\theta}_{RE^{3+}/RE}$). Based on this mechanism, at the very beginning of the electrodeposition, the first few atomic layers of the deposit have to be metallic TM with high energy ($\boldsymbol{TM}^*$), which then subsequently catalyses the reduction of the RE^{3+}.

The concentration of $\boldsymbol{TM}^*$ formed by the electrodeposition proposed in the above-mentioned model directly influences the reduction of RE^{3+}, as the formation of $\boldsymbol{TM}^*$ is controlled by the TM^{2+} concentration in the electrolyte and the applied potential/current density. Based on this, the functional relationship between the molar fraction of REE in the deposit and the concentration of TM^{2+} in the bulk solution, as well as the applied potential/current density, can be established. The solvation behavior and stable species of RE chlorides in DCA-based based ILs still need to be elaborated in the future, although the $[Fe(DCA)_5Cl]^{4-}$ complex was confirmed as the main species in [EMIM][DCA] IL by S. Begel [226]. According to the report from Q. B. Zhang [210] who speculated the $[La(DCA)_4]^-$ complex as the stable species in 1-butyl-3-methylimidazolium dicyanamide ([BMIM][DCA]) IL, the $[Nd(DCA)_4]^-$ complex is to be expected as the main species due to the chemical similarity of Nd and La. In order to clearly present the induced co-deposition process, the speciation of the Nd^{3+} and Fe^{2+} in [EMIM][DCA] are simplified as $Nd(DCA)_3$ and $Fe(DCA)_2$ which are illustrated in Figure 4.10c. Before the deposition ($t = 0$), both the TM^{2+} and RE^{3+} are adsorbed onto the cathode surface and are ready to be reduced. Once a potential or a current is applied ($t = t_1$), TM^{2+} is first reduced to $\boldsymbol{TM}^*$, whereas the TM^{2+} and RE^{3+} in the vicinity will compete to alloy with it. During the alloying, the energy is transferred from $\boldsymbol{TM}^*$ to TM^{2+} and RE^{3+} ($t = t_2$) to form the complexes of $\boldsymbol{TM}^*{\cdot}TM^{2+}$ and $\boldsymbol{TM}^*{\cdot}RE^{3+}$, which are ready to be further reduced at $t = t_3$. Since the specific amount of energy from $\boldsymbol{TM}^*$ can be absorbed by both RE^{3+} and TM^{2+}, at any instant of time t_n, all the involved reactions from t_0 to t_3 are happening at the same time, and can be expressed as follows:

i_1:
$$TM^{2+} + 2e^- \overset{k_1}{\leftrightarrow} \boldsymbol{TM}^* \tag{4.6}$$

$$RE^{3+} + \boldsymbol{TM}^* \overset{k_a}{\leftrightarrow} \boldsymbol{TM}^*{\cdot}RE^{3+} \tag{a}$$

$$TM^{2+} + \boldsymbol{TM}^* \overset{k_b}{\leftrightarrow} \boldsymbol{TM}^*{\cdot}TM^{2+} \tag{b}$$

$$\boldsymbol{TM}^{*} \overset{k_c}{\leftrightarrow} \mathrm{TM}+\mathrm{Energy} \tag{c}$$

i_2: $$\boldsymbol{TM}^{*}\cdot\mathrm{RE}^{3+}+3e^{-} \overset{k_2}{\leftrightarrow} \mathrm{TM}\cdot\mathrm{RE} \tag{4.7}$$

i_1': $$\boldsymbol{TM}^{*}\cdot\mathrm{TM}^{2+}+2e^{-} \overset{k_1}{\leftrightarrow} \boldsymbol{TM}^{*}\cdot\mathrm{TM} \tag{4.8}$$

$$\mathrm{RE}^{3+}+\boldsymbol{TM}^{*}\cdot\mathrm{TM} \overset{k_a}{\leftrightarrow} \boldsymbol{TM}^{*}\cdot\mathrm{TM}\cdot\mathrm{RE}^{3+} \tag{a}'$$

$$\mathrm{TM}^{2+}+\boldsymbol{TM}^{*}\cdot\mathrm{TM} \overset{k_b}{\leftrightarrow} \boldsymbol{TM}^{*}\cdot\mathrm{TM}\cdot\mathrm{TM}^{2+} \tag{b}'$$

$$\boldsymbol{TM}^{*}\cdot\mathrm{TM} \overset{k_c}{\leftrightarrow} 2\mathrm{TM}+\mathrm{Energy} \tag{c}'$$

i_2': $$\boldsymbol{TM}^{*}\cdot\mathrm{TM}\cdot\mathrm{RE}^{3+}+3e^{-} \overset{k_2}{\leftrightarrow} \mathrm{TM}\cdot\mathrm{TM}\cdot\mathrm{RE} \tag{4.9}$$

i_1'': $$\boldsymbol{TM}^{*}\cdot\mathrm{TM}\cdot\mathrm{TM}^{2+}+2e^{-} \overset{k_1}{\leftrightarrow} \boldsymbol{TM}^{*}\cdot\mathrm{TM}\cdot\mathrm{TM} \tag{4.10}$$

……

where k_1 and k_2 are the electrochemical rate constants, and k_a, k_b and k_c are the equilibrium constants.

Since the lifetimes for the activated species are very short (a mean life of 10^{-14} to 10^{-13} s [221]), the complex reactions of $\boldsymbol{TM}^{*}$ with RE^{3+} and TM^{2+} are considered to be in equilibrium at all times and the corresponding reverse reaction rates are neglected compared to the forward reaction rates. Therefore, the Tafel kinetics is assumed to be valid for these reactions, the partial current densities, i_j, can thus be expressed as a function of the kinetic constants, k_j:

$$i_j=n_jAFk_jc_j(1-\theta_j)e^{-\alpha_j\eta_jF/RT}$$

where n_j is the number of electrons transferred in the electrochemical reaction j, where $n_1 = n_1' = n_1'' = 2$, $n_2 = n_2' = n_2'' = 3$ in these cases, A is the frequency factor, F is the Faraday constant, c_j is the ion concentration in the bulk solution, θ_j is the adsorption coverage, α_j is the transfer coefficient, η_j is the over-potential, R is the universal gas constant, and T is the absolute temperature.

Since most of the surface area is covered by the IL, the surface coverage of TM^{2+} and RE^{3+} with their intermediates is considered small; therefore, we make the term $1-\theta_j$ constant as $1-\theta$ and let $f = F/RT$. The corresponding equations are as follows:

$$i_1=2AFk_1(1-\theta)\mathrm{c}(\mathrm{TM}^{2+})e^{-\alpha_1\eta_1f} \tag{4.11}$$

$$c(\boldsymbol{TM}^{*}\cdot\mathrm{RE}^{3+})=k_ac(\boldsymbol{TM}^{*})c(\mathrm{RE}^{3+}) \tag{4.12}$$

$$c(\boldsymbol{TM}^{*}\cdot\mathrm{TM}^{2+})=k_bc(\boldsymbol{TM}^{*})c(\mathrm{TM}^{2+}) \tag{4.13}$$

$$c(\mathrm{TM})=k_cc(\boldsymbol{TM}^{*}) \tag{4.14}$$

$$i_2=3AFk_2(1-\theta)c(\boldsymbol{TM}^{*}\cdot\mathrm{RE}^{3+})e^{-\alpha_2\eta_2f} \tag{4.15}$$

$$i_1'=2AFk_1(1-\theta)c(\boldsymbol{TM}^{*}\cdot\mathrm{TM}^{2+})e^{-\alpha_1\eta_1f} \tag{4.16}$$

$$c(\boldsymbol{TM}^{*}\cdot\mathrm{TM}\cdot\mathrm{RE}^{3+})=k_a c(\boldsymbol{TM}^{*}\cdot\mathrm{TM})\,c(\mathrm{RE}^{3+}) \tag{4.17}$$

$$c(\boldsymbol{TM}^{*}\cdot\mathrm{TM}\cdot\mathrm{TM}^{2+})=k_b c(\boldsymbol{TM}^{*}\cdot\mathrm{TM})\,c(\mathrm{TM}^{2+}) \tag{4.18}$$

$$c(2\mathrm{TM})=k_c c(\boldsymbol{TM}^{*}\cdot\mathrm{TM}) \tag{4.19}$$

$$i_2^{'}=3AFk_2(1-\theta)\,c(\boldsymbol{TM}^{*}\cdot\mathrm{TM}\cdot\mathrm{RE}^{3+})\,e^{-\alpha_2\eta_2 f} \tag{4.20}$$

$$i_1^{''}=2AFk_1(1-\theta)\,c(\boldsymbol{TM}^{*}\cdot\mathrm{TM}\cdot\mathrm{TM}^{2+})\,e^{-\alpha_1\eta_1 f} \tag{4.21}$$

……

Clearly,

$$\frac{i_1^{'}}{i_1}=\frac{i_1^{''}}{i_1^{'}}=\cdots=\frac{i_1^{n}}{i_1^{n-1}}=k_b c(\boldsymbol{TM}^{*})=\frac{i_2^{'}}{i_2}=\frac{i_2^{''}}{i_2^{'}}=\cdots=\frac{i_2^{n}}{i_2^{n-1}} \tag{4.22}$$

Therefore, for simplicity, the current efficiency is assumed as 100%, and the total current density i_t can be expressed as:

$$i_t=i_1+i_2+i_1^{'}+i_2^{'}+i_1^{''}+i_2^{''}+\cdots+i_1^{n}+i_2^{n}=\frac{1-[k_b c(\boldsymbol{TM}^{*})]^{n+1}}{1-k_b c(\boldsymbol{TM}^{*})}(i_1+i_2) \tag{4.23}$$

Since the reactions (4.6), (a), (b), (c) and (4.7) are considered as a unit that is repeated by the reaction (4.8), (a)', (b)', (c)' and (4.9) (second unit) and the reactions afterwards (the rest units). In terms of the calculation of the molar fraction of REE (X_{RE}) in the deposit, e.g., the alloy, X_{RE} should always be the same in all units. Thus, only one unit can be considered for the calculation. At any time interval, Δt, the number of electrons resulting from the total concentration change of the reduced TM ($c(\mathrm{TM})_{\mathrm{T}}$) is equal to the electrons flowing through i_1, while the number of electrons for the RE^{3+} reduction is equal to the electrons flowing through i_2. Therefore,

$$\frac{i_1\Delta t}{n_1 FV}=\Delta c(\boldsymbol{TM}^{*})+\Delta c(\boldsymbol{TM}^{*}\cdot\mathrm{RE}^{3+})+\Delta c(\boldsymbol{TM}^{*}\cdot\mathrm{TM}^{2+})+\Delta c(\mathrm{TM})+\Delta c(\mathrm{TM}\cdot\mathrm{RE}) \tag{4.24}$$

$$\frac{i_2\Delta t}{n_2 FV}=\Delta c(\mathrm{TM}\cdot\mathrm{RE}) \tag{4.25}$$

where V is the effective volume covering all the electro-active species involved in all the reactions happening near/on the cathode surface.

Inserting equations (4.11)–(4.15) into (4.24) and (4.25), we obtain,

$$c(\boldsymbol{TM}^{*})=\frac{Ak_1(1-\theta)c(\mathrm{TM}^{2+})\,e^{-\alpha_1\eta_1 f}}{k_c V+Ak_2(1-\theta)k_a c(\mathrm{RE}^{3+})\,e^{-\alpha_2\eta_2 f}}\left(1-e^{-\frac{k_c V+Ak_2(1-\theta)k_a c(\mathrm{RE}^{3+})e^{-\alpha_2\eta_2 f}}{V+k_a Vc(\mathrm{RE}^{3+})+k_b Vc(\mathrm{TM}^{2+})}}\right) \tag{4.26}$$

Based on these kinetic equations, X_{RE} of the deposit is calculated from the partial current densities according to the following equation:

$$X_{\mathrm{RE}}=\frac{\frac{i_2+i_2^{'}+i_2^{''}+\cdots+i_2^{n}}{n_2FV}}{\frac{i_1+i_1^{'}+i_1^{''}+\cdots+i_1^{n}}{n_1FV}+\frac{i_2+i_2^{'}+i_2^{''}+\cdots+i_2^{n}}{n_2FV}} \tag{4.27}$$

Inserting equations (4.11) and (4.15) and combining with equation (4.26), equation (4.27) is rewritten as follows:

$$X_{\mathrm{RE}}=\frac{\frac{i_2}{3}}{\frac{i_1}{2}+\frac{i_2}{3}}=\frac{k_2k_ac(\boldsymbol{TM}^{*})c(\mathrm{RE}^{3+})e^{-\alpha_2\eta_2 f}}{k_1c(\mathrm{TM}^{2+})e^{-\alpha_1\eta_1 f}+k_2k_ac(\boldsymbol{TM}^{*})c(\mathrm{RE}^{3+})e^{-\alpha_2\eta_2 f}}$$

$$=1-\frac{1}{1+\frac{Ak_2(1-\theta)k_ac(\mathrm{RE}^{3+})e^{-\alpha_2\eta_2 f}}{k_cV+Ak_2(1-\theta)k_ac(\mathrm{RE}^{3+})e^{-\alpha_2\eta_2 f}}(1-e^{-\frac{k_cV+Ak_2(1-\theta)k_ac(\mathrm{RE}^{3+})e^{-\alpha_2\eta_2 f}}{V+k_aVc(\mathrm{RE}^{3+})+k_bVc(\mathrm{TM}^{2+})}})} \tag{4.28}$$

Equation (4.28) indicates that the REE content in the deposit depends on the applied over-potential and the concentration of TM^{2+} in the bulk solution. A higher applied over-potential or a lower TM^{2+} concentration results in a higher REE content in the deposit. Theoretically, this kinetic model can be generally applied to describe the induced co-deposition phenomenon for all RE–TM systems.

4.2.3 Validation of the Theoretical Mathematical Model

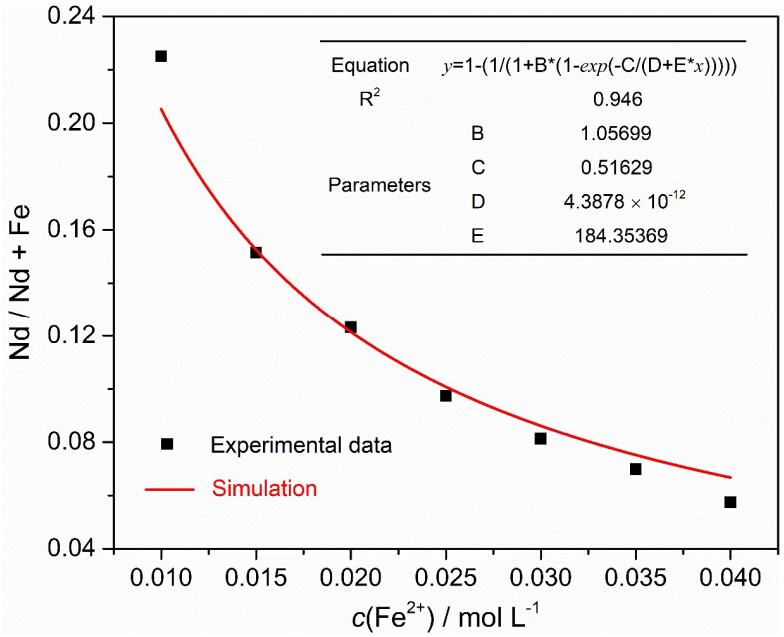

Figure 4.11: Nd content [Nd/(Nd + Fe)] in the deposit as a function of varied Fe^{2+} concentration in bulk solution from $NdCl_3$ (0.1 mol L^{-1})-[EMIM][DCA] baths. Applied potential of –1.40 V *vs.* Pt, t = 300 s, agitation rate: 400 rpm, 110 ℃.

Experiments for the Nd–Fe electrodeposition were performed by chronoamperometry at –1.40 V *vs.* Pt, which is slightly higher than the peak potential for Nd–Fe co-deposition (P_{4a}), shown in Figure 4.9a. Figure 4.11 shows the experimental and simulated Nd contents for different Fe^{2+} concentrations from 0.01 mol L^{-1} to 0.04 mol L^{-1}. The Nd content decreases from 22.5 at.% to 5.7 at.% when the Fe^{2+} concentration increases from 0.01 mol L^{-1} to 0.04 mol L^{-1}. The experimental data fits the kinetic model with a high correlation coefficient (R^2) of 0.946, validating the proposed co-deposition mechanism that describes the catalytic role of $\boldsymbol{Fe^*}$ in the co-deposition behaviour of Nd–Fe. The rate constants of k_a and k_b derived from the simulated parameters D and E show that k_a is significantly smaller than k_b, thus it can be concluded that $\boldsymbol{Fe^*}$ is preferentially combined with Fe^{2+} instead of Nd^{3+}, resulting in a relatively low Nd content in the deposit.

4.2.4 Electrodeposition of Nd–Fe Films Using the Pulse-Current Technique

In order to achieve a homogenous deposition and to avoid any concentration polarization, the pulse-current technique [227] was applied. An example of the current-pulse waveform with the corresponding potential response during current-pulse polarization is shown in Figure 4.12a.

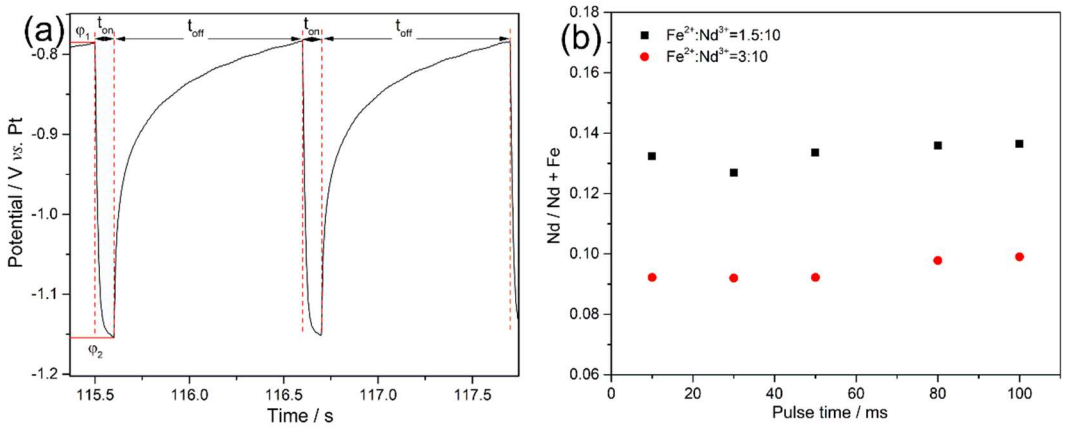

Figure 4.12: (a) Current pulse waveform with potential response at I_{on} = –16 mA cm^{-2} in $FeCl_2$ (0.015 mol L^{-1})-$NdCl_3$ (0.1 mol L^{-1})-[EMIM][DCA] (Fe^{2+}:Nd^{3+} = 1.5:10) and (b) atomic ratio of Nd [Nd/(Nd + Fe)] in the deposit as a function of pulse duration at I_{on} = –16 mA cm^{-2} for the total t_{on} of 300 s in $FeCl_2$ (0.015 mol L^{-1})-$NdCl_3$ (0.1 mol L^{-1})–[EMIM][DCA] (Fe^{2+}:Nd^{3+} = 1.5:10) and $FeCl_2$ (0.03 mol L^{-1})-$NdCl_3$ (0.1 mol L^{-1})–[EMIM][DCA] (Fe^{2+}:Nd^{3+} = 3:10) baths. Agitation rate: 400 rpm, 110 °C.

During the resting period, t_{off} (1 s), the potential remained at around –0.78 V (φ_1). When a cathodic current of –16 mA cm^{-2} was applied during the deposition period, t_{on} (0.1 s) the potential shifted suddenly to a less-noble value of –1.16 V (φ_2), at the end of t_{on}. An increase in the electrodeposition potential during t_{on} corresponds to the growth of a concentration polarization layer on the surface during each cycle and the introduction of t_{off} after t_{on} recovered the surface concentration of the Nd^{3+} and Fe^{2+} ions [227]. According to the Nernst equation, a lower deposition potential is needed for Nd and Fe deposition at higher concentrations of Nd^{3+} and Fe^{2+} ions, which helps to reduce the possibility of $[EMIM]^+$ decomposition. Figure 4.12b shows the relative atomic ratio of Nd [Nd/(Nd + Fe)] in the Nd–Fe thin film as a function of pulse duration (10–100 ms). No obvious increase in Nd [Nd/(Nd + Fe)] for both the applied concentration ratios of Fe^{2+}/Nd^{3+} 3:10 and

1.5:10, where the Nd content was almost constant at ~9 at.% and ~13 at.%, respectively, with an increase in the pulse duration. This is because t_{on} (10–100 ms) was short, where the average corresponding potentials stayed at almost the same value with the same applied current density.

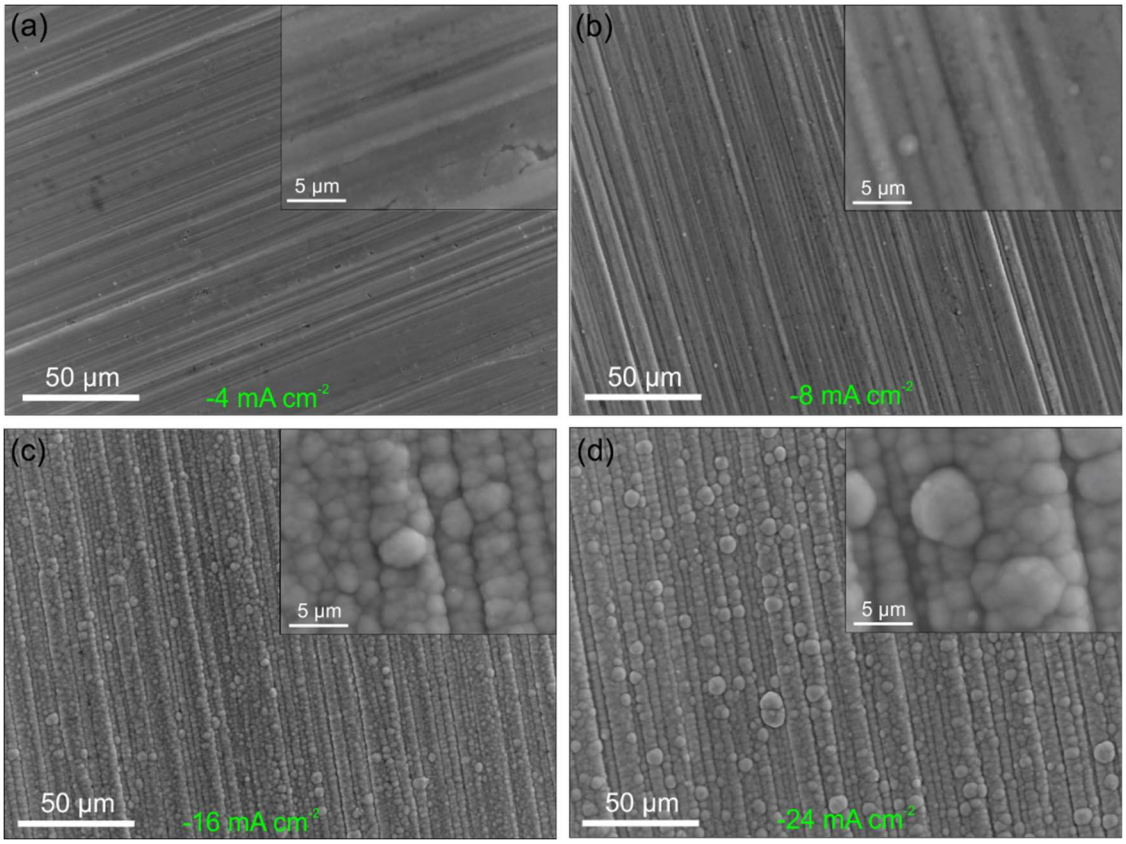

Figure 4.13: SE-SEM images of the as-deposited films from $FeCl_2$ (0.03 mol L^{-1})-$NdCl_3$ (0.1 mol L^{-1})-[EMIM][DCA] (Fe^{2+}:Nd^{3+}) = 3:10) bath with current density I_{on} = (a) –4, (b) –8, (c) –16, (d) –24 mA cm^{-2} at a total t_{on} of 300 s. Agitation rate: 400 rpm, 110 ℃.

Figure 4.13 shows SE-SEM images of the as-deposited Nd–Fe film on a Cu substrate with a pulse current density from –4 to –32 mA cm^{-2}. The granular structure (diameter, d ≤ 5 µm) without cracks is visible. The grain size increases with the increasing current density due to the larger total charge consumed at the same deposition time of 300 s. Figure 4.14 shows the relative atomic ratio of Nd [Nd/(Nd + Fe)] in the Nd–Fe thin film as a function of the pulse current (–4 to –32 mA cm^{-2}). The Nd content increases from 7.5 at.% to 9.9 at.% at the concentration ratio of Fe^{2+}/Nd^{3+} 3:10 with the increasing pulse current, and it increases at a higher rate in the electrolyte with a lower Fe^{2+} concentration (Fe^{2+}/Nd^{3+}) 1.5:10. It should be noted that the current efficiency of the Nd–Fe deposition at –16 mA cm^{-2} with the Fe^{2+} concentration (Fe^{2+}/Nd^{3+}) of 1.5:10 was calculated as 69.8%, which is lower than the other report on TM deposition from [EMIM][DCA] IL (97–99%) [228]. The loss of current efficiency for Nd–Fe deposition may be attributed to the decomposition of the IL that is in correspondence with the EDS analysis that detected the presence of carbon and nitrogen in the deposits.

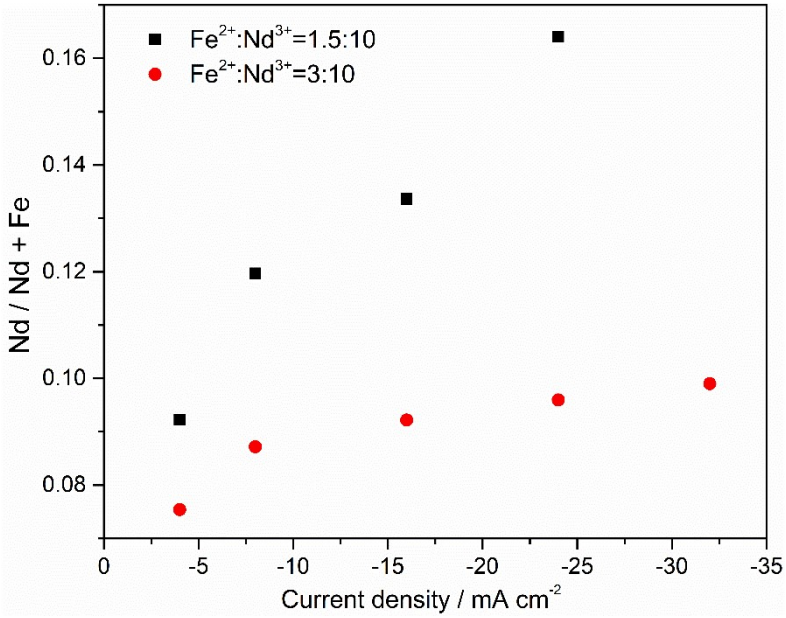

Figure 4.14: Atomic ratio of Nd [Nd/(Nd + Fe)] in the deposit as a function of pulse current density (t_{on} = 50 ms) in $FeCl_2$ (0.015 mol L^{-1})-$NdCl_3$ (0.1 mol L^{-1})-[EMIM][DCA] (Fe^{2+}:Nd^{3+} = 1.5:10) and $FeCl_2$ (0.03 mol L^{-1})-$NdCl_3$ (0.1 mol L^{-1})-[EMIM][DCA] (Fe^{2+}:Nd^{3+} = 3:10) baths. Agitation rate: 400 rpm, 110 ℃.

4.2.5 TEM Analysis of Nd–Fe Deposits

Although the electrodeposition of Nd using imidazolium and phosphonium-based ILs was reported [160-163], oxygen contents up to 50 at.% in the deposits make these materials of little practical value. The origin of these Nd oxides formed during the electrodeposition (or after) is unresolved. To find an answer, it is necessary to determine the valence state of the Nd, i.e., Nd^{3+} or Nd^{2+} or Nd^0, in the deposited materials. Although XPS was used in these earlier studies [229, 230], the valence state of the Nd deposit was unclear. This is because the binding energies of metallic Nd (Nd^0) and Nd_2O_3 are very close, i.e., 980.5–981.5 eV and 981.7–982.3 eV, respectively, making it almost impossible to differentiate between the two states [164]. In order to precisely determine the oxygen content of the deposit and reveal the deposition mechanism, the chemistry and phase composition of the deposit were investigated by means of TEM, combined with EDS and EELS. The amorphous nature of as-deposited Nd–Fe films was confirmed by the XRD analysis (Figure 4.15a), as already described in the literature [154]. Therefore, a thermal treatment of the deposit is necessary to form the crystalline alloy phases, e.g., the Nd_2Fe_{17} phase. Based on the phase diagram for Nd–Fe [231], the deposit with a Nd content of 12 at.% that would correspond to the Nd_2Fe_{17} phase stoichiometry after annealing, was selected for a thermal treatment. According to the results of the TGA, the IL starts to decompose above 250 ℃ (Figure 4.15b). Therefore, in order to remove the unstable organic compounds, the deposited film was annealed at 350 ℃ under argon for 30 min. The sample with the same initial composition was annealed at 750 ℃ under argon for 30 min, which is the temperature to obtain the Nd–Fe crystalline phase [232].

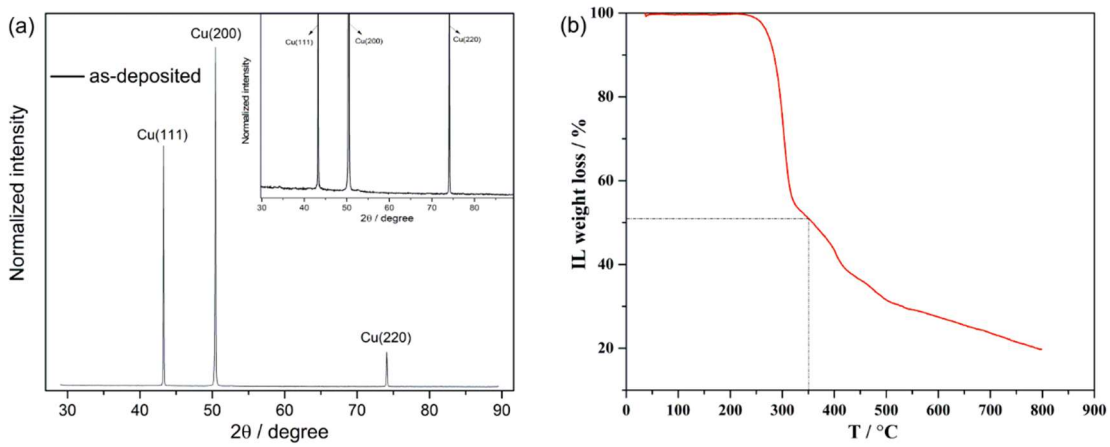

Figure 4.15: (a) XRD pattern of the as-deposited thin film, inset is the enlargement of the pattern and (b) Thermogravimetric trace for [EMIM][DCA] IL.

The TEM images of the cross-section of the deposit annealed at 350 ℃ and 750 ℃ are shown in Figure 4.16. Figure 4.16a shows a homogeneous layer of the deposit annealed at 350 ℃ on the Cu substrate. The sample annealed at 350 ℃ remained amorphous, as confirmed by the absence of diffraction spots in the selected-area electron-diffraction pattern (SAED). Figure 4.16b shows the same layer after the annealing at 750 ℃, which resulted in the formation of the porous nanocrystalline structure (as confirmed by the sharp diffraction reflections in the corresponding SAED pattern).

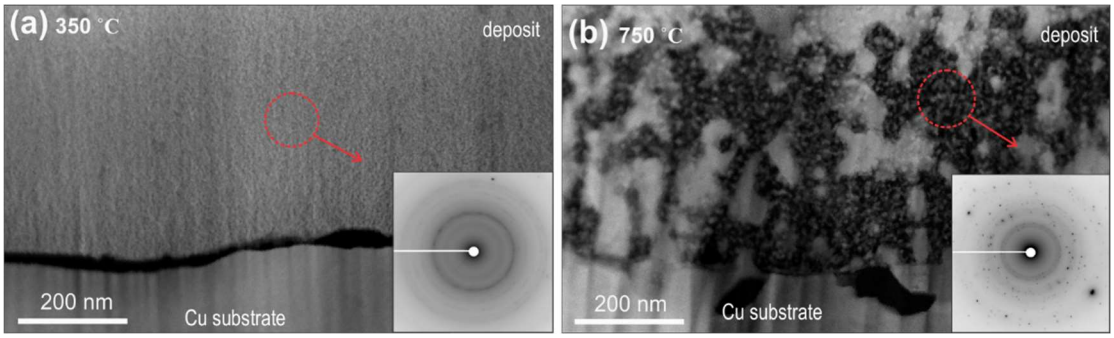

Figure 4.16: TEM images of the cross-section of the deposit (12 at.% of Nd) (a) annealed at 350 ℃ with a corresponding SAED pattern and (b) (same initial composition deposit) annealed at 750 ℃ with a corresponding SAED pattern.

Figure 4.17a shows a high-angle annular dark-field scanning TEM (HAADF-STEM) image of a representative example of the cross-section of the deposit (12 at.% of Nd) annealed at 350 ℃. A porous structure of the deposit formed on the Cu substrate is observed. A thin layer (labelled by two white dashed lines in Figure 4.17a), located between the Cu substrate and the porous deposit is shown along with the Cu substrate. Figure 4.17b shows the compositional change with the deposition depth (the red arrow line in Figure 4.17a), determined by EELS. The Fe content increases in the region between 0 nm and 3 nm, whereas Nd is not detected at all. After 3 nm from the Cu substrate, the Fe content reaches a peak value and the Nd starts to appear, showing that the Fe was deposited on the Cu substrate first. According to the proposed co-deposition mechanism, Fe is reduced first to catalyse the subsequent reduction of Nd^{3+}. Therefore, the above-

mentioned EELS spectra directly prove the proposed co-deposition mechanism. The compositional fluctuations in the EELS spectra and the relatively broad transition region of the composition change are possibly caused by the unevenness of the Cu substrate (inclination) and the heterogeneous distribution of the deposit after the annealing. The oxygen content increases from the base content of ~3 at.% to the peak content of ~18 at.%, where the Nd content reaches its peak content of ~28 at.%. It can also clear that the oxygen content fluctuates along with the change in the Nd content. This indicates that oxygen in the deposit most probably originates from NdO/Nd_2O_3. The Nd oxide(s) can be explained by the surface oxidation during the sample's transportation from the FIB to the TEM.

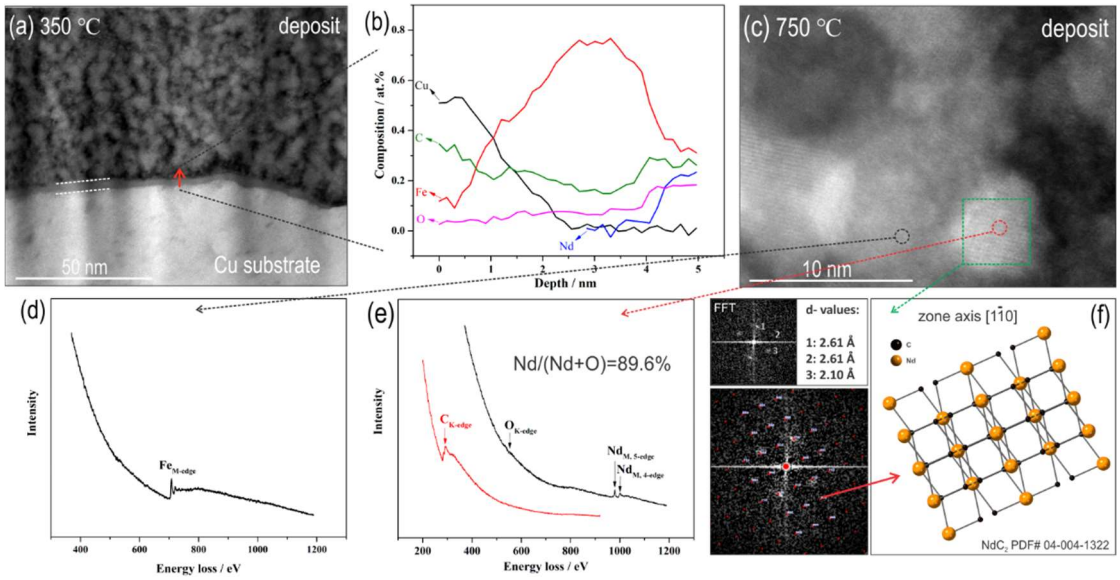

Figure 4.17: (a) HAADF-STEM image of the cross-section of the sample (12 at.% of Nd) annealed at 350 °C. (b) Compositional depth profile as obtained by EELS line scan in the image (a) (red arrow), (c) HAADF-STEM image of the cross-section of the sample (12 at.% of Nd) annealed at 750 °C. The corresponding EELS spectrum of (d) the light grey particle (black-dashed circle) and (e) the white particle (red-dashed circle) from image (c), and (f) Zone axis calculation from FFT pattern of the white particle (green-dashed square) as a comparison with the NdC_2 (PDF# 04-004-1322).

Figure 4.17c shows a HAADF-STEM image of the nanoparticles that formed during the annealing at 750 °C. The dark-grey part of Figure 4.17c are the pores formed by annealing, while the light-grey particles (black-dashed circle) are metallic Fe, confirmed by the EELS (Figure 4.17d). The white particle labelled with the red-dashed square is a single crystal (~7 nm in size) of NdC_2 observed in the (110) zone axis, confirmed by a fast Fourier transform (FFT) pattern (Figure 4.17f). Figure 4.17e shows EELS spectra of the same single crystal (red-dashed circle), mainly composed of Nd and C with a minor oxygen content. A quantitative analysis of the EELS spectrum (black curve) shows that the Nd content [Nd/(Nd + O)] is close to 90 at.%. Thus, it can be concluded that the majority of the Nd in the annealed Nd–Fe deposit is in the zero-valence state, Nd^0, either as metallic Nd or in the form of NdC_2.

Thermodynamically, it is possible to obtain NdC_2 at 750 °C, since the Gibbs free energy (ΔG) of the reaction, $Nd+2C=NdC_2$, is negative, as shown in Table 4.2. Therefore, there are two reaction paths existing to form Nd^0: i) Nd^{3+} is reduced to Nd^0 during the electrodeposition, ii) Nd^{3+} is reduced to Nd^{2+} during electrodeposition, and then further

reduced to Nd^0 by C (from the pyrolysis of organic compounds in the deposit). However, thermodynamically the Nd^{2+} cannot be reduced by C or H_2 at 750 ℃, not even at 1500 ℃, since all the ΔG are above 0 (Table 4.2). Therefore, the Nd^0 can only be obtained by the electro-reduction of Nd^{3+}.

Table 4.2: Gibbs free energy (ΔG) of chemical reactions calculated by HSC Chemistry 6.

Reaction equations	Temperature (℃)	ΔG (kcal)
$Nd+2C=NdC_2$	750	–49.035
$2NdCl_2+C=2Nd+CCl_4(g)$	750	251.377
	1500	174.203
$NdCl_2+H_2(g)=Nd+2HCl(g)$	750	71.973
	1500	19.648
$2Nd_2O_3+3C=4Nd+3CO_2(g)$	1500	340.922
$Nd_2O_3+3H_2(g)=2Nd+3H_2O(g)$	1500	205.707

The induced co-deposition of Nd, a REE and Fe, a TM, was investigated in the [EMIM][DCA] electrolyte using electrochemical measurements and SEM- and TEM-based analysis. An induced co-deposition mechanism for RE (Nd) and TM (Fe) is derived and supported by a mathematical model that considers the effect of the Fe^{2+} concentration on the Nd content in the deposit, in which the $\boldsymbol{Fe^*}$ is formed during the electrodeposition, catalysing the co-deposition of Nd and Fe. Upon annealing, NdC_2 is formed through the reaction of the electrodeposited Nd^0 with C as the ΔG of the reaction is negative. The developed RE–TM co-deposition mechanism that is valid for the Nd^{3+}-Fe^{2+}-[EMIM][DCA] IL system creates tremendous opportunities for RE–TM PM recycling and thin film production with a low environmental impact. A development of longer alkyl chains ILs would be a direction to follow in the future in order to increase the ILs stability [178] and the current efficiency. A proven electrodeposition of Nd–Fe from the [EMIM][DCA] electrolyte at a mild temperature thus contributes to the green character of this process which can be considered as a sustainable and green alternative to high-temperature molten salt electrolysis.

4.3 Selective Recovery of the REEs and Fe Metal from the Sintered Nd–Fe–B Magnets

The sintered Nd–Fe–B PMs typically contain 28–35 wt.% REEs (Pr, Nd, Tb, and Dy), which means that the sintered Nd–Fe–B magnet scraps are an important secondary resource for REEs. Recovering REEs from the sintered Nd–Fe–B magnet scraps is, therefore, going to be the key strategy for overcoming the serious supply risks associated with the REEs and making the REEs available for other applications, e.g., solid-oxide fuel cells and nuclear reactors [105].

Various approaches for REEs recovery, such as glass-slag extraction [79, 81], gas-phase extraction [82, 233], and hydrometallurgy [53, 117] are currently at various technology-readiness levels. Among them, hydrometallurgy is currently the only realistic route to recover REEs from the sintered Nd–Fe–B magnet scraps as it can be incorporated into the existing REE separation plants. But such methods require 2172 kg of H_2SO_4 and 1600 kg of NaOH to treat 1000 kg Nd–Fe–B magnets, together with the generation of around 10000 liters of wastewater [101]. The acid and alkali

cannot be recycled in a closed-loop and the wastewater and solid waste, e.g., jarosite [71], have to be further treated, all of which adds to the costs. The state-of-the-art methods, including the electrochemical and thermal pre-treatment of the magnets that facilitate the separation of REEs from Fe, still cannot avoid the generation of wastewater.

In this section, we develop a greener and more facile electrochemical method for the sintered Nd–Fe–B magnet scraps recycling. The proposed procedure enables a selective REEs recovery and a simultaneous Fe metal deposition in only two steps with the total re-use of the electrolyte; thus avoiding the formation of Fe-based solid waste and the wastewater discharge.

4.3.1 Linear Sweep Voltammetry of the Sintered Nd–Fe–B Magnets

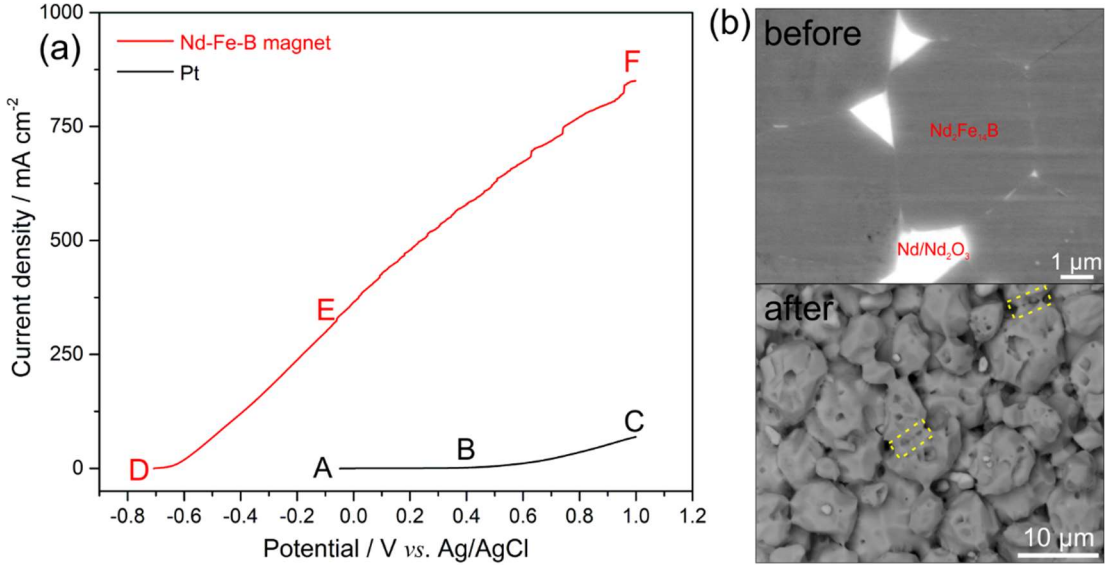

Figure 4.18: (a) LSV of a Pt-wire working electrode (black curve) and a sintered Nd–Fe–B magnet (red curve) with 0.6 mol L^{-1} $FeSO_4$, 0.4 mol L^{-1} $(NH_4)_2SO_4$, 0.175 mol L^{-1} Na_3Cit and 0.4 mol L^{-1} H_3BO_3 in the electrolyte (Conditions: scan rate of 100 mV s^{-1}, pH 4.0, room temperature). (b) BSE-SEM images of sintered Nd–Fe–B magnets before and after LSV.

Figure 4.18a shows the LSV of a Pt-wire working electrode (black curve) and the initial magnet (red curve) in the bath solution containing 1.2 mol L^{-1} $FeSO_4$, 0.4 mol L^{-1} $(NH_4)_2SO_4$, 0.125 mol L^{-1} Na_3Cit and 0.4 mol L^{-1} H_3BO_3 (pH 4.0) with a scan rate of 100 mV s^{-1}. In the potential segment AB of the black curve, the current density is stable at around 0 mA cm^{-2}. From point B on, where the potential is 0.4 V, the current density starts to increase regularly along the line BC due to the oxidation of Fe^{2+} on the Pt electrode (reaction (4.29)).

$$Fe^{2+} - e^- \rightarrow Fe^{3+} \tag{4.29}$$

$$Nd_2Fe_{14}B - 37e^- \rightarrow 2Nd^{3+} + 14Fe^{2+} + B^{3+} \tag{4.30}$$

$$2H_2O - 4e^- \rightarrow 4H^+ + O_2\uparrow \tag{4.31}$$

When the magnet was used as the working electrode, the current density starts to increase at point D with a potential of –0.70 V, shown by the red curve in Figure 4.18a.

The initial magnet generally consists of metallic $Nd_2Fe_{14}B$ (matrix phase, accounting for ~90% in terms of volume [57]), metallic $NdFe_4B_4$, metallic Nd and Nd_2O_3 phases, the increase of current density from –0.7 V is caused by the oxidation/leaching of the metallic phases, e.g., $Nd_2Fe_{14}B$ (reaction (4.30)) in the magnet. No pronounced oxidation peaks are observed, indicating that all the metallic phases in the magnet were oxidized/leached without significant selectivity. A similar result was reported in our recent study [234] where the fast leaching kinetic at high current density leads to non-selective leaching of all the metallic phases in the Nd–Fe–B magnet. The current density increases continuously along EF with the presence of kinks that are caused by the oxygen bubbles formed on the magnet surface. These bubbles were visually observed due to the side reaction of water decomposition (reaction (4.31)). Therefore, to avoid the water decomposition that decreases the leaching efficiency of the magnet, the applied potential should be more negative than 0 V (corresponding current density of 323 mA cm^{-2}). Figure 4.18b shows BSE-SEM images of the polished magnet before and after LSV. The initial magnet before LSV consists of $Nd_2Fe_{14}B$ grains surrounded by the Nd-rich GBs that are supposed to be leached preferentially, due to the more negative electrochemical potential of Nd than that of Fe [202]. After LSV, the remaining $Nd_2Fe_{14}B$ grains (grey phase) were progressively leached, indicated by the pores and pits on their surfaces. However, these $Nd_2Fe_{14}B$ grains are connecting with each other through the remaining GBs (yellow dashed lines), further demonstrating the non-selective leaching of the magnet.

4.3.2 Electrochemical Leaching of the Sintered Nd–Fe–B Magnets

Figure 4.19a shows the kinetics of leaching the magnets under applied currents of 50, 100, 150 and 200 mA (current densities of 25, 50, 75 and 100 mA cm^{-2}, respectively) on the anode. An increased leaching rate of the REEs (the slope values in Figure 4.19a) from 300.06 to 1073.92 mg L^{-1} h^{-1} with the increasing current density from 25 to 100 mA cm^{-2} is observed. The REEs leaching into the solution increased with the increase in the current density and their concentration increased linearly with the times of the electrolysis. The anodic leaching efficiency of the magnets under current densities of 25, 50, 75 and 100 mA cm^{-2} was 99.9% 99.8%, 98.7% and 92.4% with the corresponding energy consumption of 0.82, 0.96, 1.21 and 1.51 kWh per kilogram of the magnets, respectively (Table 4.3). In order to keep the leaching efficiency ~100%, the current density applied to the anode should not exceed 50 mA cm^{-2} to avoid water decomposition, which consumes the supplied charge. It should be noted that applied current densities < 50 mA cm^{-2} bring low energy consumption, but result in low leaching rates, causing low yield of the REEs. In the practical application, both the energy consumption and the yield of the REEs are needed to be considered. In this study, an anodic current density of 25 mA cm^{-2}, with an applied current of 200 mA, was used as a possible example for the electrochemical leaching of the Nd–Fe–B magnets.

$$Fe^{2+} + 2e^- \rightarrow Fe \tag{4.32}$$

$$2H^+ + 2e^- \rightarrow H_2\uparrow \tag{4.33}$$

Simultaneously, Fe metal was deposited (reaction (4.32)) on the cathode at a current density of 12.5 mA cm^{-2}. As hydrogen evolution (reaction (4.33)) occurs simultaneously with Fe deposition, this leads to an increase in pH > 7.0 at the cathode interface [235]. Consequently, both Fe^{2+} and Fe^{3+} (pH > 3.0) [235, 236] and RE^{3+}, e.g., Nd^{3+} (pH > 6.0) [237] are expected to hydrolyse and form metal hydroxides on the cathode, because of which Fe metal deposition would be limited and the overall REE recovery would be

reduced. Upon that $(NH_4)_2SO_4$ was added as a complexing agent to maintain the Fe^{2+} and Fe^{3+} as soluble species [235] at increased pH, and another complexing agent, Na_3Cit, was added to prevent the formation of RE hydroxides on the cathode [238]. However, citrate ions (Cit^{3-}) can also chelate with Fe^{2+} ($Fe(Cit)^-$), which decreases the concentration of unchelated Fe^{2+}. As a result, the over-potential for Fe deposition increases, which lowers its current efficiency [239]. Figure 4.19b shows that with the increasing concentration of Na_3Cit from 0.05 to 0.175 mol L^{-1}, the current efficiency of Fe deposition decreased from 92.9% to 74.9%.

It should be noted that in a long run, the increasing thickness of the Fe deposit will largely change the overall surface area of the cathode, leading to the change of the current efficiency. This can be avoided by removing the deposited Fe on the cathode surface using heat treatment [240] that increases the internal stress between the cathode material and deposited Fe, resulting in the detachment of the Fe deposit from the cathode material.

For a leaching efficiency of the sintered Nd–Fe–B magnets close to 100% under a constant current, approximately 70.9–75.7% of the current contributes to the leaching of Fe which can be regarded as the Fe leaching efficiency from the anode (See "Calculations" in Section 3.4.6). The concentration of total dissolved Fe (including Fe^{2+} and Fe^{3+}) in the electrolyte is a result of the Fe leaching from the anode and the Fe consumption on the cathode. Because the current efficiency is either higher than or within the Fe leaching efficiency range (indicated with blue-dashed lines in Figure 4.19b), the concentration of total dissolved Fe in the electrolyte decreased with leaching time (Figure 4.19c). A more rapid decline in Fe concentration is observed with a lower concentration of Na_3Cit in the electrolyte. It should be noted that the reducing Fe concentration in the electrolyte, in turn, results in a decrease of current efficiency [241]. Therefore, the current efficiency of the Fe deposition in the electrolyte with the Na_3Cit concentration from 0.05 to 0.175 mol L^{-1}, in the long term, is expected to decrease to a Fe leaching efficiency range of 70.9–75.7%, where the Fe leaching from the anode is balanced by the Fe consumption on the cathode. Consequently, a stable concentration of total dissolved Fe (balanced concentration) in the electrolyte will be achieved. Therefore, a lower concentration of Na_3Cit will result in a lower balanced concentration of the total dissolved Fe, favoring the next steps of selective REE precipitation and purification. In contrast, if the current efficiency of Fe deposition were to be lower than 70.9%, a continuous increase in the total dissolved Fe concentration in the electrolyte would occur. This would have adverse effects on the next steps of selective REE precipitation and purification. Moreover, the lower current efficiency resulted in more added H_2SO_4 to keep the pH of electrolyte between 3.5 and 4.5, due to the side reaction of hydrogen evolution (reaction (4.33)).

Alternatively, instead of lowering down the current efficiency of Fe deposition by adding more Na_3Cit, supplying a certain amount of Fe salt $FeSO_4$ into the electrolyte to compensate the net consumption of Fe is another option to achieve a balanced Fe concentration in the electrolyte, if the current efficiency of Fe deposition is higher than 75.7%.

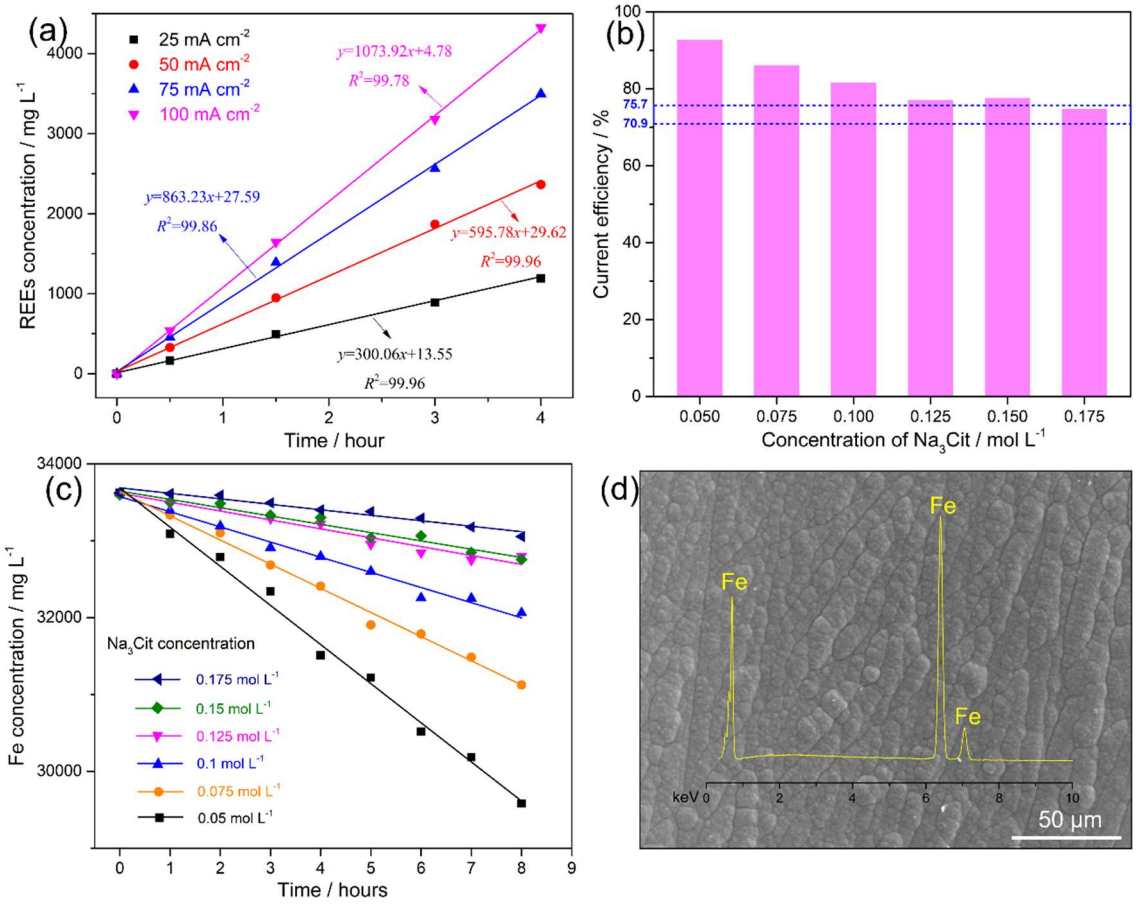

Figure 4.19: (a) Influence of current density 25–100 mA cm^{-2} on the leaching of the REEs from a Nd–Fe–B magnet anode with 0.6 mol L^{-1} $FeSO_4$, 0.4 mol L^{-1} $(NH_4)_2SO_4$, 0.4 mol L^{-1} H_3BO_3 and 0.175 mol L^{-1} Na_3Cit in the initial electrolyte. (b) Effect of Na_3Cit concentration on the current efficiency of the Fe deposition in the electrolyte (0.6 mol L^{-1} $FeSO_4$, 0.4 mol L^{-1} $(NH_4)_2SO_4$ and 0.4 mol L^{-1} H_3BO_3 in the initial electrolyte); the dashed blue line shows the operational Fe deposition current efficiency range, where the Fe concentration balance (leaching vs. deposition) is reached. (c) Effect of Na_3Cit concentration on the Fe concentration in the electrolyte (0.6 mol L^{-1} $FeSO_4$, 0.4 mol L^{-1} $(NH_4)_2SO_4$ and 0.4 mol L^{-1} H_3BO_3 in the initial electrolyte) at the anodic current density of 25 mA cm^{-2} and cathodic current density of 12.5 mA cm^{-2}. (d) The SE-SEM image of the Fe deposit with an EDS spectrum (0.6 mol L^{-1} $FeSO_4$, 0.4 mol L^{-1} $(NH_4)_2SO_4$, 0.175 mol L^{-1} Na_3Cit and 0.4 mol L^{-1} H_3BO_3 in the initial electrolyte) at the cathodic current density of 12.5 mA cm^{-2}.

Table 4.3: Effect of current density on magnet-anode dissolution, anodic leaching efficiency, and energy consumption of the electrolysis step.

Current density ($mA\ cm^{-2}$)	Mass of magnet dissolved (g)	Anodic leaching efficiency (%)	Energy consumption ($kWh\ kg^{-1}$)
25	0.220	99.9	0.82
50	0.439	99.8	0.96
75	0.651	98.7	1.21
100	0.813	92.4	1.51

Nevertheless, using 0.4 mol L^{-1} $(NH_4)_2SO_4$ and 0.175 mol L^{-1} Na_3Cit as complexing agents, it was possible to keep the current efficiency of the Fe deposition on the cathode close to the Fe leaching efficiency from the anode (~75.7%), and thus a balanced Fe (Fe^{2+} and Fe^{3+}) concentration in the electrolyte could be achieved that enables repeated electrolyte recycling. With this electrolyte bath, the Fe metal was obtained on the cathode (Figure 4.19d). As the initial magnet contains a small amount of other TMs, e.g., Co (2.13 wt.% in this study), TM alloys, e.g., Fe–Co, are expected to be deposited on the cathode with repeated recycling of the electrolyte. After electrolysis for 8 hours at an applied current of 200 mA, 1.76 g of the magnets was completely leached with a leaching efficiency of 99.9% and an energy consumption of 1.36 kWh per kilogram of the sintered Nd–Fe–B magnets. Around 1.5 mL of 4 mol L^{-1} H_2SO_4 was used to adjust the pH of the electrolyte between 3.5 and 4.5, from which the H_2SO_4 consumption is calculated to be 0.34 kg per kilogram of the sintered Nd–Fe–B magnets, which saves 84.4% of the acid usage, compared to the conventional hydrometallurgical process [101]. Although a few studies have reported on the selective leaching of the REEs from the sintered Nd–Fe–B magnet scraps, however the aspect of either the Fe-based solid waste or wastewater was not yet elaborated. For example, the REEs from the sintered Nd–Fe–B magnet scraps can be selectively leached based on the principle of the pH-dependent dissolution of the calcined magnets using the potential-pH diagram [242, 243]. Koyama and Tanaka [104] reported that the selective leaching of REEs could be realized by using 0.02 mol L^{-1} HCl in an autoclave at 180 ℃ for 2 h or at a lower temperature by increasing the initial acid concentration and having a prolonged etching time. An energy-intensive pre-treatment of the sintered Nd–Fe–B magnet scraps oxidized at 900 ℃ by roasting was needed to fit within the potential-pH diagram and the overall process operates at elevated temperatures. In the end, the REEs were precipitated out via conventional hydrometallurgy [71] with generation Fe_2O_3 and oxalic acid-containing wastewater. In this study, combining all the reactions happening on both the anode (reaction (4.30)) and the cathode (reactions (4.32) and (4.33)) in a balanced Fe (Fe^{2+} and Fe^{3+}) concentration electrolyte, the net reaction of the whole electrolysis can be expressed using reaction (4.34), which realizes the "selective leaching" of REEs, leaving the major component of metallic Fe "untouched":

$$Nd_2Fe_{14}B + 9H^+ \rightarrow 2Nd^{3+} + B^{3+} + 14Fe + 4.5H_2\uparrow \tag{4.34}$$

4.3.3 Selective Precipitation of the REEs

After the electrolysis step, a purple solution was obtained as the leachate with the pH adjusted to 3.5, in which the REEs were present as sulfate salts for further separation. Although a patent for processing Nd–Fe–B magnet slags [129] claimed that complete leaching of the magnet slags which were filled in a plating barrel as an anode and

simultaneous Fe deposition on the cathode could be achieved electrochemically in a sulfamic acid bath. The HF solution was used to precipitate the Nd as NdF_3 from the Nd- and Fe-containing leachate after electrolysis, which was then sent back to the electrolysis tank for further electrodeposition. However, as both Fe^{3+} and Fe^{2+} can precipitate as FeF_3 [130] and FeF_2 [131] by adding HF, due to their low solubility, NdF_3 could be precipitated without selectivity as a mixture of NdF_3, FeF_3 and FeF_2. How the NdF_3 was further purified from the fluoride mixture was not described in the patent.

It is well known that the sulfate double salt of the light REEs, including La, Ce, Pr, Nd and Sm, has very low solubility in an aqueous solution [49]. REEs, e.g., Nd, can be precipitated as $(Nd, Na)(SO_4)_2{\cdot}xH_2O$ by introducing Na_2SO_4, with the following reaction:

$$Nd_2(SO_4)_3 + Na_2SO_4 + 2xH_2O \rightarrow 2(Nd, Na)(SO_4)_2{\cdot}xH_2O \downarrow \quad (4.35)$$

Generally, more than 90% of REEs in the solution can be precipitated, when the addition of Na_2SO_4 at a molar ratio of Na_2SO_4 to REEs is higher than 2:1 [186]. In this study, the addition of Na_2SO_4 at a molar ratio of Na_2SO_4 to REEs was fixed to 1:1 to prevent the excess of Na_2SO_4 during repeated recycling of the electrolyte. Because the molar ratio of Na_2SO_4 to REEs higher than 2:1 for each recycling cycle, although high REE recovery would be achieved, the dissolution of Na_2SO_4 would reach saturation during repeated solution recycling, leading to the recrystallization of Na_2SO_4 as precipitate together with REE-sodium-sulfate double salts. Thus, extra washing step would be required.

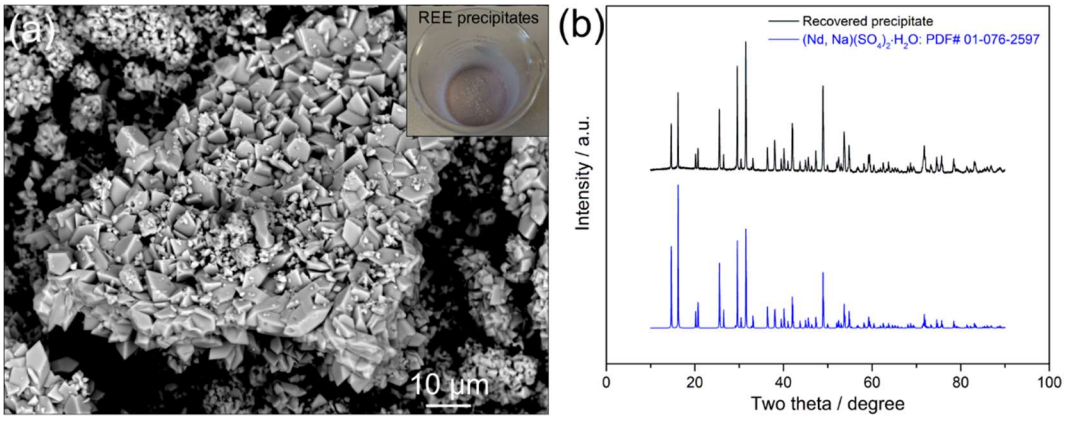

Figure 4.20: (a) BSE-SEM images with an inset of a real image and (b) XRD pattern of the REE precipitates.

As both Fe^{2+} and Fe^{3+} in the leachate stayed soluble due to the addition of $(NH_4)_2SO_4$ and Na_3Cit. Therefore, with the addition of Na_2SO_4 at a molar ratio of Na_2SO_4 to REEs of 1:1, followed by heating the solution at 70 °C for 2 hours, REEs were selectively precipitated as shown in Figure 4.20a. The XRD analysis shows that the diffraction peaks are well indexed to the $(Nd, Na)(SO_4)_2 \cdot H_2O$ (PDF# 01-076-2597) phase (Figure 4.20b). The ICP-MS analyses of the precipitates revealed that the recovered REEs were Nd (93.7%), Dy (3.1%) and Pr (2.6%), having a high purity (99.4%) and trace levels of Fe. Both the XRD and ICP-MS analysis prove that the REEs in the leachate were successfully precipitated as REE-sodium-sulfate double salts with high selectivity.

It should be noted that the recovered REEs from the sintered Nd–Fe–B magnets in the form of RE-sodium-sulfate double salts can be readily converted to either REOs by dissolving in oxalic acid and roasting in air or REF_3 by leaching in HF solution with

negligible losses of REEs [49]. However, unlike the fluoride precipitation for the REEs separation in the conventional hydrometallurgical process where NdF_3 is readily gelatinous and is, therefore, difficult to separate from the solution by filtration [49], the NdF_3 obtained from the sulfate double salt is easy to filter, which is a significant advantage of this route. Because of this, the REE-sodium-sulfate double salts are generally used for the precipitation and storage of REEs in the industry today [49].

4.3.4 Recycling of the Electrolyte

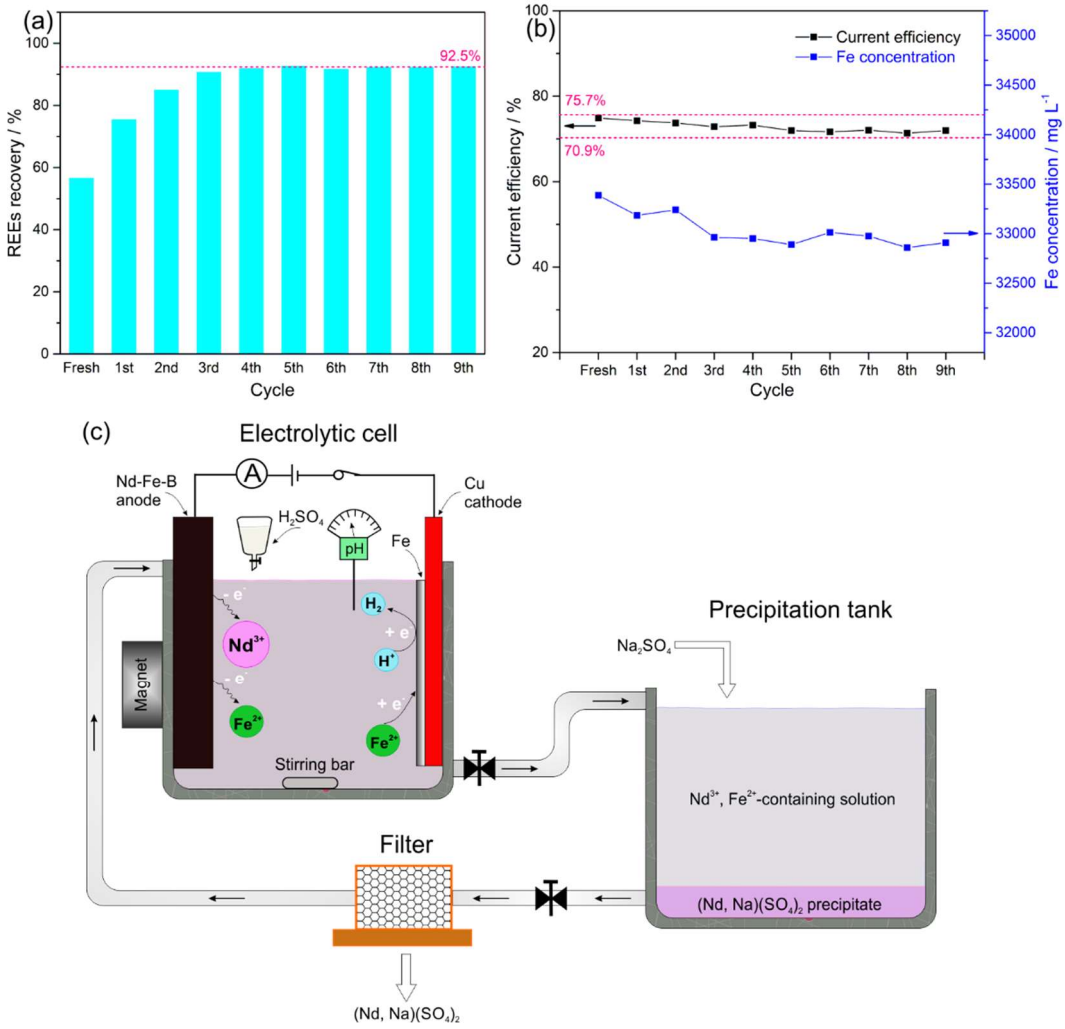

Figure 4.21: (a) Percentage extraction of the REEs. (b) Current efficiency of Fe deposition and total dissolved Fe concentration over 9 recycling cycles. (c) Schematic of the proposed closed-loop recycling route for recovering REEs from the sintered Nd–Fe–B magnets.

After filtration of the REE precipitates, the filtrate was sent back for the next electrolysis cycle. The overall REE recovery for 9 cycles is shown in Figure 4.21a. On the fresh electrolyte, the REEs recovery was only 56.8% due to the insufficient addition of Na_2SO_4 with the molar-ratio of Na_2SO_4 to REEs of 1:1, compared to 2:1 in a mole of Na_2SO_4 to REEs used in the conventional hydrometallurgical process [186]. However, with the repeated recycling, the accumulated concentrations of both Na_2SO_4 and REEs in the solution were increased, driving reaction (4.35) to the right and as a result, around 92.5% of the REEs was recovered by the fourth cycle. Because ~92.5% of the leached REEs

on the fourth cycle were precipitated with the added Na_2SO_4, leaving ~7.5% of Na_2SO_4 and REEs for the next cycle, the accumulated concentrations of Na_2SO_4 and REEs in the electrolyte after the REE precipitation increased slightly and trend to be stable, leading to a stable recovery of the REEs for the rest cycles. It has been reported that REEs, such as Nd^{3+} can form complex with Cit^-, according to the following equilibrium, and the existence of NdCit, $(NdHCit)^+$, $(NdHCit_2)^{2-}$ and $(NdCit_2)^{3+}$ was confirmed by the solution in the pH range of 2~5 [244].

$$n\mathrm{Nd}^{3+}+j\mathrm{H}^{+}+k\mathrm{Cit}^{3+}\rightarrow \mathrm{Nd}_n\mathrm{H}_j\mathrm{Cit}_k^{(3n+j-3k)} \tag{4.36}$$

However, the addition of Na_2SO_4 caused the precipitation of the REEs as REE-sodium-sulfate double salts from these REE-Cit complexes. This is probably due to the higher stability of REE-sodium-sulfate double salts than REE-Cit complexes in the solution of high sodium sulfate concentration of this study [245]. Therefore, the constant citrate concentration in this study does not influence the REE recovery in a long run.

Correspondingly, with the initial electrolyte bath of 0.6 mol L^{-1} $FeSO_4$ + 0.4 mol L^{-1} $(NH_4)_2SO_4$ + 0.175 mol L^{-1} Na_3Cit + 0.4 mol L^{-1} H_3BO_3, the current efficiency of the Fe deposition was kept within 70.9–75.7% (indicated with pink-dashed lines in Figure 4.21b), which guaranteed a relatively stable concentration of total dissolved Fe around 0.6 mol L^{-1} in 9 repeating cycles. We would expect that a stable REEs recovery of 92.5% with a relatively stable composition of the electrolyte can be achieved over the long term. Therefore, repeated cycles of re-using the electrolyte can avoid wastewater release by using the current electrolysis-selective precipitation recycling route for the REEs recovery (Figure 4.21c).

It should be noted that boron (B) was also leached out from Nd–Fe–B magnets in the form of H_3BO_3 electrochemically, according to the half-reaction [121]:

$$\mathrm{B}+3\mathrm{H_2O}-3e^{-}\rightarrow \mathrm{H_3BO_3}+3\mathrm{H}^{+} \tag{4.37}$$

In the initial electrolyte, H_3BO_3 was added as a buffer to favor the Fe electrodeposition on the cathode, because it can prevent the precipitation of metal hydroxides on the cathode surface that hinder the Fe deposition [246]. The concentration of boron increased from 0.402 mol L^{-1} in the initial electrolyte to 0.428 mol L^{-1} after the electrochemical leaching for 8 h at 200 mA (25 mA cm^{-2}), which is ascribed to the leaching of boron from the Nd–Fe–B magnet in the form of H_3BO_3. The increased concentration of H_3BO_3 in the electrolyte can strength the buffer capacity, facilitating the Fe deposition [246]. It is expected that in the long term of reusing the electrolyte, the concentration of H_3BO_3 will reach a saturation (~0.92 mol L^{-1} at 25 ℃ [247]) where H_3BO_3 will crystallize. In the REE precipitation step, H_3BO_3 will precipitate together with REE-sodium-sulfate double salts. The precipitated H_3BO_3 can be easily washed away from the precipitates with water, after which the B can be recovered as zinc borate hydrate [248] by adding zinc and raising the pH. The recycled B as zinc borate hydrate could be commercially used as a flame retardant [248].

In recent years, electrochemical recovery of REEs from the sintered Nd–Fe–B magnet scraps has been reported. P. Venkatesan et al. [44] were able to selectively recover the REEs, using membrane electrolysis to treat the partially HCl-leached Nd–Fe–B magnet within four steps. More than 95% of the REEs was leached into the solution and simultaneously Fe^{2+} was anodically oxidized and precipitated as $Fe(OH)_3$ that was removed by filtration. The remaining REEs in the electrolyte were precipitated with oxalic acid. This process facilitates the oxidation of Fe^{2+} to Fe^{3+} without extra addition of oxidants. The same group [132] further developed a two-anode system to leach Nd–Fe–B scraps and convert the Nd and Fe into the respective hydroxides without pretreatment of partial acid-

leaching. The REEs were recovered using oxalic acid, followed by calcination to obtain REOs with high purity (99.2%). The electrochemical process precipitated > 90% of the Fe in the form of solid akaganeite (FeOOH). Despite the progress achieved in the electrochemical recycling of the REEs, the methods though efficient in REEs recovery still end up with Fe-based solid waste and the oxalic acid-containing solution as wastewater that has to be treated. As a comparison, the current electrolysis-selective precipitation recycling route for the REEs recovery from the sintered Nd–Fe–B magnet scraps is greener.

In summary, we have demonstrated a facile closed-loop recycling route showing that the REEs can be selectively recovered from the sintered Nd–Fe–B magnets. In an electrolysis cell where the sintered Nd–Fe–B magnets are used as the anode, selective leaching of REEs is realized by balancing the Fe dissolution from the anode and Fe consumption on the cathode. This step saves 84.4% and 100% of acid and alkali usage, respectively, with the energy consumption of 1.36 kWh per kilogram of the sintered Nd–Fe–B magnets. After the electrolysis, the REEs were selectively precipitated as REE-sodium-sulfate double salts from the electrolyte, which are used as industrial raw materials. The electrolyte was sent back for reuse in the electrolysis cell, avoiding the wastewater generation. The addition of $(NH_4)_2SO_4$ and sodium citrate as chelating agents plays a key role in stabilizing the composition of the electrolyte for recycling and further enabling the selective precipitation of the REEs with high purity (99.4%). At the same time, Fe metal was obtained, which can be used in a wide range of industrial products. The whole process avoids the high-temperature roasting pre-treatment of magnets and the wastewater discharge, making it economically and environmentally feasible for industrial applications.

Intentionally left blank

Chapter 5

Conclusions

Rare-earth elements (REEs) are considered the most critical based on their economic importance and supply risk. The sintered neodymium-iron-boron (Nd–Fe–B) permanent magnets incorporate 20–30 wt.% of REEs that represent an important secondary REEs resource. Recycling of Nd–Fe–B magnets from End-of-Life (EoL) products will largely reduce the environmental footprint associated with the primary mining of REEs. To develop environmentally friendly and cost-effective approaches for Nd–Fe–B magnets recycling is categorised as a "key enabling technology" with the prospect of positioning REEs within the circular economy.

This thesis mainly focuses on the recycling of the sintered Nd–Fe–B magnets using electrochemistry. Three electrochemical processes were developed to recycle and reprocess sintered Nd–Fe–B magnets: i) Selective recovery of the matrix $Nd_2Fe_{14}B$ grains by electrochemical etching; ii) Electrodeposition of Nd and Fe from ionic liquid (IL)-based electrolyte and iii) Selective recovery of REEs and transition metal (TM) by a room-temperature electrolysis.

Recycling of the sintered Nd–Fe–B magnets by recovering the matrix $Nd_2Fe_{14}B$ grains was successfully achieved using electrochemical etching. The etching mechanism is based on fine-tuning of the applied potential < –0.02 V (*vs.* Pt, current density < 5 mA cm^{-2}) to exploit the etching priority series of the phases present in the pristine Nd–Fe–B magnets: metallic Nd > intergranular $NdFe_4B_4$ > matrix $Nd_2Fe_{14}B$, which allows the preferential etching of their surrounding REE-rich grain boundaries, leaving the individual $Nd_2Fe_{14}B$ grains behind for magnetic separation. The total energy consumption of the proposed electrochemical recycling route is estimated to be ~2.99 kWh kg^{-1} that is, in a long term, expected to be economically and environmentally more feasible while offering considerably more flexibility.

Electrochemical co-deposition of Nd and Fe as an alternative recycling route was realized in the IL-based electrolyte, 1-ethyl-3-methylimidizolium dicyanamide using pulse-current plating. An induced co-deposition mechanism for the RE–TM is derived and supported by a mathematical model that considers the effect of the Fe^{2+} concentration on the Nd content in the deposit, in which the transition state Fe is formed during the electrodeposition, catalyzing the co-deposition of Nd and Fe. Upon annealing, NdC_2 is formed through the reaction of the electrodeposited Nd^0 with carbon as the Gibbs free energy of the reaction is negative. The developed co-deposition mechanism for RE–TM is potentially applicable to all non-aqueous systems for REE-based thin film production.

Selective recovery of REEs from the sintered Nd–Fe–B magnets in a facile closed loop was developed. In an electrolysis cell where Nd–Fe–B magnets are used as the anode, selective leaching of REEs is realized by balancing the Fe dissolution from the anode and Fe consumption on the cathode. This step saves 84.4% and 100% of acid and alkali usage,

respectively, with the energy consumption of 1.36 kWh per kilogram of sintered Nd–Fe–B magnets. After the electrolysis, the REEs were selectively precipitated as RE-sodium-sulfate double salts from the electrolyte, which are used as industrial raw materials. The electrolyte was sent back for reuse in the electrolysis cell, avoiding the wastewater generation. The addition of $(NH_4)_2SO_4$ and sodium citrate as chelating agents plays a key role in stabilizing the composition of the electrolyte for recycling and further enabling the selective precipitation of REEs with high purity (99.4%). At the same time, Fe metal was obtained, which can be used in a wide range of industrial products.

Electrochemical recycling of RE permanent magnets provides a more flexible alternative to the existing recycling methods, as it enables both alloys recovery and REEs recovery using varied electrolyte medium in a wide range of temperature regimes. This thesis provides insight into novel recycling routes based on electrochemistry for the sintered Nd–Fe–B magnets. However, a relatively clean and bulky magnet scrap has to be used in all the processes. To electrochemically treat magnet swarf for example, that are produced from magnet finishing processes, e.g., shaping, cutting and polishing, accounting for around 20–30 wt.% of the starting material, further investigations towards efficient recycling are needed. There are two fronts for further study on magnet swarf recycling by electrochemistry:

a) For recovering REEs from the magnet swarf, complete leaching of the magnet swarf by H^+, electrochemically generated in situ on the anode, based on the oxygen evolution reaction ($2H_2O - 4e^- \rightarrow 4H^+ + O_2$, $\varphi^\theta = 1.23$ V *vs.* SHE). By balancing the dissolution and consumption of the Fe on the anode and cathode, respectively, selective leaching of the REEs could be achieved, followed by selectively precipitating REEs without wastewater discharge, as described in this thesis.
b) For making new sintered Nd–Fe–B permanent magnets (PMs) from recycled materials (including Nd–Fe–B magnet swarf and sintered Nd–Fe–B magnet scraps), a combination of molten salt electrolysis with melt-spinning would be a promising route as described by the following steps: i) sintered Nd–Fe–B magnet scraps/swarf are melted with the flux, e.g., NdF_3 + LiF, and used as the cathode, ii) the RE oxides, e.g., Nd_2O_3 dissolved in the flux in the upper layer and are reduced to metal forms by electrolysis, iii) the liquid alloys in the bottom of the cell are cast onto a water-cooled copper wheel with a high rotation speed to obtain RE alloy flakes that can be further used as master alloys for new PM making. This process is advantageous as it is applicable to both oxidized and non-oxidized magnet scraps/swarf and more importantly, no extra RE alloys are needed and the acids & alkalis consumption, as well as solid waste & wastewater generation are avoided.

References

[1] H. W. F. Sung and C. Rudowicz, "Physics behind the magnetic hysteresis loop—a survey of misconceptions in magnetism literature," *Journal of Magnetism and Magnetic Materials,* vol. 260, pp. 250-260, 2003/03/01/ 2003.

[2] B. D. Cullity and C. D. Graham, *Introduction to magnetic materials*, 2nd ed.: Wiley-IEEE Press, 2008.

[3] J. Liu. (2016) Some Design Considerations Using Permanent Magnets. . *Magnetics Business & Technology.* Available: https://magneticsmag.com/some-design-considerations-using-permanent-magnets/

[4] K. Bru, P. Christmann, J. Labbé, and G. Lefebvre, "Panorama 2014 du marché des Terres Rares," *Rapport public,* p. 194, 2015.

[5] W. Benecki, *The Global Permanent Magnet Industry*, 2016.

[6] J. M. D. Coey, *Magnetism and Magnetic Materials*: Cambridge University Press, 2010.

[7] G. V. Research, "Permanent Magnet Market Size, Share & Trend Analysis Report By Product (Ferrite Magnet, Rare Earth), By Application (Automotive, Electronics, Industrial) By Region, And Segment Forecasts, 2018 - 2024," 2016.

[8] S. Liu, "Sm–Co high-temperature permanent magnet materials," *Chinese Physics B,* vol. 28, p. 017501, 2019.

[9] C. Chen, M. H. Walmer, and S. Liu, "Thermal Stability and the Effectiveness of Coatings for Sm-Co 2: 17 High-Temperature Magnets at Temperatures up to 550^ oC," *IEEE TRANSACTIONS ON MAGNETICS MAG,* vol. 40, pp. 2928-2930, 2004.

[10] O. Gutfleisch, K.-H. Müller, K. Khlopkov, M. Wolf, A. Yan, R. Schäfer, *et al.*, "Evolution of magnetic domain structures and coercivity in high-performance SmCo 2: 17-type permanent magnets," *Acta Materialia,* vol. 54, pp. 997-1008, 2006.

[11] G. Hadjipanayis, W. Tang, Y. Zhang, S. Chui, J. Liu, C. Chen, *et al.*, "High temperature 2: 17 magnets: relationship of magnetic properties to microstructure and processing," *IEEE transactions on magnetics,* vol. 36, pp. 3382-3387, 2000.

[12] P. Long, Y. Qiuhui, H. Zhang, X. Guangliang, M. Zhang, and W. Jingdong, "Rare earth permanent magnets Sm2 (Co, Fe, Cu, Zr) 17 for high temperature applications," *Journal of Rare Earths,* vol. 26, pp. 378-382, 2008.

[13] M. Sagawa, S. Fujimura, N. Togawa, H. Yamamoto, and Y. Matsuura, "New material for permanent magnets on a base of Nd and Fe," *Journal of Applied Physics,* vol. 55, pp. 2083-2087, 1984.

[14] D. Harimoto and Y. Matsuura, "Development of High Performance Nd-Fe-B Sintered Magnets," *Hitachi Metals Technical Review,* vol. 23, pp. 69-72, 2007.

[15] J. Coey, "Permanent magnets: Plugging the gap," *Scripta Materialia,* vol. 67, pp. 524-529, 2012.

[16] O. Gutfleisch, M. A. Willard, E. Bruck, C. H. Chen, S. G. Sankar, and J. P. Liu, "Magnetic Materials and Devices for the 21st Century: Stronger, Lighter, and More Energy Efficient," *Advanced Materials,* vol. 23, pp. 821-842, Feb 15 2011.

[17] K. Binnemans, P. T. Jones, T. Muller, and L. Yurramendi, "Rare Earths and the Balance Problem: How to Deal with Changing Markets?," *Journal of Sustainable Metallurgy,* vol. 4, pp. 126-146, Mar 2018.

[18] M. P. Paranthaman, C. S. Shafer, A. M. Elliott, D. H. Siddel, M. A. McGuire, R. M. Springfield*, et al.*, "Binder Jetting: A Novel NdFeB bonded magnet fabrication process," *Jom,* vol. 68, pp. 1978-1982, 2016.

[19] C. John J, *Rapidly Solidified Neodymium-Iron-Boron Permanent Magnets*: Woodhead Publishing, 2017.

[20] T. G. Woodcock, Y. Zhang, G. Hrkac, G. Ciuta, N. M. Dempsey, T. Schrefl*, et al.*, "Understanding the microstructure and coercivity of high performance NdFeB-based magnets," *Scripta Materialia,* vol. 67, pp. 536-541, 2012/09/01/ 2012.

[21] M. A. R. Önal, "Recycling of NdFeB magnets for rare earth elememts (REE) recovery," Engineering Science (PhD), KU Leuven, 2017.

[22] M. Sagawa, S. Fujimura, H. Yamamoto, Y. Matsuura, and K. Hiraga, "Permanent magnet materials based on the rare earth-iron-boron tetragonal compounds," *IEEE transactions on Magnetics,* vol. 20, pp. 1584-1589, 1984.

[23] L. Yu, J. Zhang, S. Hu, Z. Han, and M. Yan, "Production for high thermal stability NdFeB magnets," *Journal of Magnetism and Magnetic Materials,* vol. 320, pp. 1427-1430, 2008.

[24] Y. Wenlong, Y. Shihong, Y. Dunbo, L. Kuoshe, L. Hongwei, L. Yang*, et al.*, "Influence of gadolinium on microstructure and magnetic properties of sintered NdGdFeB magnets," *Journal of Rare Earths,* vol. 30, pp. 133-136, 2012.

[25] Y. Seo and S. Morimoto, "Comparison of dysprosium security strategies in Japan for 2010–2030," *Resources Policy,* vol. 39, pp. 15-20, 2014.

[26] W. Li, H. Sepehri-Amin, T. Ohkubo, N. Hase, and K. Hono, "Distribution of Dy in high-coercivity (Nd, Dy)–Fe–B sintered magnet," *Acta Materialia,* vol. 59, pp. 3061-3069, 2011.

[27] Z. Chen, Y. Wu, M. Kramer, B. R. Smith, B.-M. Ma, and M.-Q. Huang, "A study on the role of Nb in melt-spun nanocrystalline Nd–Fe–B magnets," *Journal of magnetism and magnetic materials,* vol. 268, pp. 105-113, 2004.

[28] Y.-Q. Wu, M. Kramer, Z. Chen, B.-M. Ma, D. Ping, and K. Hono, "Microstructural control of Nb addition in nanocrystalline hard magnets with different Nd content," *IEEE transactions on magnetics,* vol. 39, pp. 2935-2937, 2003.

[29] W. Chen, R. Gao, M. Zhu, W. Pan, W. Li, X. Li*, et al.*, "Magnetic properties and coercivity mechanism of isotropic HDDR NdFeB bonded magnets with Co and Dy addition," *Journal of magnetism and magnetic materials,* vol. 261, pp. 222-227, 2003.

[30] Y. Matsuura, S. Hirosawa, H. Yamamoto, S. Fujimura, and M. Sagawa, "Magnetic properties of the Nd2 (Fe1− x Co x) 14B system," *Applied Physics Letters,* vol. 46, pp. 308-310, 1985.

[31] F. Bolzoni, F. Leccabue, O. Moze, L. Pareti, M. Solzi, and A. Deriu, "3 d and 4 f magnetism in Nd2Fe14− x Co x B and Y2Fe14− x Co x B compounds," *Journal of applied physics,* vol. 61, pp. 5369-5373, 1987.

[32] K. Ohmori, L. Li, and C. Graham, "Effect of added Cu on the Nd-rich phase in hot-deformed NdFeB magnets," *IEEE transactions on magnetics,* vol. 28, pp. 2139-2141, 1992.

[33] W. Li, T. Ohkubo, T. Akiya, H. Kato, and K. Hono, "The role of Cu addition in the coercivity enhancement of sintered Nd-Fe-B permanent magnets," *Journal of Materials Research,* vol. 24, pp. 413-420, 2009.

[34] E. Rozendaal, "Coercivity dependency of sintered NdFeB magnets on Al content and the alloying route," *IEEE Transactions on Magnetics,* vol. 26, pp. 2631-2633, 1990.

[35] G. Sadullahoğlu, B. Altuncevahir, and O. Addemir, "Effect of Al and Cu Additions on Microstructure and Magnetic Properties of NdTb–FeCo–B Magnets," *Acta Physica Polonica, A.,* vol. 125, 2014.

[36] S. Glöser-Chahoud, A. Kühn, and L. A. Tercero Espinoza. (2016). *Globale Verwendungsstrukturen der Magnetwerkstoffe Neodym und Dysprosium: Eine szenariobasierte Analyse der Auswirkung der Diffusion der Elektromobilität auf den Bedarf an Seltenen Erden.* Available: http://hdl.handle.net/10419/142767

[37] R. (2016a). "Lithium: Global industry, markets and outlook (13th ed.)," Roskill, London, UK2016.

[38] K. M. Goodenough, F. Wall, and D. Merriman, "The rare earth elements: demand, global resources, and challenges for resourcing future generations," *Natural Resources Research,* vol. 27, pp. 201-216, 2018.

[39] S. Sawyer, Q. Liming, and L. Fried, *GLOBAL WIND REPORT - Annual Market Update 2017*, 2018.

[40] M. Reimer, H. Schenk-Mathes, M. Hoffmann, and T. Elwert, "Recycling Decisions in 2020, 2030, and 2040—When Can Substantial NdFeB Extraction be Expected in the EU?," *Metals,* vol. 8, p. 867, 2018.

[41] Z. Weng, N. Haque, G. M. Mudd, and S. M. Jowitt, "Assessing the energy requirements and global warming potential of the production of rare earth elements," *Journal of cleaner production,* vol. 139, pp. 1282-1297, 2016.

[42] B. K. Reck and T. E. Graedel, "Challenges in metal recycling," *Science,* vol. 337, pp. 690-695, 2012.

[43] E. Commission. (2018, 22, May). *Circular Economy: New rules will make EU the global front-runner in waste management and recycling.* Available: http://europa.eu/rapid/press-release_IP-18-3846_en.htm

[44] P. Venkatesan, T. Vander Hoogerstraete, T. Hennebel, K. Binnemans, J. Sietsma, and Y. X. Yang, "Selective electrochemical extraction of REEs from NdFeB magnet waste at room temperature," *Green Chemistry,* vol. 20, pp. 1065-1073, Mar 2018.

[45] H. Y. Jin, P. Afiuny, S. Dove, G. Furlan, M. Zakotnik, Y. Yih*, et al.*, "Life Cycle Assessment of Neodymium-Iron-Boron Magnet-to-Magnet Recycling for Electric Vehicle Motors," *Environmental Science & Technology,* vol. 52, pp. 3796-3802, Mar 2018.

[46] M. V. Reimer, H. Y. Schenk-Mathes, M. F. Hoffmann, and T. Elwert, "Recycling Decisions in 2020, 2030, and 2040—When Can Substantial NdFeB Extraction be Expected in the EU?," *Metals,* vol. 8, p. 867, 2018.

[47] Y. X. Yang, A. Walton, R. Sheridan, K. Guth, R. Gauss, O. Gutfleisch*, et al.*, "REE Recovery from End-of-Life NdFeB Permanent Magnet Scrap: A Critical Review," *Journal of Sustainable Metallurgy,* vol. 3, pp. 122-149, Mar 2017.

[48] R. Schulze and M. Buchert, "Estimates of global REE recycling potentials from NdFeB magnet material," *Resources, Conservation and Recycling,* vol. 113, pp. 12-27, 2016.

[49] H. Zhongsheng, "Rare Earth Recycling from NdFeB," in *Sustainable Inorganic Chemistry*, D. A. Aatwood, Ed., ed Lexington, USA: John Wiley & Sons, 2016.

[50] Y. Xu, L. S. Chumbley, and F. Laabs, "Liquid metal extraction of Nd from NdFeB magnet scrap," *Journal of Materials Research,* vol. 15, pp. 2296-2304, 2000.

[51] Z. Hua, J. Wang, L. Wang, Z. Zhao, X. Li, Y. Xiao*, et al.*, "Selective extraction of rare earth elements from NdFeB scrap by molten chlorides," *ACS Sustainable Chemistry & Engineering,* vol. 2, pp. 2536-2543, 2014.

[52] K. Habib and H. Wenzel, "Exploring rare earths supply constraints for the emerging clean energy technologies and the role of recycling," *Journal of Cleaner Production,* vol. 84, pp. 348-359, 2014.

[53] C. Tunsu, "8 - Hydrometallurgy in the recycling of spent NdFeB permanent magnets," in *Waste Electrical and Electronic Equipment Recycling*, F. Vegliò and I. Birloaga, Eds., ed: Woodhead Publishing, 2018, pp. 175-211.

[54] K. Habib, P. K. Schibye, A. P. Vestbø, O. Dall, and H. Wenzel, "Material flow analysis of NdFeB magnets for Denmark: a comprehensive waste flow sampling and analysis approach," *Environmental science & technology,* vol. 48, pp. 12229-12237, 2014.

[55] D. Schüler, M. Buchert, R. Liu, S. Dittrich, and C. Merz, "Study on rare earths and their recycling: final report for the Greens/EFA Group in the European Parliament," *Oko-Institute eV, Darmstad,* 2011.

[56] R. Moss, E. Tzimas, H. Kara, P. Willis, and J. Kooroshy, "Critical metals in strategic energy technologies," *JRC-scientific and strategic reports, European Commission Joint Research Centre Institute for Energy and Transport,* 2011.

[57] J. Holc, S. Besenič ar, and D. Kolar, "A study of Nd2Fe14B and a neodymium-rich phase in sintered NdFeB magnets," *Journal of Materials Science,* vol. 25, pp. 215-219, January 01 1990.

[58] K. Lee, K. Yoo, H.-S. Yoon, C. J. Kim, and K. W. Chung, "Demagnetization followed by remagnetization of waste NdFeB magnet for reuse," *Geosystem Engineering,* vol. 16, pp. 286-288, 2013/12/01 2013.

[59] M. Zakotnik, I. Harris, and A. Williams, "Possible methods of recycling NdFeB-type sintered magnets using the HD/degassing process," *Journal of Alloys and Compounds,* vol. 450, pp. 525-531, 2008.

[60] A. Walton, H. Yi, N. A. Rowson, J. D. Speight, V. S. J. Mann, R. S. Sheridan*, et al.*, "The use of hydrogen to separate and recycle neodymium–iron–boron-type magnets from electronic waste," *Journal of Cleaner Production,* vol. 104, pp. 236-241, 2015/10/01/ 2015.

[61] J. Meakin, J. Speight, R. Sheridan, A. Bradshaw, I. Harris, A. Williams*, et al.*, "3-D laser confocal microscopy study of the oxidation of NdFeB magnets in atmospheric conditions," *Applied Surface Science,* vol. 378, pp. 540-544, 2016.

[62] M. Awais, F. Coelho, M. Degri, E. Herraiz, A. Walton, and N. Rowson, "Hydrocyclone Separation of Hydrogen Decrepitated NdFeB," *Recycling,* vol. 2, p. 22, 2017.

[63] E. H. Lalana, M. J. Degri, A. Bradshaw, and A. Walton, "Recycling of Rare Earth Magnets by Hydrogen Processing and Re-Sintering," in *European Congress and Exhibition on Powder Metallurgy. European PM Conference Proceedings*, 2016, pp. 1-6.

[64] A. Lixandru, I. Poenaru, K. Guth, R. Gauss, and O. Gutfleisch, "A systematic study of HDDR processing conditions for the recycling of end-of-life Nd-Fe-B magnets," *Journal of Alloys and Compounds,* vol. 724, pp. 51-61, Nov 2017.

[65] O. Diehl, M. Schönfeldt, E. Brouwer, A. Dirks, K. Rachut, J. Gassmann*, et al.*, "Towards an Alloy Recycling of Nd–Fe–B Permanent Magnets in a Circular Economy," *Journal of Sustainable Metallurgy,* vol. 4, pp. 163-175, 2018.

[66] M. Zakotnik and C. Tudor, "Commercial-scale recycling of NdFeB-type magnets with grain boundary modification yields products with 'designer properties' that exceed those of starting materials," *Waste management,* vol. 44, pp. 48-54, 2015.

[67] M. Firdaus, M. A. Rhamdhani, Y. Durandet, W. J. Rankin, and K. McGregor, "High temperature oxidation of rare earth permanent magnets. Part 2-Kinetics," *Corrosion Science,* vol. 133, pp. 318-326, Apr 2018.

[68] D. Brown, Z. Wu, F. He, D. Miller, and J. Herchenroeder, "Dysprosium-free melt-spun permanent magnets," *Journal of Physics: Condensed Matter,* vol. 26, p. 064202, 2014.

[69] O. Gutfleisch, "Controlling the properties of high energy density permanent magnetic materials by different processing routes," *Journal of Physics D: Applied Physics,* vol. 33, p. R157, 2000.

[70] R. Gauß, O. Diehl, E. Brouwer, A. Buckow, K. Güth, and O. Gutfleisch, "Verfahren zum Recycling von seltenerdhaltigen Permanentmagneten," *Chemie Ingenieur Technik,* vol. 11, pp. 1477-1485, 2015.

[71] K. Binnemans, P. T. Jones, B. Blanpain, T. Van Gerven, Y. Yang, A. Walton*, et al.*, "Recycling of rare earths: a critical review," *Journal of cleaner production,* vol. 51, pp. 1-22, 2013.

[72] O. Takeda, K. Nakano, and Y. Sato, "Recycling for the waste derived from rare earth magnets by using molten fluoride," *Rare earths,* pp. 32-33, 2009.

[73] H. J. Chae, Y. Do Kim, B. S. Kim, J. G. Kim, and T.-S. Kim, "Experimental investigation of diffusion behavior between molten Mg and Nd–Fe–B magnets," *Journal of Alloys and Compounds,* vol. 586, pp. S143-S149, 2014.

[74] H. Okamoto, "Mg-Nd (magnesium-neodymium)," *Journal of phase equilibria,* vol. 12, pp. 249-250, 1991.

[75] A. Nayeb-Hashemi, J. Clark, and L. Swartzendruber, "The Fe— Mg (Iron-Magnesium) system," *Journal of Phase Equilibria,* vol. 6, pp. 235-238, 1985.

[76] O. Takeda, T. H. Okabe, and Y. Umetsu, "Phase equilibria of the system Fe–Mg–Nd at 1076 K," *Journal of alloys and compounds,* vol. 392, pp. 206-213, 2005.

[77] O. Takeda, T. H. Okabe, and Y. Umetsu, "Recovery of neodymium from a mixture of magnet scrap and other scrap," *Journal of Alloys and Compounds,* vol. 408, pp. 387-390, 2006.

[78] O. Takeda, T. Okabe, and Y. Umetsu, "Phase equilibrium of the system Ag–Fe–Nd, and Nd extraction from magnet scraps using molten silver," *Journal of alloys and compounds,* vol. 379, pp. 305-313, 2004.

[79] T. Saito, H. Sato, S. Ozawa, J. Yu, and T. Motegi, "The extraction of Nd from waste Nd–Fe–B alloys by the glass slag method," *Journal of alloys and compounds,* vol. 353, pp. 189-193, 2003.

[80] T. Saito, H. Sato, and T. Motegi, "Recovery of rare earths from sludges containing rare-earth elements," *Journal of alloys and compounds,* vol. 425, pp. 145-147, 2006.

[81] Y. Bian, S. Guo, L. Jiang, K. Tang, and W. Ding, "Extraction of Rare Earth Elements from Permanent Magnet Scraps by FeO–B 2 O 3 Flux Treatment," *Journal of Sustainable Metallurgy,* vol. 1, pp. 151-160, 2015.

[82] J. Jiang, T. Ozaki, K.-i. Machida, and G.-y. Adachi, "Separation and recovery of rare earths via a dry chemical vapour transport based on halide gaseous complexes," *Journal of alloys and compounds,* vol. 260, pp. 222-235, 1997.

[83] T. Uda, K. T. Jacob, and M. Hirasawa, "Technique for enhanced rare earth separation," *Science,* vol. 289, pp. 2326-2329, 2000.

[84] T. Uda, "Recovery of rare earths from magnet sludge by FeCl2," *Materials Transactions,* vol. 43, pp. 55-62, 2002.

[85] S. Shirayama, "Selective extraction of Nd and Dy from rare earth magnet scrap into molten salt," in *The Minerals, Metals and Materials Society-3rd International Conference on Processing Materials for Properties 2008*, 2009, pp. 469-474.

[86] C.-H. Lee, Y.-J. Chen, C.-H. Liao, S. R. Popuri, S.-L. Tsai, and C.-E. Hung, "Selective leaching process for neodymium recovery from scrap Nd-Fe-B magnet," *Metallurgical and Materials Transactions A,* vol. 44, pp. 5825-5833, 2013.

[87] J. W. Lyman and G. R. Palmer, "Scrap treatment method for rare earth transition metal alloys," United States Patent 5129945, 1992.

[88] T. Ellis, F. Schmidt, and L. Jones, "Methods and opportunities in the recycling of rare earth based materials," Ames Lab., IA (United States)1994.

[89] D. D. München, A. M. Bernardes, and H. M. Veit, "Evaluation of Neodymium and Praseodymium Leaching Efficiency from Post-consumer NdFeB Magnets," *Journal of Sustainable Metallurgy,* vol. 4, pp. 288-294, 2018.

[90] H. Vogel and B. Friedrich, "Development and research trends of the neodymium electrolysis–a literature review," in *Proceedings of the 8th European Metallurgical Conference, Düsseldorf*, 2015.

[91] J. P. Rabatho, W. Tongamp, Y. Takasaki, K. Haga, and A. Shibayama, "Recovery of Nd and Dy from rare earth magnetic waste sludge by hydrometallurgical process," *Journal of Material Cycles and Waste Management,* vol. 15, pp. 171-178, 2013.

[92] P. Venkatesan, Z. H. I. Sun, J. Sietsma, and Y. X. Yang, "An environmentally friendly electro-oxidative approach to recover valuable elements from NdFeB magnet waste," *Separation and Purification Technology,* vol. 191, pp. 384-391, Jan 2018.

[93] M. A. R. Önal, C. R. Borra, M. Guo, B. Blanpain, and T. Van Gerven, "Recycling of NdFeB magnets using sulfation, selective roasting, and water leaching," *Journal of Sustainable Metallurgy,* vol. 1, pp. 199-215, 2015.

[94] B. Morgan and O. Lahav, "The effect of pH on the kinetics of spontaneous Fe (II) oxidation by O2 in aqueous solution–basic principles and a simple heuristic description," *Chemosphere,* vol. 68, pp. 2080-2084, 2007.

[95] X. Wei, R. C. Viadero Jr, and K. M. Buzby, "Recovery of iron and aluminum from acid mine drainage by selective precipitation," *Environmental Engineering Science,* vol. 22, pp. 745-755, 2005.

[96] H.-S. Yoon, C.-J. Kim, J.-Y. Lee, S.-D. Kim, J.-S. Kim, and J.-C. Lee, "Separation of Neodymium from NdFeB Permanent Magnetic Scrap," *Journal of the Korean Institute of Resources Recycling,* vol. 12, pp. 57-63, 2003.

[97] J.-c. Lee, W.-b. Kim, J. Jeong, and I. Yoon, "Extraction of neodymium from Nd-Fe-B magnet scraps by sulfuric acid," *Journal of the Korean Institute of Metals and Materials(South Korea),* vol. 36, pp. 967-972, 1998.

[98] M. A. R. Önal, C. Jönsson, W. Zhou, T. Van Gerven, M. Guo, A. Walton*, et al.*, "Comparative oxidation behavior of Nd-Fe-B magnets for potential recycling methods: Effect of hydrogenation pre-treatment and magnet composition," *Journal of Alloys and Compounds,* vol. 728, pp. 727-738, 2017.

[99] T. Vander Hoogerstraete, B. Blanpain, T. Van Gerven, and K. Binnemans, "From NdFeB magnets towards the rare-earth oxides: a recycling process consuming only oxalic acid," *RSC Advances,* vol. 4, pp. 64099-64111, 2014.

[100] H.-S. Yoon, C.-J. Kim, K. W. Chung, S.-J. Lee, A.-R. Joe, Y.-H. Shin*, et al.*, "Leaching kinetics of neodymium in sulfuric acid from E-scrap of NdFeB permanent magnet," *Korean Journal of Chemical Engineering,* vol. 31, pp. 706-711, 2014.

[101] M. Tanaka, T. Oki, K. Koyama, H. Narita, and T. Oishi, "Recycling of rare earths from scrap," in *Handbook on the physics and chemistry of rare earths*. vol. 43, ed: Elsevier, 2013, pp. 159-211.

[102] S. Behera and P. Parhi, "Leaching kinetics study of neodymium from the scrap magnet using acetic acid," *Separation and Purification Technology,* vol. 160, pp. 59-66, 2016.

[103] M. Gergoric, C. Ravaux, B.-M. Steenari, F. Espegren, and T. Retegan, "Leaching and Recovery of Rare-Earth Elements from Neodymium Magnet Waste Using Organic Acids," *Metals,* vol. 8, p. 721, 2018.

[104] K. Koyama, A. Kitajima, and M. Tanaka, "Selective leaching of rare-earth elements from an Nd-Fe-B magnet," *Kidorui,* vol. 54, pp. 36-37, 2009.

[105] J. H. L. Voncken, *The rare earth elements: an introduction*: Springer, 2016.

[106] C. Tunsu and T. Retegan, "Hydrometallurgical processes for the recovery of metals from WEEE," in *WEEE Recycling*, ed: Elsevier, 2016, pp. 139-175.

[107] K. L. Nash, "A review of the basic chemistry and recent developments in trivalent f-elements separations," *Solvent Extraction and Ion Exchange,* vol. 11, pp. 729-768, 1993.

[108] M. Gergoric, C. Ekberg, B. M. Steenari, and T. Retegan, "Separation of Heavy Rare-Earth Elements from Light Rare-Earth Elements Via Solvent Extraction from a Neodymium Magnet Leachate and the Effects of Diluents," *Journal of Sustainable Metallurgy,* vol. 3, pp. 601-610, Sep 2017.

[109] T. Elwert, D. Goldmann, and F. Römer, "Separation of lanthanides from NdFeB magnets on a mixer-settler plant with PC-88A," *World Metall,* vol. 67, pp. 287-296, 2014.

[110] H.-S. Yoon, C.-J. Kim, K. Chung, S.-D. Kim, and J. Kumar, "Process development for recovery of dysprosium from permanent magnet scraps leach liquor by hydrometallurgical techniques," *Canadian Metallurgical Quarterly,* vol. 54, pp. 318-327, 2015.

[111] H. S. Yoon, C. J. Kim, K. W. Chung, S. D. Kim, J. Y. Lee, and J. R. Kumar, "Solvent extraction, separation and recovery of dysprosium (Dy) and neodymium (Nd) from aqueous solutions: Waste recycling strategies for permanent magnet processing," *Hydrometallurgy,* vol. 165, pp. 27-43, Oct 2016.

[112] Y. Kikuchi, M. Matsumiya, and S. Kawakami, "Extraction of rare earth ions from Nd-Fe-B magnet wastes with TBP in tricaprylmethylammonium nitrate," *Solvent Extraction Research and Development, Japan,* vol. 21, pp. 137-145, 2014.

[113] A. Rout and K. Binnemans, "Separation of rare earths from transition metals by liquid–liquid extraction from a molten salt hydrate to an ionic liquid phase," *Dalton Transactions,* vol. 43, pp. 3186-3195, 2014.

[114] Y. Liu, H. S. Jeon, and M. S. Lee, "Solvent extraction of Pr and Nd from chloride solution by the mixtures of Cyanex 272 and amine extractants," *Hydrometallurgy,* vol. 150, pp. 61-67, 2014.

[115] N. Panda, N. Devi, and S. Mishra, "Solvent extraction of neodymium (III) from acidic nitrate medium using Cyanex 921 in kerosene," *Journal of Rare Earths,* vol. 30, pp. 794-797, 2012.

[116] B. N. Kumar, B. R. Reddy, M. L. Kantam, J. R. Kumar, and J. Y. Lee, "Synergistic solvent extraction of neodymium (III) from chloride solutions using a mixture of triisooctylamine and bis (2, 4, 4-trimethylpentyl) monothiophosphinic acid," *Separation Science and Technology,* vol. 49, pp. 130-136, 2014.

[117] N. Swain and S. Mishra, "A review on the recovery and separation of rare earths and transition metals from secondary resources," *Journal of Cleaner Production,* vol. 220, pp. 884-898, May 20 2019.

[118] M. Gergoric, C. Ekberg, M. R. S. J. Foreman, B.-M. Steenari, and T. Retegan, "Characterization and leaching of neodymium magnet waste and solvent extraction of the rare-earth elements using TODGA," *Journal of Sustainable Metallurgy,* vol. 3, pp. 638-645, 2017.

[119] D. Dupont and K. Binnemans, "Recycling of rare earths from NdFeB magnets using a combined leaching/extraction system based on the acidity and thermomorphism of the ionic liquid [Hbet][Tf 2 N]," *Green Chemistry,* vol. 17, pp. 2150-2163, 2015.

[120] T. Vander Hoogerstraete, S. Wellens, K. Verachtert, and K. Binnemans, "Removal of transition metals from rare earths by solvent extraction with an undiluted phosphonium ionic liquid: separations relevant to rare-earth magnet recycling," *Green Chemistry,* vol. 15, pp. 919-927, 2013.

[121] D. C. Harris, *Quantitative chemical analysis*, 8th Edition ed.: W. H. Freeman, 2010.

[122] Y. Kamimoto, T. Itoh, K. Kuroda, and R. Ichino, "Recovery of rare-earth elements from neodymium magnets using molten salt electrolysis," *Journal of Material Cycles and Waste Management,* pp. 1-5, 2016.

[123] T. Oishi, H. Konishi, T. Nohira, M. Tanaka, and T. Usui, "Separation and recovery of rare earth metals by molten salt electrolysis using alloy diaphragm," *Kagaku Kogaku Ronbunshu,* vol. 36, pp. 299-303, 2010.

[124] H. Konishi, H. Ono, E. Takeuchi, T. Nohira, and T. Oishi, "Electrochemical separation of Dy from Nd magnet scraps in molten LiCl-KCl," *Transactions of the Institutions of Mining and Metallurgy Section C-Mineral Processing and Extractive Metallurgy,* vol. 125, pp. 216-220, 2016.

[125] L. Schultz, A. M. El-Aziz, G. Barkleit, and K. Mummert, "Corrosion behaviour of Nd–Fe–B permanent magnetic alloys," *Materials Science and Engineering: A,* vol. 267, pp. 307-313, 1999/07/31/ 1999.

[126] S. Mao, H. Yang, Z. Song, J. Li, H. Ying, and K. Sun, "Corrosion behaviour of sintered NdFeB deposited with an aluminium coating," *Corrosion Science,* vol. 53, pp. 1887-1894, 2011/05/01/ 2011.

[127] S. Mao, H. Yang, J. Li, F. Huang, and Z. Song, "Corrosion properties of aluminium coatings deposited on sintered NdFeB by ion-beam-assisted deposition," *Applied Surface Science,* vol. 257, pp. 5581-5585, 2011/04/15/ 2011.

[128] A. A. El-Moneim, A. Gebert, F. Schneider, O. Gutfleisch, and L. Schultz, "Grain growth effects on the corrosion behavior of nanocrystalline NdFeB magnets," *Corrosion Science,* vol. 44, pp. 1097-1112, 2002/05/01/ 2002.

[129] B. Greenberg, "Neodymium recovery process," 5362459, 1994.

[130] D. L. Perry, *Handbook of inorganic compounds*: CRC press, 2016.

[131] P. Patnaik, *Handbook of inorganic chemicals*: McGraw-Hill, 2002.

[132] P. Venkatesan, T. Vander Hoogerstraete, K. Binnemans, Z. Sun, J. Sietsma, and Y. Yang, "Selective Extraction of Rare-Earth Elements from NdFeB Magnets by a Room-Temperature Electrolysis Pretreatment Step," *ACS Sustainable Chemistry & Engineering,* vol. 6, pp. 9375-9382, 2018/07/02 2018.

[133] M. Schwartz, N. Myung, and K. Nobe, "Electrodeposition of iron group-rare earth alloys from aqueous media," *Journal of The Electrochemical Society,* vol. 151, pp. C468-C477, 2004.

[134] B. D. Falola and I. I. Suni, "Low temperature electrochemical deposition of highly active elements," *Current Opinion in Solid State & Materials Science,* vol. 19, pp. 77-84, Apr 2015.

[135] A. Bard, *Standard potentials in aqueous solution*: Routledge, 1985.

[136] W. Simka, D. Puszczyk, and G. Nawrat, "Electrodeposition of metals from non-aqueous solutions," *Electrochimica Acta,* vol. 54, pp. 5307-5319, Sep 30 2009.

[137] C. Baes and R. Mesmer, "The Hydrolysis of Cations," ed: Wiley, New York, 1976.

[138] J. Zhang, P. Evans, and G. Zangari, "Electrodeposition of Sm–Co nanoparticles from aqueous solutions," *Journal of Magnetism and Magnetic Materials,* vol. 283, pp. 89-94, 11// 2004.

[139] D. Gao, J. Fu, Y. Xu, and D. Xue, "Preparation and magnetic properties of Nd5Fe95-xBx nanowire arrays," *Materials Letters,* vol. 62, pp. 3070-3072, Jun 30 2008.

[140] Z.-n. Yang, C. Wang, Y. Zhang, and Y. Xie, "Electroplating mechanism of nanocrystalline NdFeB film," *Transactions of Nonferrous Metals Society of China,* vol. 25, pp. 832-837, 3// 2015.

[141] C. A. Berger, M. Arkhipova, G. Maas, and T. Jacob, "Dysprosium electrodeposition from a hexaalkylguanidinium-based ionic liquid," *Nanoscale,* vol. 8, pp. 13997-14003, 2016.

[142] L.-X. Luo, Y.-L. Liu, N. Liu, L. Wang, L.-Y. Yuan, Z.-F. Chai*, et al.*, "Electrochemical and thermodynamic properties of Nd (III)/Nd (0) couple at liquid Zn electrode in LiCl-KCl melt," *Electrochimica Acta,* vol. 191, pp. 1026-1036, Feb 10 2016.

[143] K. Yasuda, K. Kondo, S. Kobayashi, T. Nohira, and R. Hagiwara, "Selective Formation of Rare-Earth-Nickel Alloys via Electrochemical Reactions in NaCl-KCl Molten Salt," *Journal of the Electrochemical Society,* vol. 163, pp. D140-D145, 2016 2016.

[144] C. Nourry, L. Massot, P. Chamelot, and P. Taxil, "Formation of Ni-Nd alloys by Nd(III) electrochemical reduction in molten fluoride," *Journal of New Materials for Electrochemical Systems,* vol. 10, pp. 117-122, Apr 2007.

[145] H. Zhu, "Rare earth metal production by molten salt electrolysis," in *encyclopedia of applied electrochemistry*, ed: Springer, 2014, pp. 1765-1772.

[146] H. Konishi, H. Ono, E. Takeuchi, T. Nohira, and T. Oishi, *Electrochemical Formation of Nd Alloys Using Liquid Metal Electrodes in Molten LiCl-KCl Systems*, 2017.

[147] W. Han, M. Li, M. L. Zhang, and Y. D. Yan, "Progress in preparation of rare earth metals and alloys by electrodeposition in molten salts," *Rare Metals,* vol. 35, pp. 811-825, Nov 2016.

[148] H.-Y. Ryu, J.-H. Lee, W.-G. Kim, H. H. Nersisyan, G.-G. Lee, S.-K. Jo*, et al.*, "Electrochemical behavior of Nd in its pyrometallurgical recovery from waste magnet," *Rare Metals,* vol. 34, pp. 111-117, Feb 2015.

[149] A. P. Abbott, J. C. Barron, K. S. Ryder, and D. Wilson, "Eutectic - Based Ionic Liquids with Metal - Containing Anions and Cations," *Chemistry – A European Journal,* vol. 13, pp. 6495-6501, 2007.

[150] J. Kestin, M. Sokolov, and W. A. Wakeham, "Viscosity of liquid water in the range– 8 C to 150 C," *Journal of Physical and Chemical Reference Data,* vol. 7, pp. 941-948, 1978.

[151] E. L. Smith, A. P. Abbott, and K. S. Ryder, "Deep Eutectic Solvents (DESs) and Their Applications," *Chemical Reviews,* vol. 114, pp. 11060-11082, 2014/11/12 2014.

[152] Q. Zhang, K. D. O. Vigier, S. Royer, and F. Jérôme, "Deep eutectic solvents: syntheses, properties and applications," *Chemical Society Reviews,* vol. 41, pp. 7108-7146, 2012.

[153] E. Gómez, P. Cojocaru, L. Magagnin, and E. Valles, "Electrodeposition of Co, Sm and SmCo from a deep eutectic solvent," *Journal of electroanalytical chemistry,* vol. 658, pp. 18-24, 2011.

[154] J. X. Li, H. Lai, B. Q. Fan, B. Zhuang, L. H. Guan, and Z. G. Huang, "Electrodeposition of RE-TM (RE = La, Sm, Gd; TM = Fe, Co, Ni) films and magnetic properties in urea melt," *Journal of Alloys and Compounds,* vol. 477, pp. 547-551, May 2009.

[155] P. Liu, Y.-P. Du, Q.-Q. Yang, G.-R. Li, and Y.-X. Tong, "Electrochemical behavior of Fe(II) in acetamide-urea-NaBr-KBr melt and magnetic properties of inductively codeposited Nd-Fe film," *Electrochimica Acta,* vol. 52, pp. 710-714, Oct 25 2006.

[156] L. Peng, Y. Qiqin, Y. Yansheng, and T. Yexiang, "Electrodeposition of Rare Earth Metals and Their Alloys in Organic Electrolytes," *稀土学报 (英文版),* vol. 2, 1999.

[157] R. D. Rogers and G. A. Voth, "Ionic Liquids," *Accounts of Chemical Research,* vol. 40, pp. 1077-1078, 2007/11/01 2007.

[158] F. Liu, Y. Deng, X. Han, W. Hu, and C. Zhong, "Electrodeposition of metals and alloys from ionic liquids," *Journal of Alloys and Compounds,* vol. 654, pp. 163-170, Jan 5 2016.

[159] M. Galinski, A. Lewandowski, and I. Stepniak, "Ionic liquids as electrolytes," *Electrochimica Acta,* vol. 51, pp. 5567-5580, Aug 15 2006.

[160] X. Yang, L. He, S. Qin, G.-H. Tao, M. Huang, and Y. Lv, "Electrochemical and Thermodynamic Properties of Ln(III) (Ln = Eu, Sm, Dy, Nd) in 1-Butyl-3-Methylimidazolium Bromide Ionic Liquid," *Plos One,* vol. 9, Apr 21 2014.

[161] H. Kondo, M. Matsumiya, K. Tsunashima, and S. Kodama, "Investigation of oxidation state of the electrodeposited neodymium metal related with the water content of phosphonium ionic liquids," *ECS Transactions,* vol. 50, pp. 529-538, 2013.

[162] H. Kondo, M. Matsumiya, K. Tsunashima, and S. Kodama, "Attempts to the electrodeposition of Nd from ionic liquids at elevated temperatures," *Electrochimica Acta,* vol. 66, pp. 313-319, Apr 1 2012.

[163] M. Matsumiya, M. Ishii, R. Kazama, and S. Kawakami, "Electrochemical analyses of diffusion behaviors and nucleation mechanisms for neodymium complexes in

DEME TFSA ionic liquid," *Electrochimica Acta,* vol. 146, pp. 371-377, Nov 10 2014.

[164] J. Chastain, R. C. King, and J. Moulder, *Handbook of X-ray photoelectron spectroscopy: a reference book of standard spectra for identification and interpretation of XPS data*: Physical Electronics Division, Perkin-Elmer Corporation Eden Prairie, Minnesota, 1992.

[165] A. Brenner, "Introduction to Electrodeposition of Some of the More Important Alloys of the Iron-Group Metals, with Special Reference to Anomalous Codeposition*," in *Electrodeposition of Alloys*, ed: Academic Press, 1963, pp. 191-193.

[166] D. Weston, S. Harris, P. Shipway, N. Weston, and G. Yap, "Establishing relationships between bath chemistry, electrodeposition and microstructure of Co–W alloy coatings produced from a gluconate bath," *Electrochimica Acta,* vol. 55, pp. 5695-5708, 2010.

[167] M. D. Obradovic, R. M. Stevanovic, and A. R. Despic, "Electrochemical deposition of Ni-W alloys from ammonia-citrate electrolyte," *Journal of Electroanalytical Chemistry,* vol. 552, pp. 185-196, Jul 2003.

[168] L. Ma, X. Xi, Z. Nie, T. Dong, and Y. Mao, "Electrodeposition and Characterization of Co-W Alloy from Regenerated Tungsten Salt," *International Journal of Electrochemical Science,* pp. 1034-1051, 2017.

[169] T. Akiyama and H. Fukushima, "Recent study on the mechanism of the electrodeposition of iron-group metal alloys," *ISIJ international,* vol. 32, pp. 787-798, 1992.

[170] N. Zech, E. Podlaha, and D. Landolt, "Anomalous codeposition of iron group metals: II. Mathematical model," *Journal of the Electrochemical Society,* vol. 146, pp. 2892-2900, 1999.

[171] M. Holt and L. Vaaler, "Electrolytic reduction of aqueous tungstate solutions," *Journal of The Electrochemical Society,* vol. 94, pp. 50-58, 1948.

[172] W. E. Clark and M. Lietzke, "The mechanism of the tungsten alloy plating process," *Journal of The Electrochemical Society,* vol. 99, pp. 245-249, 1952.

[173] O. Younes-Metzler, L. Zhu, and E. Gileadi, "The anomalous codeposition of tungsten in the presence of nickel," *Electrochimica Acta,* vol. 48, pp. 2551-2562, 2003.

[174] S. Belevskii, S. Yushchenko, and A. Dikusar, "Anomalous electrodeposition of Co-W coatings from a citrate electrolyte due to the formation of multinuclear heterometallic complexes in the solution," *Surface Engineering and Applied Electrochemistry,* vol. 48, pp. 97-98, 2012.

[175] T. Woodcock and O. Gutfleisch, "Multi-phase EBSD mapping and local texture analysis in NdFeB sintered magnets," *Acta Materialia,* vol. 59, pp. 1026-1036, 2011.

[176] K. Hono and H. Sepehri-Amin, "Strategy for high-coercivity Nd–Fe–B magnets," *Scripta Materialia,* vol. 67, pp. 530-535, 2012/09/01/ 2012.

[177] Y. MATSUDA, T. FUJII, N. YOSHIMOTO, M. MORITA, and H. Masaki, "Studies on Electrodeposition of Dy-Fe in Organic Electrolyte Solution," *Journal of The Surface Finishing Society of Japan,* vol. 43, pp. 36-40, 1992.

[178] F. Endres, D. MacFarlane, and A. Abbott, *Electrodeposition from ionic liquids*: John Wiley & Sons, 2008.

[179] M. N. Torrico, R. A. Boll, and M. Matos, "Electrodeposition of actinide compounds from an aqueous ammonium acetate matrix: Experimental development and optimization," *Nuclear Instruments & Methods in Physics Research Section a-Accelerators Spectrometers Detectors and Associated Equipment,* vol. 790, pp. 64-69, Aug 1 2015.

[180] K. Mech, J. Mech, P. Zabinski, R. Kowalik, and M. Wojnicki, "Electrochemical deposition of alloys in Ru3+-Co2+-Cl--H2O system," *Journal of Electroanalytical Chemistry,* vol. 748, pp. 76-81, Jul 1 2015.

[181] O. Berkh, N. Eliaz, and E. Gileadi, "The Initial Stages of Electrodeposition of Re-Ni Alloys," *Journal of the Electrochemical Society,* vol. 161, pp. D219-D226, 2014 2014.

[182] O. Younes and E. Gileadi, "Electroplating of Ni/W alloys I. Ammoniacal citrate baths," *Journal of The Electrochemical Society,* vol. 149, pp. C100-C111, 2002.

[183] Sigma-Aldrich. (2004). *Material safety data sheet.* Available: http://terpconnect.umd.edu/~choi/MSDS/Sigma-Aldrich/N,N-DIMETHYLFORMAMIDE.pdf

[184] G. Bai, R. Gao, Y. Sun, G. Han, and B. Wang, "Study of high-coercivity sintered NdFeB magnets," *Journal of magnetism and magnetic materials,* vol. 308, pp. 20-23, 2007.

[185] N. Yoshimoto, O. Shinoura, H. Miyauchi, M. Ishikawa, and Y. Matsuda, "Nd-Fe Electrodeposition in Organic Electrolyte (E)," *Denki Kagaku Oyoki Kogyo Butsuri Kagaku,* vol. 62, pp. 982-984, 1994.

[186] H.-S. Yoon, C.-J. Kim, J.-Y. Lee, S.-D. Kim, J.-S. Kim, and J.-C. Lee, "Separation of Neodymium from NdEeB Permanent Magnetic Scrap," *Journal of the Korean Institute of Resources Recycling,* vol. 12, pp. 57-63, 2003.

[187] D. A. Jones, *Principles and prevention of corrosion*, 2nd edition ed. Upper Saddle River, New Jersey: Pearson Education, 1996.

[188] K. Hennemann, H. L. Lukas, and H. Schaller, "Constitution and thermodynamics of Fe-Nd alloys," *Zeitschrift für Metallkunde,* vol. 84, pp. 668-674, 1993.

[189] A. P. H. A. A. W. W. A. W. E. Federation., "Standard methods for the examination of water and wastewater," ed. Washington DC: American Public Health Association/American Water Works Association/Water Environment Federation., 1998.

[190] M. Firdaus, M. A. Rhamdhani, Y. Durandet, W. J. Rankin, and K. McGregor, "Review of high-temperature recovery of rare earth (Nd/Dy) from magnet waste," *Journal of Sustainable Metallurgy,* vol. 2, pp. 276-295, 2016.

[191] M. Farr, "Production of anisotropic injection moulded NdFeB magnets from end-of-life sintered magnets," University of Birmingham, 2018.

[192] M. Zakotnik, I. Harris, and A. Williams, "Multiple recycling of NdFeB-type sintered magnets," *Journal of Alloys and Compounds,* vol. 469, pp. 314-321, 2009.

[193] H. Sepehri-Amin, T. Ohkubo, M. Zakotnik, D. Prosperi, P. Afiuny, C. Tudor, *et al.*, "Microstructure and magnetic properties of grain boundary modified recycled

Nd-Fe-B sintered magnets," *Journal of Alloys and Compounds,* vol. 694, pp. 175-184, 2017.

[194] W. F. Li, T. Ohkubo, K. Hono, and M. Sagawa, "The origin of coercivity decrease in fine grained Nd–Fe–B sintered magnets," *Journal of Magnetism and Magnetic Materials,* vol. 321, pp. 1100-1105, 2009/04/01/ 2009.

[195] Y. Shinba, T. Konno, K. Ishikawa, K. Hiraga, and M. Sagawa, "Transmission electron microscopy study on Nd-rich phase and grain boundary structure of Nd–Fe–B sintered magnets," *Journal of applied physics,* vol. 97, p. 053504, 2005.

[196] L. Yanfeng, Z. Minggang, L. Anhua, F. Haibo, S. HUANG, L. Wei*, et al.*, "Relationship between controllable preparation and microstructure of NdFeB sintered magnets," *Journal of Rare Earths,* vol. 32, pp. 628-632, 2014.

[197] X. Xu, T. Sasaki, Y. Une, H. Kubo, T. Ohkubo, M. Sagawa*, et al.*, "Origin of the coercivity difference in Nd-Fe-B sintered magnets processed from hydrogenation-disproportionation-desorption-recombination powder and jet-milled powder," *Acta Materialia,* vol. 151, pp. 293-300, 2018.

[198] K. Oesterreicher and H. Oesterreicher, "On the phase NdFe4B4 and its implication in the magnetic hardening of Nd2Fe14B permanent magnets," *Journal of the Less Common Metals,* vol. 104, pp. 19-21, 1984.

[199] S. Wang and Y. Li, "In situ TEM study of Nd-rich phase in NdFeB magnet," *Journal of Magnetism and Magnetic Materials,* vol. 285, pp. 177-182, 2005.

[200] S.-i. Ishiguro, K. Ozutsumi, and H. Ohtaki, "Calorimetric and spectrophotometric studies of chloro complexes of manganese (II) and cobalt (II) ions in N, N-dimethylformamide," *Journal of the Chemical Society, Faraday Transactions 1: Physical Chemistry in Condensed Phases,* vol. 84, pp. 2409-2419, 1988.

[201] W. Grzybkowski and M. Pilarczyk, "Stability of monochloride complexes of some divalent transition-metal cations in N, N-dimethylformamide," *Journal of the Chemical Society, Faraday Transactions 1: Physical Chemistry in Condensed Phases,* vol. 82, pp. 1745-1753, 1986.

[202] L. Schultz, A. El-Aziz, G. Barkleit, and K. Mummert, "Corrosion behaviour of Nd–Fe–B permanent magnetic alloys," *Materials Science and Engineering: A,* vol. 267, pp. 307-313, 1999.

[203] E. Isotahdon, E. Huttunen-Saarivirta, S. Heinonen, V.-T. Kuokkala, and M. Paju, "Corrosion mechanisms of sintered Nd–Fe–B magnets in the presence of water as vapour, pressurised vapour and liquid," *Journal of Alloys and Compounds,* vol. 626, pp. 349-359, 2015.

[204] F. Fabiano, F. Celegato, A. Giordano, C. Borsellino, L. Bonaccorsi, L. Calabrese*, et al.*, "Assessment of corrosion resistance of Nd–Fe–B magnets by silanization for orthodontic applications," *Physica B: Condensed Matter,* vol. 435, pp. 92-95, 2014.

[205] E. Isotahdon, E. Huttunen-Saarivirta, V.-T. Kuokkala, and M. Paju, "Corrosion behaviour of sintered Nd–Fe–B magnets," *Materials Chemistry and Physics,* vol. 135, pp. 762-771, 2012.

[206] A. J. Bard, L. R. Faulkner, J. Leddy, and C. G. Zoski, *Electrochemical methods: fundamentals and applications, 2nd Edition* vol. 2: Wiley New York, 2000.

[207] M. Zakotnik, C. O. Tudor, L. T. Peiró, P. Afiuny, R. Skomski, and G. P. Hatch, "Analysis of energy usage in Nd–Fe–B magnet to magnet recycling," *Environmental Technology & Innovation,* vol. 5, pp. 117-126, 2016/04/01/ 2016.

[208] A. K. Pathak, M. Khan, K. A. Gschneidner Jr, R. W. McCallum, L. Zhou, K. Sun, *et al.*, "Cerium: an unlikely replacement of dysprosium in high performance Nd–Fe–B permanent magnets," *Advanced Materials,* vol. 27, pp. 2663-2667, 2015.

[209] M. Bidikoudi, L. F. Zubeir, and P. Falaras, "Low viscosity highly conductive ionic liquid blends for redox active electrolytes in efficient dye-sensitized solar cells," *Journal of Materials Chemistry A,* vol. 2, pp. 15326-15336, 2014.

[210] Q. Zhang, C. Yang, Y. Hua, Y. Li, and P. Dong, "Electrochemical preparation of nanostructured lanthanum using lanthanum chloride as a precursor in 1-butyl-3-methylimidazolium dicyanamide ionic liquid," *Physical Chemistry Chemical Physics,* vol. 17, pp. 4701-4707, 2015.

[211] D. MacFarlane, S. Forsyth, J. Golding, and G. Deacon, "Ionic liquids based on imidazolium, ammonium and pyrrolidinium salts of the dicyanamide anion," *Green Chemistry,* vol. 4, pp. 444-448, 2002.

[212] T. Simons, P. Howlett, A. Torriero, D. MacFarlane, and M. Forsyth, "Electrochemical, transport, and spectroscopic properties of 1-ethyl-3-methylimidazolium ionic liquid electrolytes containing zinc dicyanamide," *The Journal of Physical Chemistry C,* vol. 117, pp. 2662-2669, 2013.

[213] A. A. Torriero, *Electrochemistry in Ionic Liquids: Volume 1: Fundamentals*: Springer, 2015.

[214] N.-C. Lo, P.-C. Chung, W.-J. Chuang, S. C. N. Hsu, I. W. Sun, and P.-Y. Chen, "Voltammetric Study and Electrodeposition of Ni(II)/Fe(II) in the Ionic Liquid 1-Butyl-1-Methylpyrrolidinium Dicyanamide," *Journal of the Electrochemical Society,* vol. 163, pp. D9-D16, 2016 2016.

[215] Y.-l. Zhu, Y. Katayama, and T. Miura, "Electrochemistry of fe (ii)/fe in a hydrophobic amide-type ionic liquid," *Journal of The Electrochemical Society,* vol. 159, pp. D699-D704, 2012.

[216] H. Zhou, P. Lv, Y. Shen, J. Wang, and J. Fan, "Identification of degradation products of ionic liquids in an ultrasound assisted zero-valent iron activated carbon micro-electrolysis system and their degradation mechanism," *Water research,* vol. 47, pp. 3514-3522, 2013.

[217] H. Zhou, Y. Shen, P. Lv, J. Wang, and J. Fan, "Degradation of 1-butyl-3-methylimidazolium chloride ionic liquid by ultrasound and zero-valent iron/activated carbon," *Separation and Purification Technology,* vol. 104, pp. 208-213, 2013.

[218] D. M. Dryden, T. Sun, R. McCormick, R. Hickey, R. Vidu, and P. Stroeve, "Anomalous Deposition of Co-Ni Alloys in Film and Nanowire Morphologies from Citrate Baths," *Electrochimica Acta,* vol. 220, pp. 595-600, 2016/12/01/ 2016.

[219] P. Zanello, *Inorganic electrochemistry: theory, practice and application*: Royal Society of Chemistry, 2003.

[220] S. Oue, H. Nakano, S. Kobayashi, and H. Fukushima, "Structure and codeposition behavior of Ni–W alloys electrodeposited from ammoniacal citrate solutions," *Journal of the Electrochemical Society,* vol. 156, pp. D17-D22, 2009.

[221] H. Eyring, "The activated complex and the absolute rate of chemical reactions," *Chemical Reviews,* vol. 17, pp. 65-77, 1935.

[222] E. Pollak and J.-L. Liao, "A new quantum transition state theory," *The Journal of chemical physics,* vol. 108, pp. 2733-2743, 1998.

[223] R. Hernandez and W. H. Miller, "Semiclassical transition state theory. A new perspective," *Chemical physics letters,* vol. 214, pp. 129-136, 1993.

[224] Y. Georgievskii and S. J. Klippenstein, "Long-range transition state theory," *The Journal of chemical physics,* vol. 122, p. 194103, 2005.

[225] D. G. Truhlar, B. C. Garrett, and S. J. Klippenstein, "Current status of transition-state theory," *The Journal of physical chemistry,* vol. 100, pp. 12771-12800, 1996.

[226] S. Begel, F. W. Heinemann, G. Stopa, G. Stochel, and R. van Eldik, "The classic "brown-ring" reaction in a new medium: Kinetics, mechanism, and spectroscopy of the reversible binding of nitric oxide to iron (II) in an ionic liquid," *Inorganic chemistry,* vol. 50, pp. 3946-3958, 2011.

[227] J. Tang and K. Azumi, "Optimization of pulsed electrodeposition of aluminum from AlCl 3-1-ethyl-3-methylimidazolium chloride ionic liquid," *Electrochimica Acta,* vol. 56, pp. 1130-1137, 2011.

[228] M.-J. Deng, I. W. Sun, P.-Y. Chen, J.-K. Chang, and W.-T. Tsai, "Electrodeposition behavior of nickel in the water- and air-stable 1-ethyl-3-methylimidazolium-dicyanamide room-temperature ionic liquid," *Electrochimica Acta,* vol. 53, pp. 5812-5818, 2008/08/01/ 2008.

[229] L. Sanchez-Cupido, J. M. Pringle, A. L. Siriwardana, A. Unzurrunzaga, M. Hilder, M. Forsyth*, et al.*, "Water-Facilitated Electrodeposition of Neodymium in a Phosphonium-Based Ionic Liquid," *The journal of physical chemistry letters,* vol. 10, pp. 289-294, 2019.

[230] H. Ota, M. Matsumiya, N. Sasaya, K. Nishihata, and K. Tsunashima, "Investigation of electrodeposition behavior for Nd (III) in [P 2225][TFSA] ionic liquid by EQCM methods with elevated temperatures," *Electrochimica Acta,* vol. 222, pp. 20-26, 2016.

[231] D. Givord, J. Nozieres, M. Rossignol, D. Taylor, I. Harris, D. Fruchart*, et al.*, "Structural analysis of the hard ferromagnetic phase observed in quenched Nd-Fe alloys of hyper-eutectic composition," *Journal of alloys and compounds,* vol. 176, pp. L5-L11, 1991.

[232] Y. Sui, Z. Zhang, Q. Xiao, W. Liu, T. Zhao, X. Zhao*, et al.*, "Structure, phase transformation and magnetic properties of Nd–Fe–C alloys made by mechanical alloying and subsequent annealing," *Journal of alloys and compounds,* vol. 267, pp. 215-223, 1998.

[233] K. Murase, K.-i. Machida, and G.-y. Adachi, "Recovery of rare metals from scrap of rare earth intermetallic material by chemical vapour transport," *Journal of alloys and compounds,* vol. 217, pp. 218-225, 1995.

[234] X. Xu, S. Sturm, Z. Samardzija, J. Vidmar, J. Scancar, and K. Zuzek Rozman, "A novel concept for direct Nd - Fe - B magnets recycling based on the Nd2Fe14B grains recovery via acid - free electrochemical etching," *ChemSusChem,* vol. 12, pp. 4754-4758, 2019.

[235] K. Osseo-asare, M. E. Deelo, and K. Weil, "Electrodeposition of iron in aqueous ferrous sulfate solution: Role of ammonium ion," *ECS Transactions,* vol. 2, pp. 293-302, 2006.

[236] M. Schlesinger and M. Paunovic, *Modern electroplating* vol. 55: John Wiley & Sons, 2011.

[237] R. Mesmer and C. Baes, *The hydrolysis of cations*: Ed. Wiley, EUA, 1976.

[238] M. A. Brown, A. J. Kropf, A. Paulenova, and A. V. Gelis, "Aqueous complexation of citrate with neodymium (III) and americium (III): a study by potentiometry, absorption spectrophotometry, microcalorimetry, and XAFS," *Dalton Transactions,* vol. 43, pp. 6446-6454, 2014.

[239] C. Chu and C. Wan, "The effect of chelating agents on the cathodic polarization and the electrodeposition of iron powders," *Journal of materials science,* vol. 27, pp. 6700-6706, 1992.

[240] S. Yoshimura, S. Yoshihara, T. Shirakashi, E. Sato, and K. Ishii, "Magnetic Properties and Structures of Electrodeposited Iron Films," *IEEE Translation Journal on Magnetics in Japan,* vol. 9, pp. 112-117, 1994.

[241] E. Zhelibo, K. Aryupina, and É. Natanson, "Formation of fine iron powder on the cathode," *Powder Metallurgy and Metal Ceramics,* vol. 12, pp. 97-101, 1973.

[242] N. Takeno, "Atlas of Eh-pH diagrams," *Geological survey of Japan open file report,* vol. 419, p. 102, 2005.

[243] M. Pourbaix, *Atlas of electrochemical equilibria in aqueous solutions*. New York: Pergamon Press, 1966.

[244] M. A. Brown, A. J. Kropf, A. Paulenova, and A. V. Gelis, "Aqueous complexation of citrate with neodymium(III) and americium(III): a study by potentiometry, absorption spectrophotometry, microcalorimetry, and XAFS," *Dalton Transactions,* vol. 43, pp. 6446-6454, 2014 2014.

[245] G. Senanayake, S. Jayasekera, A. Bandara, E. Koenigsberger, L. Koenigsberger, and J. Kyle, "Rare earth metal ion solubility in sulphate-phosphate solutions of pH range— 0.5 to 5.0 relevant to processing fluorapatite rich concentrates: effect of calcium, aluminium, iron and sodium ions and temperature up to 80° C," *Minerals Engineering,* vol. 98, pp. 169-176, 2016.

[246] N. Zech and D. Landolt, "The influence of boric acid and sulfate ions on the hydrogen formation in Ni · Fe plating electrolytes," *Electrochimica acta,* vol. 45, pp. 3461-3471, 2000.

[247] Wikipedia, "Boric acid," ed.

[248] J. Lyman and G. Palmer, "Recycling of rare earths and iron from NdFeB magnet scrap," *High Temperature Materials and Processes,* vol. 11, pp. 175-188, 1993.

Intentionally left blank

Bibliography

Publications Related to the Thesis

Journal Articles

X. Xu, S. Šturm, J. Zavašnik, and K. Žužek Rožman, "Electrodeposition of a rare-earth iron alloy from an ionic-liquid electrolyte," *ChemElectroChem,* vol. 6, no. 11, pp. 2860–2869, 2019. (Cover feature)

X. Xu, S. Šturm, Z. Samardžija, J. Vidmar, J. Scancar, and K. Žužek Rožman, "A novel concept for direct Nd–Fe–B recycling based on the $Nd_2Fe_{14}B$ grains recovery via acid-free electrochemical etching," *ChemSusChem*, vol. 12, pp. 4754–4758, 2019.

X. Xu, S. Šturm, Z. Samardžija, J. Scancar, K. Marković and K. Žužek Rožman, "A facile method for the simultaneous recovery of the rare-earth elements and transition metals from Nd–Fe–B magnets," submitted to *Green Chemistry*, 2019.

Patents

X. Xu, S. Šturm, and K. Žužek Rožman, "A method for recovery of $Nd_2Fe_{14}B$ grains from bulk sintered Nd–Fe–B magnet scraps by electrochemical etching," *European Patent*, EP18208508.4, 2018.

X. Xu, S. Šturm, and K. Žužek Rožman, "A method for selective recovery of the rare earth elements and transition metals from Nd–Fe–B magnets based on electrolysis," *European Patent*, EP19197716.4, 2019.

Scientific Conference Contribution Abstracts Related to the Thesis

X. Xu, S. Šturm, and K. Žužek Rožman, "Induced co-deposition of neodymium and iron from an ionic-liquid electrolyte," European Congress and Exhibition on Advanced Materials and Processes 2019 (EUROMAT 2019), 1–5 September, 2019, Stockholm, Sweden. Book of abstracts.

X. Xu, S. Šturm, and K. Žužek Rožman, "Selective recovering the 2:14 grains from sintered Nd–Fe–B magnets by electrochemical etching at room temperature," The 9th International Conference on Rare Earth Development and Application & Annual Meeting of the Chinese Society of Rare Earths 2019 (ICRE2019), May 13–15, 2019, Beijing, China. Book of abstracts. (Excellent oral lecture award)

X. Xu, S. Šturm, and K. Žužek Rožman, "Induced co-deposition of NdFe-based thin film by pulse plating technique in 1-ethyl-3-methylimidizolium dicyanamide," 6th International Conference on Ionic Liquids for Electrochemical Devices, September 9–11, 2018, Rome, Italy. Book of abstracts.

X. Xu, Š. Trafela, A. Ikram, M. F. Mehmood, S. Šturm, and K. Žužek Rožman, "Development of $NdFe_{12}$-based magnetic films by electrodeposition from aqueous-

and ionic liquid-based electrolytes as an alternative reprocessing route for recycled Nd–Fe–B permanent magnets", European Congress on Exhibition on Advanced Materials and Processes, September 17–22, 2017, Thessaloniki, Greece. Federation of European Materials Society.

X. Xu, Š. Trafela, S. Kobe, and K. Žužek Rožman, "Electrodeposition of NdFe-based thin films from aqueous solution: the mechanism of Nd and Fe incorporation", 12th International Workshop on Electrodeposited Nanostructures, ED NANO, March 16–22, 2017, Sofia, Bulgaria. Book of abstracts, pp. 40.

X. Xu, Š. Trafela, S. Kobe, and K. Žužek Rožman, "Electrodeposition of Nd–Fe-based alloy from aqueous solution", 24th International Conference on Materials and Technology, September 28–30, 2016, Portorož, Slovenia. Programme and book of abstracts, pp. 225.

Other Publications

Conference Paper

E. Anas, A. Ikram, M. F. Mehmood, **X. Xu**, S. Šturm, K. Žužek Rožman, and Š. Irena, "Hydrogen decrepitation and spark plasma sintering to produce recycled $SmCo_5$ magnets with high coercivity," *IEEE magnetics letters*, vol. 9, pp. 5503504-1-5503504-5, 2018.

Scientific Conference Contribution Abstracts

K. Žužek Rožman, **X. Xu**, K. Spomenka, and S. Šturm, "Development of Nd–Fe-based magnetic films by electrode-position from ionic liquids as an alternative reprocessing route for recycled Nd–Fe–B permanent magnets," 62nd Annual Conference on Magnetics, MMM, November 6–10, 2017, Pittsburgh, USA. Programme and book of abstracts, The IEEE Magnetics Society Society.

Š. Trafela, **X. Xu**, S. Kobe, and K. Žužek Rožman, "A novel electrochemical sensor based on modified Ni electrodes for formaldehyde detection in alkaline media," 8th International Workshop on Surface Modification for Chemical and Biochemical Sensing, SMCBS, November 3–7, 2017, Żelechów, Poland. Programme and book of abstracts, The Bioelectrochemical Society, pp. 228–229.

Š. Trafela, **X. Xu**, S. Kobe, and K. Žužek Rožman, "Electrodeposition and electro-catalytic properties of Ni based nanomaterials for formaldehyde detection in alkaline media," 25th International Conference on Materials and Technology, October 16–19, 2017, Portorož, Slovenia. Programme and book of abstracts, pp. 187–188.

K. Žužek Rožman, P. Darja, A. M. Shahid, Š. Trafela, **X. Xu**, S. Šturm, P. M. P. Mariana, V. Manuel, W. Ulli, N. Volker, E. Mateja, H. Samo, K. Spomenka, and K. Nina, "Magnetic nanostructures with added functionalities for future magnetic and medical applications," NANOAPP 2017, Nanomaterials & Application, June 14–18, 2017, Bled, Slovenia. Programme and book of abstracts.

Biography

The author of this thesis Xuan Xu was born on September 26, 1989, in Wuhan, Hubei Province, People's Republic of China. He started his university study programme in Agricultural Resources and Environment at the College of Plant Science at the Tarim University, China. He obtained his Bachelor of Agriculture degree in June, 2012. In September 2012, he continued his Master study on Environmental Science at the Chongqing Institute of Green and Intelligent Technology, Chinese Academy of Sciences, China. The research topic of his Master Thesis was "Establishing electro-Fenton system of high oxygen utilization and its application in DMP degradation". He obtained his Master of Engineering degree in June, 2015. In 2016, he began his doctoral study at the Jožef Stefan International Postgraduate School. He is employed at the Department for Nanostructured Materials (K7), Jožef Stefan Institute. His work was framed in the European Training Network for the Design and Recycling of Rare-Earth Permanent Magnet Motors and Generators in Hybrid and Full Electric Vehicles (ETN-DEMETER) towards the development of electrodeposition of $NdFe_{12}N_x$ thin and thick films. His research interests are recycling of rare-earth permanent magnets, recovery of rare-earth elements and other noble metals, and synthesis of active electrocatalysts for new energy applications.

Intentionally left blank